Title
Mechanisms of biofoulant-membrane interactions for ultrafiltration and microfiltration membranes

Author
Jun, Dukwoo

Publication Date
2016

Peer reviewed|Thesis/dissertation

UNIVERSITY OF CALIFORNIA

Los Angeles

Mechanisms of Biofoulant-Membrane Interactions for Ultrafiltration and Microfiltration Membranes

A dissertation submitted in partial satisfaction

of the requirements for the degree Doctor of Philosophy

in Civil Engineering

by

Dukwoo Jun

2016

ABSTRACT OF THE DISSERTATION

Mechanisms of Biofoulant-Membrane Interactions for Ultrafiltration and Microfiltration Membranes

by

Dukwoo Jun

Doctor of Philosophy in Civil Engineering

University of California, Los Angeles, 2016

Professor Eric M.V. Hoek, Chair

Since the majority of biofouling occurs on the surface of the polymeric membranes, key interfacial interactions between a membrane surface and a biofoulant play a pivotal role in biofouling phenomena. In thermodynamic perspective, biofouling can be interpreted as adhesion of two different entities, a biofoulant and a membrane, through a media, (herein, water), to be a combined column. Therefore, adhesion accompanies a structural change of interfaces existing in the aqueous system. This interface-transitive nature of biofouling phenomena leads that surface tension-based theories are adopted in the fundamental understanding of the membrane biofouling. Among those theories, the van Oss approach has been considered prominent because of its satisfactory prediction for experimental results of biofouling tests. According to van Oss

approach, in aqueous media, Lewis acid-base interaction occurs between the electron-acceptor in hydrogen atoms of water and lone pairs of atoms of a solid, basically having an analogous concept with hydrogen-bonding. The membrane surface with polar properties is able to hold water molecules and form a hydration cell layer on its surface, which may impede the access of biofoulant to the membrane surface. Because the biofoulant also has the electron-donating and accepting potentials, other interfacial interactions also occur in biofoulant-water and biofoulant–membrane surface. Therefore, better thermodynamic understanding on the biofouling phenomena need a perspective that ponders the three different but deeply interconnected interfacial interactions existing in membrane-water, water-biofoulant and biofoulant-membrane. The purpose of this dissertation is to investigate the biofouling phenomena in the molecular basis that can qualitatively and quantitatively evaluate the roles of physicochemical properties of water, membranes and biofoulants in biofoulant-membrane interaction for aqueous system.

First, this study investigated the water-membrane interaction in terms of surface tension properties of a membrane and their discrete interactions with water in Chapter 2. This chapter simulated the available surface tension parameters of polymeric porous membranes using different presumptions on polar properties of water and evaluates the effect of each surface tension parameter of a membrane on water-membrane interactions. The simulated libraries of surface tension parameters revealed that polymeric porous membranes highly tend to fall into a category of electron-donor monopolar or semi-monopolar solids. The high electron-accepticity of water emphasized the role of γ^- of a membrane in the interfacial interaction between a membrane and water (ΔG_{131}^{tot}) and caused the polar adhesion between electron-donor sites of a membrane and electron-acceptor sites of water to be a major interaction component in ΔG_{131}^{tot} than other components. The high Lewis acidity of water highlighted the role of γ^- of a

membrane in its wettability as well. A higher electron-donicity of a membrane has little impact on the total surface tension of the membrane surface (γ_1), but successfully favors the electron-acceptor sites of water forming a significantly lower surface tension of the water-membrane interface (γ_{13}) and thus a greater affinity between the membrane and water ($-\Delta G_{13}^{tot}$).

Chapter 3 investigated the effects of water-solids interactions on biofouling phenomena and explored fining key physicochemical properties of a membrane for biofouling resistance. The high electron-accepticity of water emphasized the importance of γ^- of a membrane and a biofoulant in their interfacial interaction through water and drove acid-base interaction to be a major interaction component in the interfacial interactions between membranes and a biofoulant (ΔG_{132}). The surfaces of various biofoulants were characterized with highly variable electron-donicities and the biofoulant with lower electron donicity can be more vulnerable to biofouling due to the inferior hydration energy formed on the surface of the biofoulant. The inferior hydration energy by a low electron-donicity of a biofoulant can be compensated by an enhanced electron-donicity of a membrane; this fact leads to propose a standard of an electron-donicity demand for a membrane to have a positive ΔG_{132} with a given biofoulant. Experimental results of a microbial adhesion test and biofouling tests qualitatively correlated well with tendencies of electron-donicities of the test membranes, proving an electron-donicity of a membrane to be a reasonable indicator for the anti-biofouling property of the membrane.

Chapter 4 attempted to impart membranes with hydrophilic and anti-biofouling properties by grafting hydrophilic polymers to the surface. Photoactive perfluorophenyl azides (PFPAs) were utilized to generate highly reactive nitrenes (when exposed to UV light) that can covalently bind to the membranes' surfaces. Three different types of small molecule PFPA derivatives were applied and the experimental data directed us to modify the UF membrane surfaces with water-

soluble small molecules to maintain the membranes' high permeability. The effects of small molecule PFPA derivatives on surface tension characteristics of a polymeric membrane were analyzed by van Oss method. Modeling data indicated that the electron-donicity of membranes plays an essential role in foulant adhesion forces. The analyzed physicochemical properties of the modified membranes were compared to the experimental results of a biofouling test with alginate solution. The modified membranes with higher electron-donicity exhibit outstanding foul-resistance against sodium alginate, a model foulant, during operation.

The dissertation of Dukwoo Jun is approved.

Michael K. Stenstrom

Shaily Mahendra

Richard B. Kaner

Eric M.V. Hoek, Committee Chair

University of California, Los Angeles

2016

Dedication

To my God Almighty and Lord,

who is my everything and without whom I am nothing.

Table of Contents

List of Figures

List of Tables

Acknowledgements

First and foremost I would like to thank my advisor, Professor Eric M.V. Hoek for his unstinted support and encouragement. I am highly grateful to him that I am offered an invaluable chance to study at UCLA, which is as I have experienced the center of fervent creativity in art and science. I would also like to thank the other members of my doctoral committee, Professor Stenstrom, Professor Mahendra, and Professor Kaner for their guidance and feedback.

I would like to thank my good friends, Brian McVerry, Saeedreza Hafeznezami, Jinwen Wang, Mavis Wong, Catalina Marambio-Jones, Xinwei Huang, Kristofer Marsh and Na He for their great encouragements and contributions to my research.

I would like to show my deep appreciation for my mother. Her prayer and love are a spiritual and mental fuel that enables me to enjoy this journey.

Finally, I want to express my highest gratitude to my beloved wife, Sarah for her selfless support and sincere encouragement throughout this journey. I love you.

VITA

Education

2009 M.S. Civil & Environmental Engineering, Seoul National University, Korea

2003 B.S. Geosystem Science, Seoul National University, Korea

Professional Experience

2009 – 2012 Research Engineer, Eco-energy Department, Technology Development Division, Hyundai Engineering and Construction Co. Ltd., Korea

2003 – 2006 Engineering Officer, Korean Army
(2005, Served at Civil Affair Team in Afghanistan)

Teaching Experience

Fall 2014 Teaching assistant, CEE 155: Unit Operations and Processes for Water and Wastewater Treatment

Publications and Conference Presentations

Andy Tay, Anja Kunze, **Dukwoo Jun**, Eric M.V. Hoek and Dino Di Carlo, "The Age of Cortical Neural Networks Affects Their Interactions with Nanoparticles," *Small*, Submitted

Brian T. McVerry, **Dukwoo Jun**, Robert Jordan, Xinwei Huang, Kristofer L. Marsh, Ethan Rao, Yves Rubin, Eric M.V. Hoek, Richard B. Kaner, "Novel, Small Molecule Perfluorophenylazide Coatings for Fouling-resistant Membrane Bioreactors," *Advanced Functional Materials*, in preparation.

Dukwoo Jun, Kwansun Yoo, Eric M.V. Hoek, Young O Kim and Jeonghwan Kim, "Inorganic Scaling Mechanisms in the Anaerobic Membrane Bioreactor Treating High-Strength Organic Wastewater," *Journal of Membrane Science*, in preparation.

Dukwoo Jun and Eric M.V. Hoek, "A Modified Blasius Equation for Power Law Fluids in Turbulent Flow: Development of a New Explicit Friction Model and Rheological Characterization Method," *Chemical Engineering Journal*, in preparation.

Dukwoo Jun and Eric M.V. Hoek, "Mechanisms of Biofoulant-Membrane Interfacial Interactions: Implications of Electron-Donicity in Membrane Biofouling," *Journal of Membrane Science*, in preparation.

Chapter 1

INTRODUCTION

1.1. Biofouling problem in membrane bioreactor

Membrane bioreactor (MBR) is water and wastewater treatment process that integrates a biological process with a membrane. Although MBR has become a trustworthy option to replace the conventional activated sludge process and an alternative for many domestic and industrial applications, membrane biofouling is considered the one of main factors to limit the widespread application of MBRs.[1,2] Membrane biofouling can be defined as "the undesirable deposition and accumulation of microorganisms, organic colloids, solutes, and cell debris within pores or on membrane surface".[2] According to the survey result with MBR specialists, it is found that a high range of MBR stakeholders still attributed the limitation of MBR application to membrane fouling as shown in Figure 1.1.[3] They answered that membrane biofouling is a main problematic issue in membrane operation because the biofouling increases operation cost and requires membrane cleaning with making the operation more complicated.

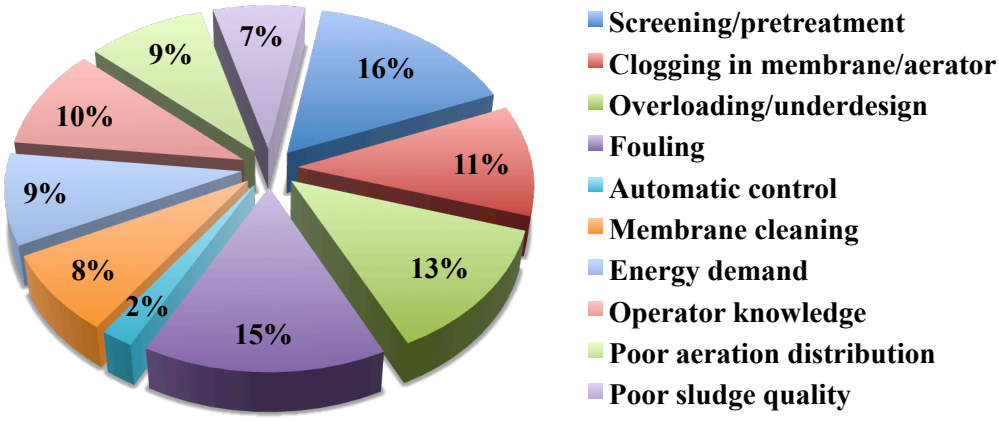

Figure 1.1. Key factors challenging MBR operation[3]

It is difficult to generalize the principle of membrane fouling in MBRs. However, the characteristics and extent of fouling are deeply affected by three factors: biomass properties, operating conditions, and membrane features (Figure 1.2). Although some operating parameters such as SRT, HRT and food to microorganism ratio (F/M) do not directly affect membrane fouling, those conditions influence the sludge characteristics, which are able to determine the fouling phenomena.[4,5]

Membrane fouling is determined by the interaction between the membrane material and the components of the activated sludge liquor such as bioflocs and soluble and colloidal compounds. Thus, the properties and amount of biomass in mixed liquor critically affects on the membrane fouling. Generally, the mixed liquor in bioreactor is a complex and heterogeneous suspension, which contains feed components, biomass and biological metabolites produced by the biomass. Each component of the mixed liquor, including the suspended solids and soluble and colloidal exopolymers like extracellular polymeric substances (EPS), is cable to contribute significantly to membrane fouling.[2,4,6]

Moreover, the composition of biomass is not fixed but varies with both feed water condition and the operating conditions; this variable property of biomass makes the membrane fouling in MBRs more complicated. In order to elucidate the complexity of the relation between biomass and membrane fouling, it is required to understand how the membrane fouling occurs in MBRs in presence of biomass. Therefore, this study reviews the fundamental mechanisms of fouling existing in MBRs and the possible effects of biomass on the fouling process.

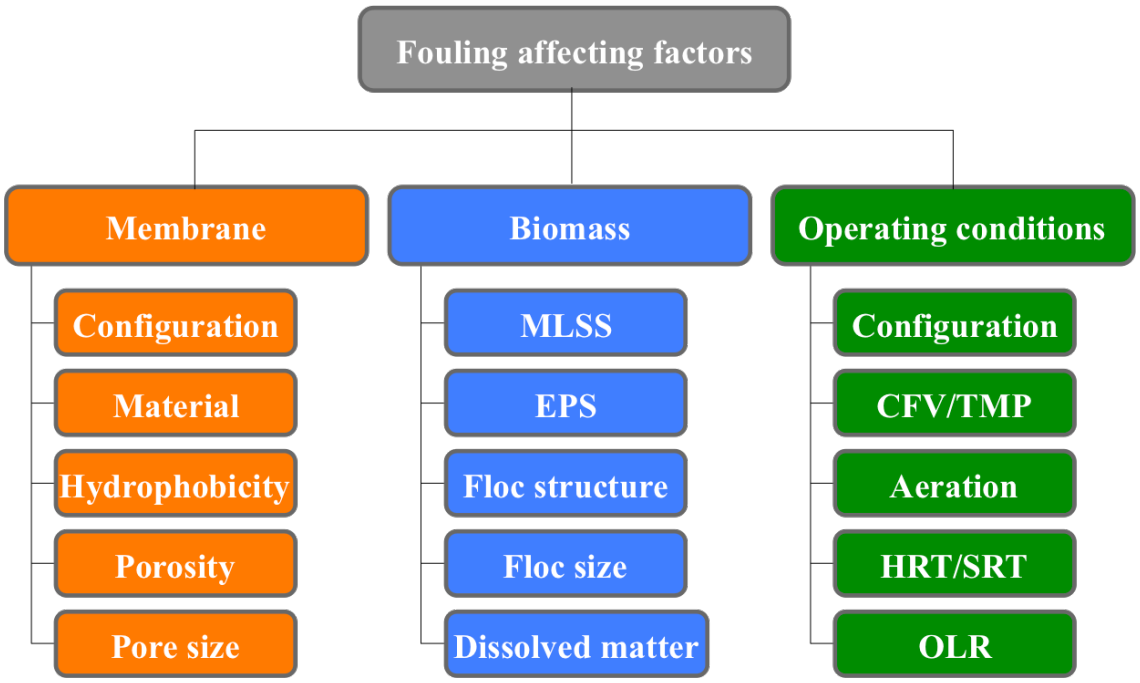

Figure 1.2. Factors influencing membrane fouling in membrane bioreactor process[2]

1.2. Biofouling mechanism in MBRs

1.2.1. Force balance

In a bulk fluid along the membrane surface, the total momentum of a particle is controlled by the sum of all the forces exerted on the particle, as schematically described in Figure. 1.3. Since the total momentum determines the movement of a particle, the tendency of attachment and deposition of a particle can be changed with the combination of each force component. Generally, permeation drag force and shear-induced diffused force are mainly attributed to the membrane fouling since they affect the movement of suspended particles, which is considered a major resistance in MBRs. It is known that at a certain permeation flux there is a particle size range above which the particles can be moved backward away from membrane surface by hydrodynamic force like cross-flow velocity and below which the particles tend to

move toward the membrane resulting in membrane fouling. At the field of MBRs, the permeation flux is called critical flux (Jc) if the flux below Jc does not cause the suspended solids such as biomass to move onto membrane so that there is no observation of cake formation during a certain period.[7]

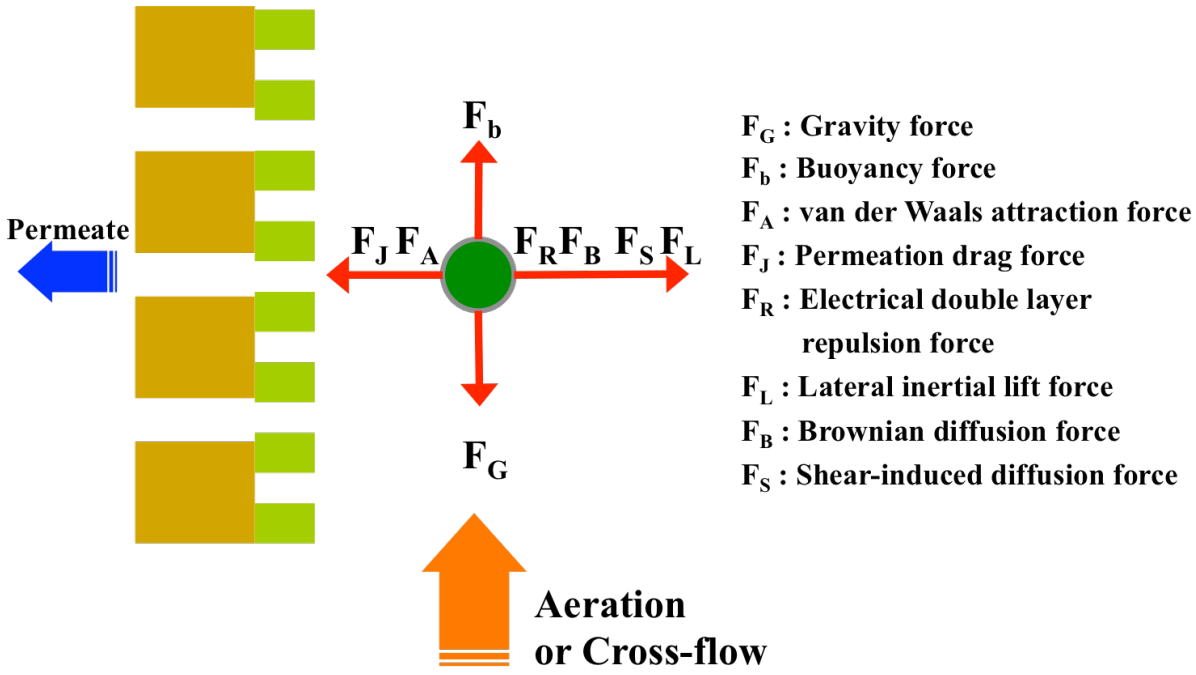

Figure 1.3. Force balance imposed on a particle in fluid stream along membrane surface

1.2.2. Biofouling model

Figure 1.4-1. shows the fouling procedure that could occur in MBR. It is considered that membrane pores into which small particles can access in the first stage of filtration, could undergo internal fouling (standard or complete pore blocking) and that this initial fouling could decrease the effective pore density and finally result in a cake layer formation. Some researchers assume that at the initial filtration stage a membrane pore can undergo both internal fouling

phenomena (standard and complete pore blocking) simultaneously.[8]. However, as shown in Figure 1.5, cake formation is thought to occur only after the internal obstruction of the pores happens.[8,9]

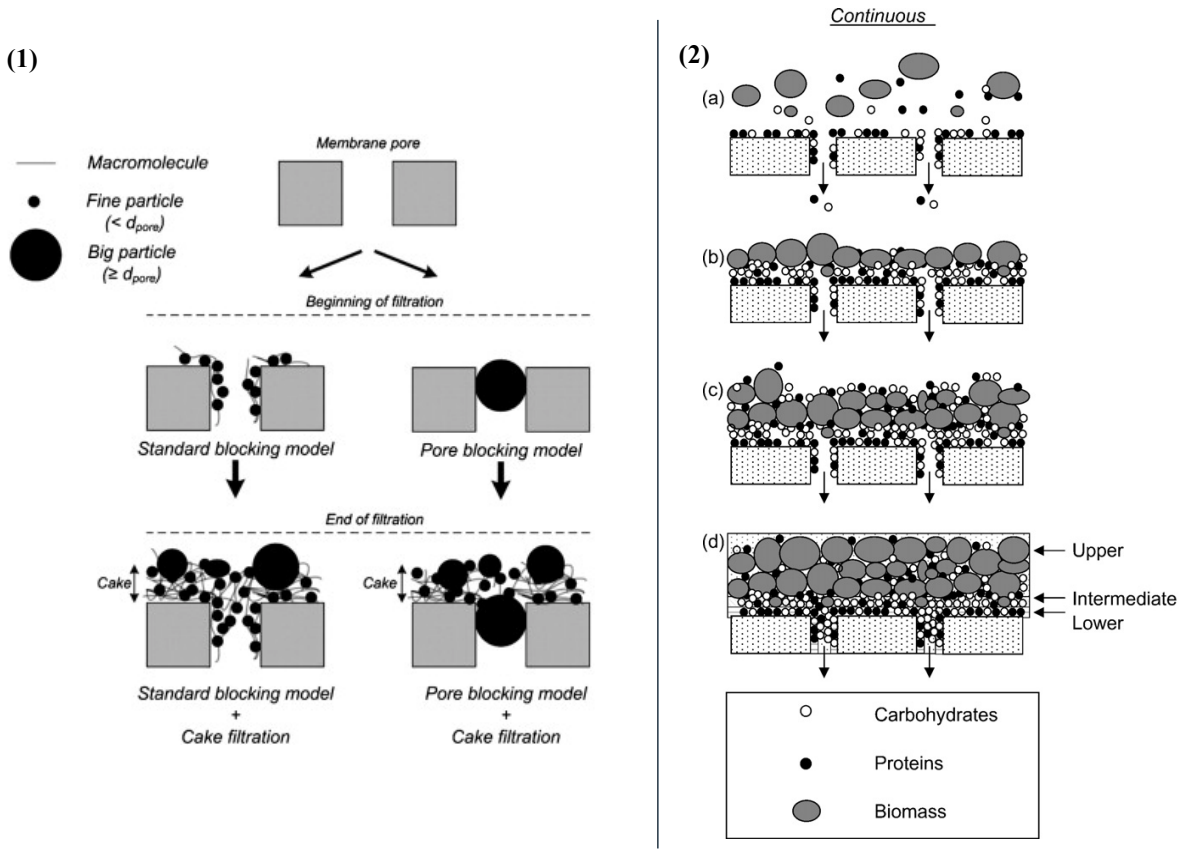

Figure 1.4. Models describing the fouling in MBR (left: [8], right:[10])

More detailed model to simulate the cake formation in MBRs can be described as Figure 1.4-2, which shows cake multilayers as well as the interaction between biofocs and their exopolymers. Within the initial stage of filtration, small particles like soluble microbial product (SMP) preferentially approaches the membrane surface and forms a thin conditioning layer, resulting in "size-differentiated conditioning layer" (Figure 1.4-2a). These attached biopolymers enhance the stickiness of the membrane surface as well as the attraction force, leading to more ready attachment and deposition of bioflocs on the membrane (Figure 1.4-2b). Then, a sludge

cake layer begins to form and more biomass flocs and exopolymers attach to the cake layer, developing a porous cake layer (Figure 1.4-2c). Due to shear forces exerted on the particles, the thickness of the cake layer reaches equilibrium. This cake layer can have a function to prefilter the small particles as a secondary membrane, called a dynamic membrane, and delay the deposition of the small particles on the pores. However, due to porous structure of the cake layer, small particles are capable to diffuse through the cake layer and join to the membrane until their coverage on the membrane reaches equilibrium (Figure 1.4-2d).[10]

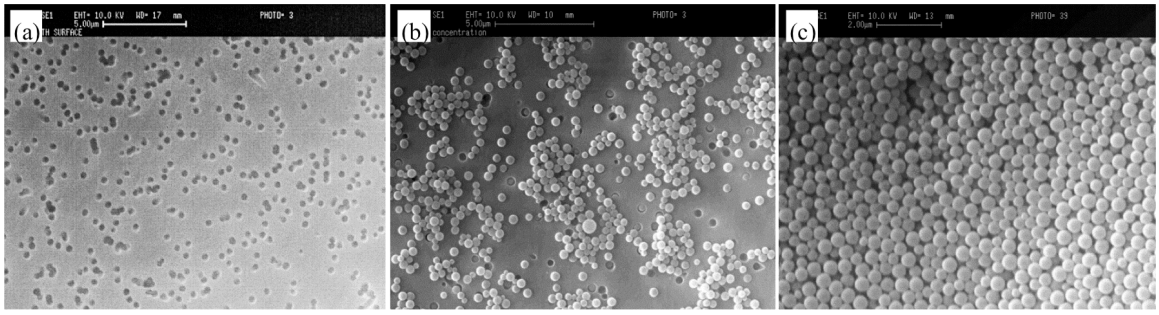

Figure 1.5. Filtering surface of iso-pore membrane: (a) clean membrane, (b) at the end of the pore blocking filtration stage, (c) at the transition from blocking to cake formation.[9]

1.2.3. Types of Fouling resistance in MBR

Based on the above models, the resistance that occurs in MBRs can be defined as the below equation:

$$R_T = R_M + R_C + R_B + R_P + R_A \tag{1.1}$$

where R_T is the total resistance, R_M the inherent membrane resistance, R_C the cake layer resistance, R_B the biofilm resistance, R_P the pore blocking resistance and R_A the adsorption resistance. Sometimes, R_B, R_P and R_A are considered a unified fouling resistance, R_F, which represents the irreversible fouling resistance in contrast to the reversible fouling, R_C.[7]

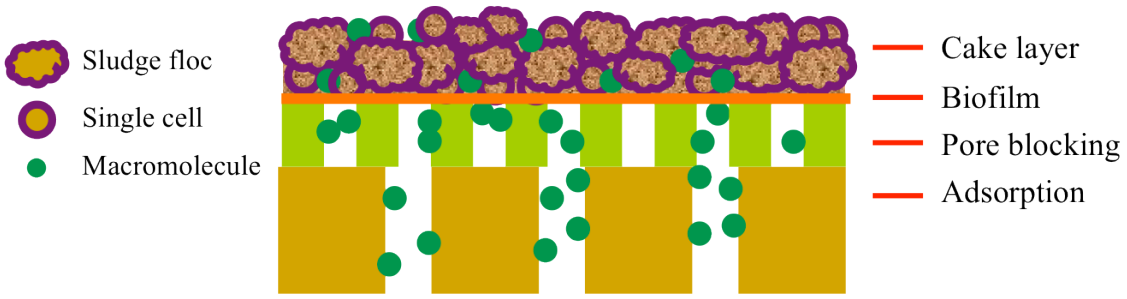

Figure 1.6. Resistance schematic for membrane fouling in MBR

It is widely reported that the sludge cake formation is the main cause of fouling in MBRs and that the initial transmembrane pressure (TMP) increase under super-critical flux operation or the steady flux decline under the constant TMP operation are attributed to the formation of cake layer on membrane surface. The sludge cake layer appears to have a high filtration resistance; a sludge cake with a 1mm thickness might have a filtration resistance of 1.7×10^{13} m^{-1}, which is the corresponding resistance causing a pressure drop of about 0.5×10^{5} Pa for the permeating stream of 0.25 m/d.[7]

Table 1.1. Analysis results of α, R_T, R_M, R_P and R_C in MBRs. [7]

MLSS (g/L)	α (m/kg)	Resistance (10^{12} m^{-1})				Cake resistance ratio (%) R_c/R_t
		R_m	R_p	R_c	R_t	
8.0–12.0	4.9E + 13	–	4.0	9.0	–	–
2.0–3.0	3–60E + 12	0.49–0.50	0.35–0.81	2.94–3.39	4.24	69.0–80.0
3.1–3.4	–	1.3–1.9	0.6–1.1	32.2–38.0	35.2–39.9	92.0–95.0
1.8–4.6	–	1.1	0.8–0.9	8.8–8.9	10.8	81.5–82.4
4.7 ± 0.25	–	0.20	0.80	15.40	16.40	93.9
6.0	–	0.48	0.40	4.66	5.54	84.1
6.0	2.3–5.2E + 13	0.11	0.25–0.42	0.59–1.38	0.98–1.74	53.0–79.4
1.0–2.0, 7.0–12.0	1–100E + 12	1.16–1.17	0.38–0.46	4.14–4.23	5.77[a]	72.0–73.0
0.09–3.7	0.7–18.5E + 8	0.89–1.56	1.16–1.51	2.06–5.39	4.49–7.44	40.2–72.4
5.2–10.0	0.6–1.2E + 12	–	–	–	–	–

[a]resistance values calculated at 30 kPa.

Table 1.1. presents various resistances (R_T, R_M, R_C and R_P) and specific cake resistance in MBRs. Even though the extents of cake resistance vary with researches, the cake resistance is observed as being the main contributor to the total resistance. The sludge cake generally has a high specific resistance of the order of 10^{12}~10^{14} m/kg, which is more than two orders of magnitude higher than the resistance of the bulk sludge suspension (about 10^{11} m/kg). It was argued that a pool of biopolymers within the sludge cake and its interaction with bioflocs might result in the higher specific filtration resistance of the sludge cake layer.[7]

The biomass supernatants (generally defined as EPS and SMP) can contribute to overall membrane fouling significantly; it has been reported that their relative contribution ranges from 17% to 81%, as shown in Figure 1.7.[6]. The relative contribution of biopolymers on membrane fouling is depending on biological states of the sludge suspension and properties of membrane used in MBRs. Especially, operating conditions can also determine the role of biopolymers on fouling; if MBR is operated with sub-critical flux, pore blocking and biofilm derived by the biopolymers can become the dominant fouling phenomena over cake formation. [6]

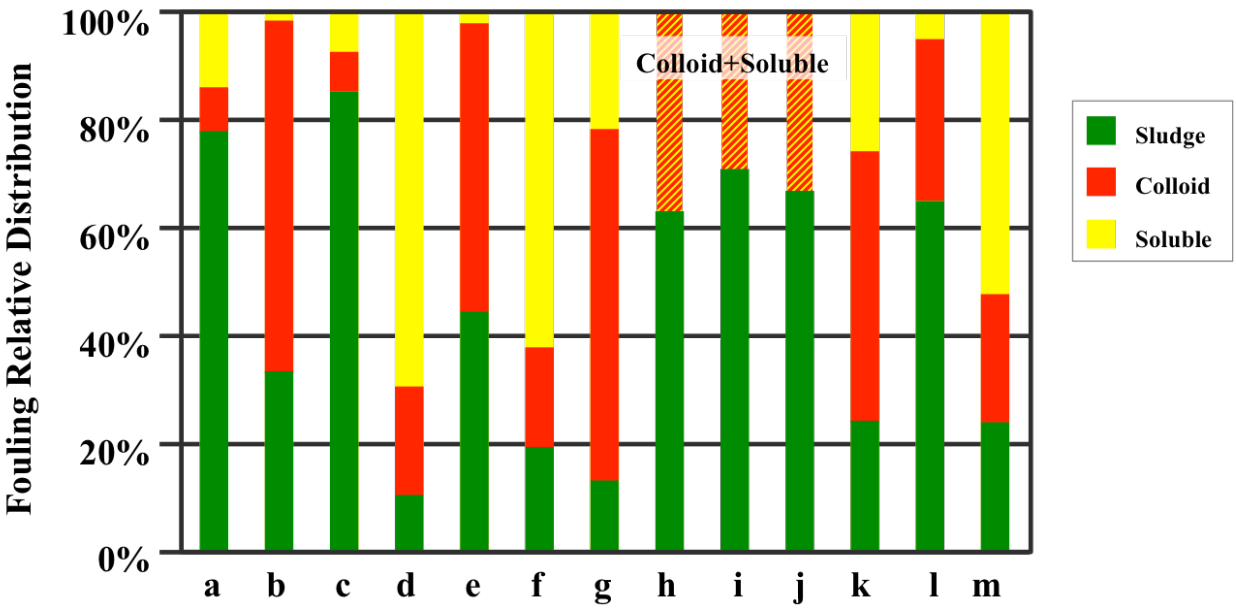

Figure 1.7. Relative contributions of the different biomass fractions to MBR fouling.[6]

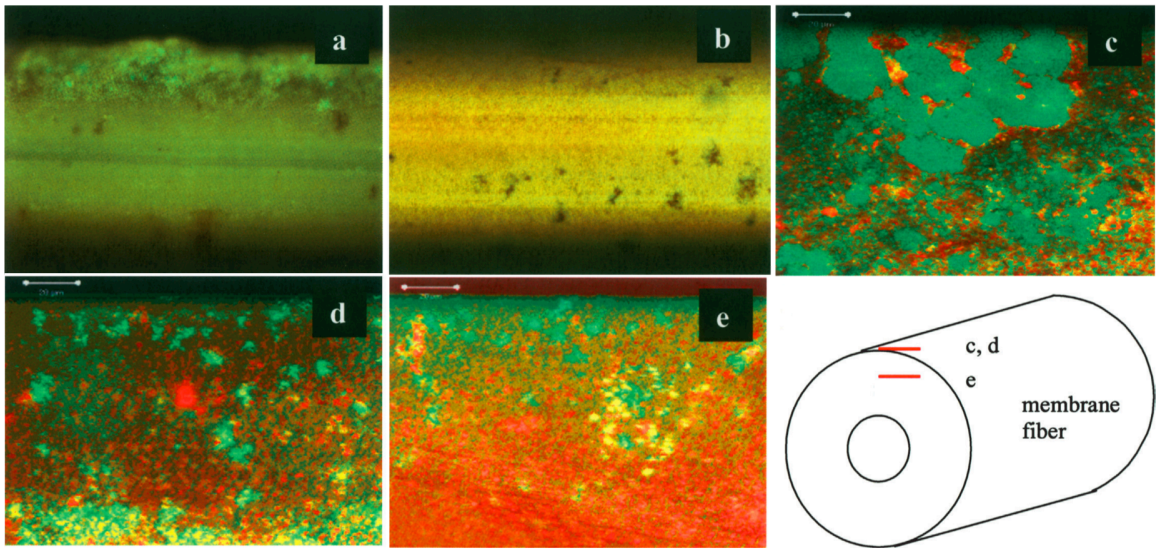

Figure 1.8. CLSM photographs of membrane fouling and sludge cake coverage: (a) a membrane fiber with partial sludge cake coverage at the top before a physical wash; (b) a membrane fiber after a brief physical wash removing the sludge cake; (c) bacteria clusters (green) and associated polysaccharides (red) in the sludge cake attached to the membrane surface; (d) polysaccharides and bacteria that remained on the membrane surface after a physical wash; and (e) penetration and accumulation of polysaccharides into the membrane pores.[11]

Despite the discrepancy of the relative filtration resistance of biopolymer, long-term operation of MBR needs to take account for control of biopolymer deposition on membrane because biopolymers can accumulate on membrane surface and even penetrate onto pores inside membrane. Accumulation of biopolymers on membrane can modify the membrane property, accelerating the membrane fouling. Figure 1.8 shows that the irreversible fouling occurs with the deposition of biopolymers on membrane pores. When Chu and Li (2005) identified bacteria (green) and polysaccharide-based biopolymers (red) with different confocal laser scanning microscopy (CLSM) probes, they detected that biopolymers still remained on the membrane surface after removing sludge cake with a physical wash (Figure. 1.8d). Furthermore, polysaccharides were spread through inside the membrane fiber, 100 μm below the surface; biopolymers were able to intrude into the membrane pores and remained adsorbed on the pores (Figure. 1.8e). This accumulation of biopolymers added to the pore fouling resistance (R_P) estimated by the filtration test. They claimed that the biopolymer residue could modify the feature of membrane surface and make it stickier, resulting in more ready accumulation of biomass and formation of sludge cake on membrane. They concluded that periodical chemical cleaning to remove biopolymer residues is very essential for sustainable long-term operation.

1.2.4. Approaches to control biofouling and their limitation

Transport of foulants is regulated by convection force toward the membrane surface and the back-transport force imposed on the particles. Shear-induced diffusion with aeration or mixed liquor recirculation is known very effective to enhance the back transport of suspended solids. However, it is difficult to control the back transport of colloids and solutes only by

enhancing aeration intensity and mixed liquor recirculation because the detachment of small substances generally requires a high level of shear intensity, which can consume energy appreciably.[2,4]

In the fields of MBR plants, the operators can control the biopolymers by two approaches: adjustment of operating factors (i.e., SRT, HRT, DO, temperature) and usage of adsorbents or coagulants. Many researchers and engineers have been investigating the optimum operating conditions and the best protocol using chemicals in order to reduce the biopolymers in MBRs. Meng et al.[2] and Lin et al.[12] summarized the key results of the strategies to control biopolymers in MBRs; however, wide discrepancies are found at the control approaches due to different feed conditions and microbiological composition of biomass existed in the bioreactors.

1.3. Thermodynamic understanding on biofouling

1.3.1. Adhesion of biofoulant on membrane surface

As discussed in Section 1.1, the origin of biofouling is rooted on deposition of biofoulant either on the membrane surface or on the internal membrane pore structure. In macroscopic basis, the biofouling is a mass transport phenomenon where the transport of biofoulant determined by different physicochemical forces exerted on the biofoulant. Several driving forces interact with each other and control the movement of the biofoulant on the membrane. In this perspective, a biofoulant experiences a variety of distinct forces and reaches an equilibrium state specific to the given physicochemical condition. For instance, if the back-transport forces such as shear-induced diffusion are greater than the forward-transport forces, which are mainly dominated by the permeate dragging force, the membrane theoretically should encounter little deposition of biofoulants and thus no/little biofouling. For this macroscopic perspective, the

biofouling phenomena can be theoretically described by cake formation theory or film theory or gel polarization theory, which predict the biofouling magnitude mainly with the diffusion intensity.

Because this macroscopic basis established its mass transport of a biofoulant with a mass balance of the biofoulant, the role of water enters the macroscopic frame very marginally; its theoretical theories treat water just as a physical media that are given specific hydrodynamic conditions and enable the mass transport of biofoulants to occur in the body of media. However, water is not a physical fluid that allows a continuum flow but also a physicochemical cluster of small strongly polar molecules, which interact with each other and chemically react with given entities such as membranes and biofoulants. Recognizing water in molecular basis leads to the necessity of understanding the biofouling in terms of the interfacial interactions between a membrane and a biofoulant *through* water, which take the water-membrane and water-biofoulant interactions into account as well. In this microscopic perspective, the biofouling is recognized an interfacial phenomenon that several distinct interfaces encounter each other and can be reconstructed according to thermodynamic mechanisms.

In thermodynamic perspective, biofouling can be interpreted as adhesion of two different entities, a biofoulant and a membrane, to be a combined column through a media (herein, water). Therefore, adhesion accompanies the structural change of interfaces existing in the aqueous system (i.e. from two interfaces of biofoulant-water and membrane-water to a interface of biofoulant-membrane) as illustrated in Figure 1.9. According to surface chemistry, the change of interfaces demands free energy because each entity has its own inward attraction (cohesion) and different levels of outward attractions (adhesion) with given substances. Thermodynamically, contacting entities reorganize their interfaces to minimize the enthalpy, which result in lowering

the interfaces of those different entities in accordance with intensities of their cohesion and adhesion. For examples, if the entities have low cohesive attractions but high adhesive attraction with each other, they will be much less forced to contract to the smallest possible interface area than the entities having high inward attractions and low outward attraction with each other and thus the first pair of entities will equip larger interface area than the latter pair. In terms of biofouling, the entities can be a membrane and a biofoulant so that their own interfacial characteristics will determine their interfacial free energy (γ_{12}) as well as their adhesive tendency. However, as will be discussed in the following section, biofouling in aqueous system involves a third entity, water, which has a strong cohesive attraction and robust polar properties that severely differentiate the interfacial free energies with other substances (herein, a membrane and a biofoulant). The involvement of water in the interfacial interaction between a membrane and a biofoulant makes the biofouling be a more complex interfacial phenomenon over calculation of a single interfacial free energy (γ_{12}) between a membrane and a biofoulant.

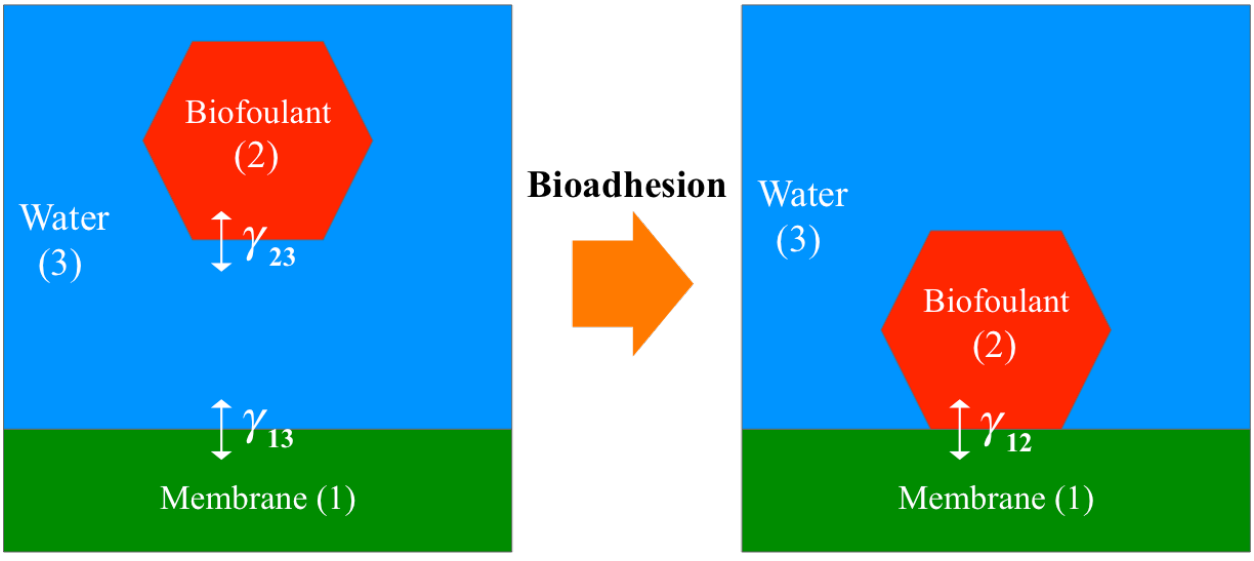

Figure 1.9. Change of interfacial interactions between two entities before and after bioadhesion.

1.3.2. Measurement of surface tensions of solids with a contact angle method

Surface tension (γ) of a material is the force that works inwards from the surface perpendicularly and enforces minimizing the surface area. Due to the inward force, enlargement of the surface area demand energy, which leads to a definition of surface tension as the work to create a new surface having a unit area ($1m^2$):

$$\gamma = \frac{dW}{dA} = \frac{-dG}{dA} (mJ / m^2) \tag{1.2}$$

In practice, it is physically impossible to measure the liquid-vacuum surface tension for the real surface tensions of liquids due to their instant evaporation in a complete vacuum condition. Since the air molecules are highly dilute in a room condition and normally inert to the majority of liquids (especially, for water), the liquid-air surface tension is measured as the surface tensions of liquids. By virtue of the ready shape-conformability of liquids and their satisfactory capillarity, there are several methods for direct measurement of the surface tensions of liquids such as du Noüy ring method and Pendant drop method. [13]

In contrast with liquids, the solids have strict elastic restraints because of their high viscosities and rigidities and invalidate the direct measurement methods of the surface tension, which need a flexible shape conformation. The low mobility of a solid compared to any liquid necessitates the use of indirect methods for measuring the surface tension of a solid. The indirect methods generally utilize the liquids, the surface tensions of which are already known, and make the liquids (3) contact the target solid to estimate the surface tension (γ_1) of the solid (1) by the interfacial free energies (γ_{13}) between the liquids and the solid. Since the interfacial property of a liquid resting on a solid can be characterized by a contact angle of the liquid, various

fundamental theories have employed a contact angle method to develop indirect measurements of surface tensions of solids. [14]

T. Young (1805) was the first founder who defined the contact angle equilibrium in terms of interfacial free energies.{Young:1805ii} He described the vertorial equilibrium for a liquid drop resting on a solid with the solid-vapor (γ_1), liquid-vapor (γ_3), and liquid-solid (γ_{13}) interactions as depicted in Figure 1.10. This contact angle equilibrium was mathematically formulated as

$$\gamma_1 = \gamma_{13} + \gamma_3 \cos\theta_{13} \tag{1.3}$$

, which is known as Young equation. θ_{13} is the contact of the liquid (3) with the solid (1).

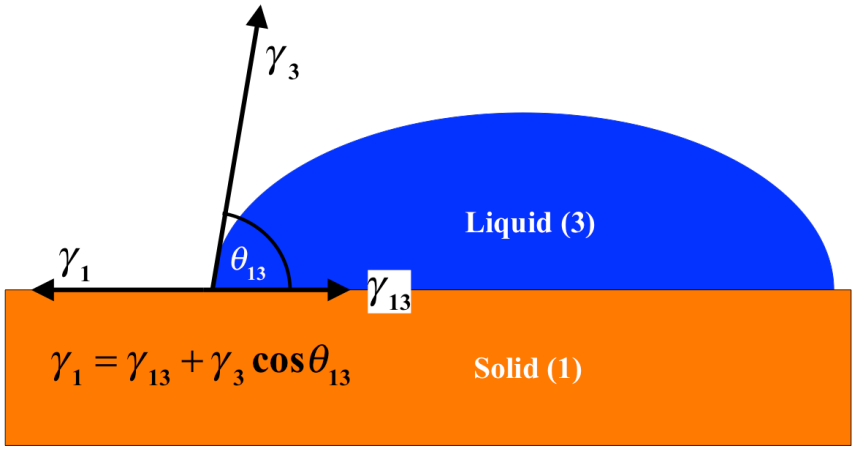

Figure 1.10. Diagram for Young's contact angle equilibrium.

Dupré (1869) defined the work of adhesion as the work, per unit area, required to separate a column of two different liquids or solids into two different new equilibrium surfaces of two distinct materials. [15] He formulated the work of adhesion in terms of surface tensions of two contacting substances and their interfacial tension:

$$W_{13}^a = -\Delta G_{13}^a = \gamma_1 + \gamma_3 - \gamma_{13} \tag{1.4}$$

Positive W_{13}^{a} means a supplementary work needed to separate the material 1 and material 3 from their favorably adhered status. Dupré incorporated his definition of the work of adhesion into Young's equation (Eqn. 1.3), resulting in Young-Dupré equation:

$$W_{13}^{a} = -\Delta G_{13}^{a} = \gamma_3(1+\cos\theta_{13}) \tag{1.5}$$

It should be noted that if the contacting substances are identical (1=3=i), W_{13}^{a} becomes W_i^{c}, the work of cohesion, with a zero contact angle ($\theta_{13} = 0$), resulting in

$$W_i^{c} = 2\gamma_i \tag{1.6}$$

Young-Dupré equation successfully revealed that the contact angle is a thermodynamic output quantitatively determined by the work of adhesion in terms of enthalpy and explains which types of the interfacial interaction two contacting entities may have. In the case for water resting on a membrane, θ_{13} less than 90° (or W_{13}^{a} greater than γ_3) indicates the membrane is wetting because it has a strong interaction with water and tends to spread water molecules on its surface. θ_{13} identical to zero has $W_{13}^{a} = 2\gamma_3$ and represents complete wetting of the membrane. θ_{13} greater than 90° (or W_{13}^{a} smaller than γ_3) implies a weak interaction between the membrane and water, leading to non-wetting of the membrane. If $\theta_{13} = 180°$, W_{13}^{a} becomes zero, which means that no additional work is demanded to separate water from the membrane surface because they are spontaneously divided to independent surfaces of two pure entities. [14] However, because Young-Dupré equation does not contain the term of the surface tension of a solid but only the one of a liquid, Young-Dupré equation is unable to estimate the surface tension of a solid on its own and needs an additional theoretical scheme that defines W_{13}^{a} in terms of surface tension components of a solid and a liquid.

Fowkes (1964) proposed to break the work of adhesion into dispersion (d), polar (p), induction (i), and hydrogen-bonding (h) components: [16]

$$W^a = W_d^a + W_p^a + W_i^a + W_h^a \tag{1.7}$$

and adopted a geometric-mean approach to define the dispersion component of the work of adhesion (W_{13}^a) between a solid (1) and a liquid (3) in terms of their own cohesive dispersion components such as:

$$W_d^a = \sqrt{(W_d^c)_1 (W_d^c)_3} \tag{1.8}$$

Based on the definition of the work of cohesion as given in Eqn. 1.6, the dispersive component of the work of cohesion can be calculated by

$$W_d^c = 2\gamma_i^d \tag{1.9}$$

so that Eqn. 1.8 can be specified as

$$W_d^a = 2\sqrt{\gamma_1^d \gamma_3^d} \tag{1.10}$$

This geometric-mean approach for the dispersive component of W_{13}^a has been widely accepted in the modern surface chemistry.

Owens and Wendt (1969) simplified the concept of W_{13}^a with only two separate components, dispersive component (W_d^a) and polar one (W_p^a), and applied the geometric approach to the polar component as well: [14]

$$W_p^a = 2\sqrt{\gamma_1^p \gamma_3^p} \tag{1.11}$$

They assumed that the dispersive and polar components of the surface tension are additive such as

$$\gamma_i = \gamma_i^d + \gamma_i^p \tag{1.12}$$

Owens and Wendt were the first proposers who employed the additive concept on integration of the dispersive and polar components of the surface tension and established a complete method to estimate the surface tension of a solid with the contact angle measurement. Although Owens and Wendt's approach had been used for a considerable time, their theory incorrectly estimated the surface tensions of substances, even the values of which were well known. The main cause for the inaccuracy of Owens and Wendt's equation is originated from their erroneous assumption with the geometric-mean approach for W_p^a (Eqn. 1.11). In principle, the polar interaction is based on Lewis acid-base interaction, which can occur only between electron-donating potential and electron-accepting one. This asymmetric nature of the polar interaction causes the geometric-mean method to fail estimating the correct quantities of W_p^a and γ_i^p. For instance, if the contacting substances have identical types of polar potentials (i.e. electron-donor sites but no electron-accepter sites on those entities), the participating substances will not have any polar interaction although they may have significant quantities in polar components.

1.3.3. van Oss approach

Following the simplicity of Owens and Wendt's approach, van Oss and Good proposed that the surface tension is composed of only two separate components: Lifshitz-van Der Waals (LW) interaction and acid-base (AB) interaction.[17] van Oss assumed that LW interaction comprises dispersion, dipolar and induction interaction while AB interaction covers all of electron donor-acceptor interactions, which are basically consistent with the polar interaction. However, in order to reflect the asymmetric property of acid-base interaction, van Oss and Good

developed new parameters reflecting the electron-accepticity (γ_i^+) and electron-donicity (γ_i^-) of a substance (i) and applied Small's combing rule for defining the AB interaction component of W^a with those new polar parameters:[18]

$$W_{13}^{AB} = 2\left(\sqrt{\gamma_1^+\gamma_3^-} + \sqrt{\gamma_1^-\gamma_3^+}\right) \tag{1.13}$$

For acid-base interaction between identical substances (i), Eqn 1.13 calculates the acid-base component of the work of cohesion (W^c) such as

$$W_{AB}^c = W_i^{AB} = 4\sqrt{\gamma_i^+\gamma_i^-} \tag{1.14}$$

W_{AB}^c can be expressed in terms of the polar component of the surface tension according to Eqn. 1.6 as the below

$$W_{AB}^c = 2\gamma_i^{AB} \tag{1.15}$$

and combination of Eqn. 15 with Eqn. 1.14 generates

$$\gamma_i^{AB} = 2\sqrt{\gamma_i^+\gamma_i^-} \tag{1.16}$$

van Oss and Good followed Owens and Wendt's additive approach for the surface tension calculation with the dispersive and polar components (Eqn. 1.12) and finalized the formula for the surface tension of a substance (γ_i^{tot}) as the following:

$$\gamma_i^{tot} = \gamma_i^{LW} + \gamma_i^{AB} \tag{1.17}$$

van Oss and Good also adopted Fowke's geometric-mean approximation for LW interaction

$$W_{13}^{LW} = \sqrt{(W_c^{LW})_1(W_c^{LW})_3} = 2\sqrt{\gamma_1^{LW}\gamma_3^{LW}} \tag{1.18}$$

and combined it with Dupré's equation for LW interaction

$$W_{13}^{LW} = \gamma_1^{LW} + \gamma_3^{LW} - \gamma_{13}^{LW} \tag{1.19}$$

, which results in

$$\gamma_{13}^{LW} = \gamma_1^{LW} + \gamma_3^{LW} - 2\sqrt{\gamma_1^{LW}\gamma_3^{LW}} \tag{1.20}$$

or $$\gamma_{13}^{LW} = \left(\sqrt{\gamma_1^{LW}} - \sqrt{\gamma_3^{LW}}\right)^2 \tag{1.21}$$

They also combined Dupré's equation for AB interaction with their newly proposed definition of AB interaction (Eqn. 1.13)

$$\gamma_{13}^{AB} == 2\sqrt{\gamma_1^+\gamma_1^-} + 2\sqrt{\gamma_3^+\gamma_3^-} - 2\sqrt{\gamma_1^+\gamma_3^-} - 2\sqrt{\gamma_1^-\gamma_3^+} \tag{1.22}$$

or $$\gamma_{13}^{AB} = 2\left(\sqrt{\gamma_1^+} - \sqrt{\gamma_3^+}\right)\left(\sqrt{\gamma_1^-} - \sqrt{\gamma_3^-}\right) \tag{1.23}$$

suggested the total interfacial interaction as the sum of Eqn. 1.21 and Eqn. 1.23

$$\gamma_{13}^{tot} = \gamma_{13}^{LW} + \gamma_{13}^{AB} = \left(\sqrt{\gamma_1^{LW}} - \sqrt{\gamma_3^{LW}}\right)^2 + 2\left(\sqrt{\gamma_1^+} - \sqrt{\gamma_3^+}\right)\left(\sqrt{\gamma_1^-} - \sqrt{\gamma_3^-}\right) \tag{1.24}$$

Dupré's equation for the interfacial interaction between two substances (1 and 2) immersed in a liquid (3) can be expressed as

$$W_{132}^a = -\Delta G_{132} = \gamma_{13} + \gamma_{23} - \gamma_{12} \tag{1.25}$$

van Oss and Good substituted Eqn. 1.24 to Eqn. 1.25, leading to

$$\Delta G_{132}^{LW} = 2\left(\sqrt{\gamma_3^{LW}} - \sqrt{\gamma_1^{LW}}\right)\left(\sqrt{\gamma_2^{LW}} - \sqrt{\gamma_3^{LW}}\right) \tag{1.26}$$

and

$$\Delta G_{132}^{AB} = 2\sqrt{\gamma_3^-}\left(\sqrt{\gamma_1^+} + \sqrt{\gamma_2^+} - \sqrt{\gamma_3^+}\right) + 2\sqrt{\gamma_3^+}\left(\sqrt{\gamma_1^-} + \sqrt{\gamma_2^-} - \sqrt{\gamma_3^-}\right) - 2\left(\sqrt{\gamma_1^+\gamma_2^-} + \sqrt{\gamma_1^-\gamma_2^+}\right) \tag{1.27}$$

It should be noted that, in van Oss and Good's approach, the final expression of the surface tension (γ_i^{tot}) comprises one apolar component (γ_i^{LW}) and two polar components (γ_i^+ and γ_i^-) according to Eqn. 1.16 and Eqn. 1.17. Therefore, calculation of the surface tension necessities a

theoretical basis to estimate the three different components. van Oss and Good developed an indirect method by integrating Young-Dupré equation (Eqn. 1.5) with Eqn. 1.14 and Eqn. 1.18: [16]

$$\left(1+\cos\theta_{13}\right)\gamma_3^{tot} = 2\left(\sqrt{\gamma_1^{LW}\gamma_3^{LW}} + \sqrt{\gamma_1^{+}\gamma_3^{-}} + \sqrt{\gamma_1^{-}\gamma_3^{+}}\right) \tag{1.28}$$

Since van Oss and Good succeeded to incorporate into Young-Dupré equation a hypothetical scheme that defines W_{13}^{a} in terms of surface tension components of a solid and a liquid, Eqn. 1.28 has been successfully used to estimate the surface tension properties of a solid with the contact angle method. In order to enable Eqn. 1.28 to predict the surface tension parameters, one needs to use three different probe liquids, surface tension properties of which are already known. It is commonly recommended to use two distinct polar liquids (i.e. water, glycerol) and one completely apolar liquid (i.e. diiodomethane). van Oss and Good theory has been widely utilized to interpretation of various types of solid-liquid interactions such as membrane biofouling,[19-21] bioadhesion to flat surfaces and particles,[22] polymer phase separation,[23] polymer surface property prediction,[24] and microbial cell adhesion.

In order to specify the interfacial interaction energy with the surface tension components, van Oss adopted several well-intended assumptions such as Fowkes' geometric-mean approach for the Lifshitz-van der Waals interaction and Small's combing rule for the acid-base interaction. Even though van Oss succeeded to define the interfacial interaction equations from the wetting theories, his theory failed to propose the absolute values of polar surface tension components of a liquid or a solid. In order to overcome this quantitative defect, van Oss suggested a relative valuing system for acid-base properties of a given liquid or a solid based on water's bipolarity; he set the acid-base properties ratio of water at 20 °C equal to 1, consequently resulting in 25.5 mJ/m^2 of each polar component of water.[25,26]

The equality of the acid-base components of water does not have any experimental reasoning and, furthermore, is the main basis that the van Oss approach generates the absolute predominance of electron-donor surfaces and fails to detect the acidic natures of solids even commonly considered to contain acidic sites.[27,28] The partially impaired polarity-value system has provoked alternative development of the more realistic values of the polar components of water. Lee was the first explorer who tried to correlate the polar components ratio to the one of experimental coefficients of solvatochromic scale (1.8).[29] Along the same line, Volpe also considered that the water is stronger as Lewis acid than as Lewis base, suggesting apparently elevated acid-base properties ratios (3.2~5.5).[26,30,31] Furthermore, Volpe developed an alternative value of the water dispersive component than proposed by Fowkes and adopted by van Oss.

1.4. Research hypothesis and objectives

Because the majority of biofouling occurs on the surface of the polymeric membranes, key interfacial interactions between a membrane surface and a biofoulant play a pivotal role in biofouling phenomena.[32,33] Physicochemical basis of the solid-liquid interface such as surface tension has been a significant concept for researchers to interpret the interfacial interactions between a membrane surface and a biofoulant. In thermodynamic perspective, biofouling can be interpreted as adhesion of two different entities, a biofoulant and a membrane, through a media, (herein, water), to be a combined column. Therefore, adhesion accompanies the structural change of interfaces existing in the aqueous system (i.e. from two interfaces of biofoulant-water and membrane-water to a interface of biofoulant-membrane). This interface-transitive nature of biofouling phenomena leads that surface tension-based theories are adopted in the fundamental understanding of the membrane biofouling. Among those theories, the van Oss approach has

been considered prominent because of its satisfactory prediction for experimental results of biofouling tests either in dense membranes (NF/RO) and porous membranes (MF/UF).[19,20,34-39]

van Oss theory added Lewis acid-base interaction to conventional Derjaguin-Landau-Verwey-Overbeek (DLVO) theory and the theory has been recognized as an extended DLVO theory. According to van Oss approach, in aqueous media, Lewis acid-base interaction occurs between the electron-acceptor in hydrogen atoms of water and lone pairs of atoms of a solid, basically having an analogous concept with hydrogen-bonding. The membrane surface with high electron-donating potential is able to hold water molecules and form a hydration cell layer on its surface, which may impede the access of biofoulant to the membrane surface. Because the biofoulant also has the electron-donating and accepting potentials, other interfacial interactions also occur in biofoulant-water and biofoulant–membrane surface. Therefore, better thermodynamic understanding on the biofouling phenomena need a perspective that ponders the three different but deeply interconnected interfacial interactions existing in membrane surface-water, water-biofoulant and biofoulant-membrane surface.

It is hypothesized that understanding the molecular basis of biofouling will reveal the importance of a polar property of water molecules in water-membrane interaction as well as biofoulant-membrane interaction in aqueous system and thus emphasize the role of a polar property of a membrane in biofouling. To test the hypothesis, the dissertation has been divided into three chapters (Chapter 2~4). Chapter 2 investigates the water-membrane interaction in terms of surface tension properties of a membrane and their discrete interactions with water. This chapter simulates the available surface tension parameters of polymeric porous membranes using different presumptions on polar properties of water and evaluates the effect of each surface tension parameter of a membrane on water-membrane interactions. Electron-donor dominancy

on the polymeric membranes is statistically examined and the statistic results are compared to literature results by regression analysis.

Chapter 3 investigates the effects of water-solids interactions on biofouling phenomena and explores fining key physicochemical properties of a membrane for biofouling resistance. The membrane-biofoulant interaction in aqueous system is disassembled into three separate units of water-membrane, water-biofoulant, and biofoulant-membrane interactions and their connections with chemistries of water, membranes and biofoulants are quantitatively examined by van Oss theory incorporating experimental data and various literature results. One of surface tension parameters of a membrane is suggested to be an indicator that can represent the anti-biofouling capability of a membrane and the indicator is qualitatively and quantitatively evaluated in microbial cell adhesion test and biofouling tests.

Chapter 4 attempts to impart membranes with hydrophilic and anti-biofouling properties by grafting hydrophilic polymers to the surface. Photoactive perfluorophenyl azides (PFPAs) are utilized to generate highly reactive nitrenes (when exposed to UV light) that can covalently bind to the membranes' surfaces. Three different types of small molecule PFPA derivatives are applied and their effects on surface tension characteristics of a polymeric membrane are analyzed by van Oss method. The analyzed physicochemical properties of the modified membranes are compared to the experimental results of a biofouling test with alginate solution. Much of this chapter is taken directly from a ready-to-submit journal article, which has the identical title with the one of this chapter and for which I am listed as the second author. I have contributed to this article on the investigation of surface tension properties of the test membranes and the evaluation of their interfacial interactions with a model biofoulant.

References

(1) Judd, S. *The MBR Book*; Elsevier, 2006.

(2) Meng, F.; Chae, S.-R.; Drews, A.; Kraume, M.; Shin, H. S.; Yang, F. Recent advances in membrane bioreactors (MBRs): Membrane fouling and membrane material. *Water Research* **2009**, *43* (6), 1489–1512.

(3) Judd, S.; Judd, C. *The 2012 MBR Survey – the results*; 2012.

(4) Chang, I. S.; Le-Clech, P.; Jefferson, B. Membrane fouling in membrane bioreactors for wastewater treatment. *Journal of Environmental Engineering* **2002**.

(5) Drews, A. Membrane fouling in membrane bioreactors—characterisation, contradictions, cause and cures. *Journal of Membrane Science* **2010**, *363* (1-2), 1–28.

(6) Le-Clech, P.; Chen, V.; Fane, T. A. G. Fouling in membrane bioreactors used in wastewater treatment. *Journal of Membrane Science* **2006**, *284* (1-2), 17–53.

(7) Wang, Z.; Wu, Z. A Review of Membrane Fouling in MBRs: Characteristics and Role of Sludge Cake Formed on Membrane Surfaces. *Separation Science and Technology* **2009**, *44* (15), 3571–3596.

(8) Castaing, J. B.; Massé, A.; Séchet, V.; Sabiri, N. E.; Pontié, M.; Haure, J.; Jaouen, P. Immersed hollow fibres microfiltration (MF) for removing undesirable micro-algae and protecting semi-closed aquaculture basins. *Desalination* **2011**, *276* (1-3), 386–396.

(9) Kosvintsev, S.; Holdich, R. G.; Cumming, I. W.; Starov, V. M. Modelling of dead-end microfiltration with pore blocking and cake formation. *Journal of Membrane Science* **2002**, *208* (1-2), 181–192.

(10) Metzger, U.; Le-Clech, P.; Stuetz, R. M.; Frimmel, F. H.; Chen, V. Characterisation of polymeric fouling in membrane bioreactors and the effect of different filtration modes. *Journal of Membrane Science* **2007**, *301* (1-2), 180–189.

(11) Ping Chu, H.; Li, X.-Y. Membrane fouling in a membrane bioreactor (MBR): Sludge cake formation and fouling characteristics. *Biotechnol. Bioeng.* **2005**, *90* (3), 323–331.

(12) Lin, H.; Peng, W.; Zhang, M.; Chen, J.; Hong, H.; Zhang, Y. A review on anaerobic membrane bioreactors: Applications, membrane fouling and future perspectives. *Desalination* **2013**, *314* (C), 169–188.

(13) Drelich, J.; Fang, C.; White, C. L. Measurement of interfacial tension in fluid-fluid systems. In *Encyclopedia of Surface and Colloid Science*; Somasundaran, P., Ed.; Encyclopedia of surface and colloid …, 2002; pp 3152–3166.

(14) Erbil, H. Y. *Surface Chemistry of Solid and Liquid Interfaces*; Wiley-Blackwell, 2006.

(15) Adamson, A. W. *Physical chemistry of surfaces*; Wiley-Interscience, 1990.

(16) Van Oss, C. J. *Interfacial Forces in Aqueous Media, Second Edition*; CRC Press, 2006.

(17) van Oss, C. J.; Good, R. J.; Chaudhury, M. K. The role of van der Waals forces and hydrogen bonds in "hydrophobic interactions" between biopolymers and low energy surfaces. *Journal of colloid and Interface …* **1985**, *111* (2), 378–390.

(18) van Oss, C. J.; Good, R. J.; Chaudhury, M. K. Solubility of proteins. *J Protein Chem* **1986**, *5* (6), 385–405.

(19) Cornelissen, E. R.; van den Boomgaard, T.; Strathmann, H. Physicochemical aspects of polymer selection for ultrafiltration and microfiltration membranes. *Colloids and Surfaces A: Physicochemical and Engineering Aspects* **1998**, *138*, 283–289.

(20) Brant, J. A.; Childress, A. E. Assessing short-range membrane–colloid interactions using

surface energetics. *Journal of Membrane Science* **2002**.
(21) Subramani, A.; Hoek, E. M. V. Biofilm formation, cleaning, re-formation on polyamide composite membranes. *Desalination* **2010**, *257* (1-3), 73–79.
(22) van Oss, C. J. The forces involved in bioadhesion to flat surfaces and particles — Their determination and relative roles. *Biofouling* **1991**, *4* (1-3), 25–35.
(23) Volpe, Della, C.; Siboni, S.; Maniglio, D.; Morra, M.; Cassinelli, C.; Anderle, M.; Speranza, G.; Canteri, R.; Pederzolli, C.; Gottardi, G.; et al. Recent theoretical and experimental advancements in the application of the van Oss–Chaudhury–Good acid–base theory to the analysis of polymer surfaces II. Some peculiar cases. *Journal of Adhesion Science and Technology* **2012**, *17* (11), 1425–1456.
(24) Esumi, K. *Polymer interfaces and emulsions*, 1st ed.; CRC press: New York, 1999.
(25) van Oss, C. J. Acid—base interfacial interactions in aqueous media. *Colloids and Surfaces A: Physicochemical and Engineering Aspects* **1993**, *78*, 1–49.
(26) Volpe, C. D.; Siboni, S. Some Reflections on Acid–Base Solid Surface Free Energy Theories. *Journal of Colloid and Interface Science* **1997**, *195* (1), 121–136.
(27) Morra, M. Some Reflection on the Evaluation of the Lewis Acid–Base Properties of Polymer Surfaces by Wetting Measurements. *Journal of Colloid and Interface Science* **1996**, *182* (1), 312–314.
(28) Morra, M. On the molecular basis of fouling resistance. *Journal of Biomaterials Science, Polymer Edition* **2000**, *11* (6), 547–569.
(29) Lee, L.-H. Adhesion and Surface-Hydrogen-Bond Components for Polymers and Biomaterials. *The Journal of Adhesion* **1998**, *67* (1-4), 1–18.
(30) Volpe, Della, C.; Siboni, S. Acid–base surface free energies of solids and the definition of scales in the Good–van Oss–Chaudhury theory. *Journal of Adhesion Science and Technology* **2000**, *14* (2), 235–272.
(31) Volpe, Della, C.; Maniglio, D.; Brugnara, M.; Siboni, S.; Morra, M. The solid surface free energy calculation. *Journal of Colloid and Interface Science* **2004**, *271* (2), 434–453.
(32) Liu, F.; Du, C.-H.; Zhu, B.-K.; Xu, Y.-Y. Surface immobilization of polymer brushes onto porous poly(vinylidene fluoride) membrane by electron beam to improve the hydrophilicity and fouling resistance. *Polymer* **2007**, *48* (10), 2910–2918.
(33) Li Liu; Mark H Engelhard, A.; Mingdi Yan. *Surface and Interface Control on Photochemically Initiated Immobilization*; American Chemical Society, 2006; Vol. 128, pp 14067–14072.
(34) Kim, S.; Marion, M.; Jeong, B.-H.; Hoek, E. M. V. Crossflow membrane filtration of interacting nanoparticle suspensions. *Journal of Membrane Science* **2006**, *284* (1-2), 361–372.
(35) Kim, S.; Hoek, E. M. V. Interactions controlling biopolymer fouling of reverse osmosis membranes. *Desalination* **2007**, *202* (1-3), 333–342.
(36) Jin, X.; Huang, X.; Hoek, E. M. V. Role of Specific Ion Interactions in Seawater RO Membrane Fouling by Alginic Acid. *Environ. Sci. Technol.* **2009**, *43* (10), 3580–3587.
(37) Subramani, A.; Hoek, E. M. V. Biofilm formation, cleaning, re-formation on polyamide composite membranes. *Desalination* **2010**, *257* (1-3), 73–79.
(38) Wang, Q.; Wang, Z.; Zhu, C.; Mei, X.; Wu, Z. Assessment of SMP fouling by foulant–membrane interaction energy analysis. *Journal of Membrane Science* **2013**, *446* (C), 154–163.

(39) Wang, J.; Mo, Y.; Mahendra, S.; Hoek, E. M. V. Effects of water chemistry on structure and performance of polyamide composite membranes. *Journal of Membrane Science* **2014**, *452* (C), 415–425.

Chapter 2

INTERFACIAL INTERACTION MECHANISM OF DETERMINING THE MEMBRANE HYDROPHILICTY

2.1. Introduction

With the current and future stress from demand of clean water, low cost and high-performance measures of purifying water from a variety of different water sources have been of major importance. Membrane has successfully contributed to improve conventional water purification technologies due to its physiochemical separation function. In aqueous media, hydrophilic membrane is generally considered more cost-effective than hydrophobic membrane because hydrophilic membrane demands less energy to force water molecules access membrane surface and pass the narrow pole channels of membrane. In thermodynamic perspective, higher hydrophilicity assists the membrane surface to hold water molecules nearby forming an interfacial thin layer of hydrogen-bonding water molecules (i.e. hydration shells). Because the displacement of those water molecules bonding to hydrophilic membrane surface requires work that increases the free energy of the aqueous system, this hydration layer is perceived to play an energy barrier to biofoulant asses to membrane surface and to lower biofouling consequently.[1,2] Several studies have reported that improvement of the membrane hydrophilicity can reduce biofouling from different biofoulant sources such as microorganisms, proteins, polysaccharides, alginate, soluble microbial products, and natural organic matter.[3-10]

Thermodynamic understanding of solid and liquid interfaces has helped researchers satisfactorily interpret the interfacial interactions between a membrane surface and water molecules. Especially, several researchers have adopted the thermodynamic approach with the concept of energy barrier of adhesion such as Derjaguin-Landau-Verwey-Overbeek (DLVO) theory, which has been widely applied in the colloid and surface chemistry.[11] According to DLVO theory, the energy barrier of adhesion is explained by the existence of repulsive forces in electrostatic double layers. As biofoulant approaches the membrane surface, the biofoulant

experiences an energy barrier mainly governed by the electrostatic double layer forces until the attractive van der Waals forces become enough to assist the biofoulant stably reach the primary energy minimum.[12]

Although DLVO theory had extensively succeeded to understand the biofouling mechanisms in the macroscopic basis, there were several studies in which DLVO solely failed to predict the adhesion mechanism of biofoulants.[13] Particularly, the effects of the different physicochemical properties of a given medium such as ionic strength, temperature and pH were hardly considered since water or a medium marginally enters the picture of DLVO theory. With ambitious attempts to extend DLVO theory, van Oss suggested Lewis acid-base interaction, which emphasizes the role of water in aqueous media.[14-16] Since van Oss' concept on Lewis acid-base interaction in aqueous media basically is based on the hydrogen-bonding, van Oss theory declares that the electron-poor regions of hydrogen atoms of water molecules play a critical role as the "electron-acceptors" that progressively interact with the "electron-donors" of solids (i.e. lone pairs of electrons on the oxygen or nitrogen atoms).[17,18]

In order to specify the interfacial interaction energy with the surface tension components, van Oss adopted several well-intended assumptions such as Fowkes' geometric-mean approach for the Lifshitz-van der Waals interaction and Small's combing rule for the acid-base interaction. Even though van Oss succeeded to define the interfacial interaction equations from the wetting theories, his theory failed to propose the absolute values of polar surface tension components of a liquid or a solid. In order to overcome this quantitative defect, van Oss suggested a relative valuing system for acid-base properties of a given liquid or a solid based on water's bipolarity; he set the acid-base properties ratio of water at 20 °C equal to 1, consequently resulting in 25.5 mJ/m^2 of each polar component of water.[19,20]

The equality of the acid-base components of water does not have any experimental reasoning and, furthermore, is the main basis that the van Oss approach generates the absolute predominance of electron-donor surfaces and fails to detect the acidic natures of solids even commonly considered to contain acidic sites.[18,21] The partially impaired polarity-value system has provoked alternative development of the more realistic values of the polar components of water. Lee was the first explorer who tried to correlate the polar components ratio to the one of experimental coefficients of solvatochromic scale (1.8).[22] Along the same line, Volpe also considered that the water is stronger as Lewis acid than as Lewis base, suggesting apparently elevated acid-base properties ratios (3.2~5.5).[17,20,23] Furthermore, Volpe developed an alternative value of the water dispersive component than proposed by Fowkes and adopted by van Oss.

In this chapter, we generate simulated libraries of different surface tension parameters (STPs) of polymeric membranes by following the theoretical basis of the wetting method. The range of input contact angles is determined by an extensive literature survey and hypothetical development of the boundary conditions of contact angles of solvents. The simulated STPs libraries adopt three different reference value sets of STPs of solvents (van Oss, Lee and Volpe's sets) and evaluate their quantitative impacts on STPs, hydrophilicity and wettability of a membrane surface. Furthermore, this study investigates the mechanisms of interfacial interaction that determine the membrane hydrophilicity and wettability in terms of surface free energy and surface tension components and evaluates how their interconnected relationships impact the membrane hydrophilicity and wettability.

2.2. Theory

2.2.1. Basics of van Oss theory

In order to calculate the interfacial free energies (ΔG_{132}^{LW} , ΔG_{132}^{AB} , ΔG_{132}^{Tot}) the surface tensions (γ^{LW} , γ^{+} , γ^{-}) of membranes and particles should be determined with contact angles (θ) measured by using three different probe liquids, surface tensions of which are already known. The surface tensions are calculated by the extended Young-Dupré equation,[24]

$$-\Delta G_{sl} = (1+\cos\theta)\gamma_l^{tot} = 2\left(\sqrt{\gamma_s^{LW}\gamma_l^{LW}} + \sqrt{\gamma_s^{+}\gamma_l^{-}} + \sqrt{\gamma_s^{-}\gamma_l^{+}}\right) \tag{2.1}$$

where θ is the ideal contact angle formed between a droplet of liquid L and the smooth membrane surface, γ_S^{LW} and γ_L^{LW} are the apolar (Lifshitz-van der Waals) components of the surface tension of solid S (here, membrane or particle) and liquid L, γ_S^{+} , γ_L^{+} , γ_S^{-} , and γ_L^{-} are the polar (electron-acceptor and electro donor) components of the surface tension of solid S and liquid L, respectively.

The interfacial free energy at contact, ΔG_{132}^{tot} , an thermodynamic value of indicating the inherent affinity of a solid material (1) interacting through a liquid media (*3*) with another solid material (2). ΔG_{132}^{tot} can be determined as,

$$\Delta G_{132}^{tot} = \Delta G_{132}^{LW} + \Delta G_{132}^{AB} \tag{2.2}$$

ΔG_{132}^{LW} and ΔG_{132}^{AB} are the Lifshitz–van der Waals and Lewis acid–base interfacial free energies, respectively and they can be calculated from, [19]

$$\Delta G_{132}^{LW} = 2\left(\sqrt{\gamma_3^{LW}} - \sqrt{\gamma_1^{LW}}\right)\left(\sqrt{\gamma_2^{LW}} - \sqrt{\gamma_3^{LW}}\right) \tag{2.3}$$

$$\Delta G_{132}^{AB} = 2\sqrt{\gamma_3^{-}}\left(\sqrt{\gamma_1^{+}} + \sqrt{\gamma_2^{+}} - \sqrt{\gamma_3^{+}}\right) + 2\sqrt{\gamma_3^{+}}\left(\sqrt{\gamma_1^{-}} + \sqrt{\gamma_2^{-}} - \sqrt{\gamma_3^{-}}\right) - 2\left(\sqrt{\gamma_1^{+}\gamma_2^{-}} + \sqrt{\gamma_1^{-}\gamma_2^{+}}\right) \tag{2.4}$$

The solid surface 1 and 2 will be same when the interfacial interaction between identical particles is calculated (ΔG_{131}^{tot}). ΔG_{131}^{tot} indicates the thermodynamic affinity of a solid material (1) with a given liquid media (3). For instance, ΔG_{131}^{tot} implies the hydrophilicity of the membrane surface in case that a membrane is submerged in aqueous media. ΔG_{131}^{tot} can be simply expressed as

$$\Delta G_{131}^{tot} = -2\left(\sqrt{\gamma_1^{LW}} - \sqrt{\gamma_3^{LW}}\right)^2 - 4\sqrt{\gamma_3^+\gamma_3^-} - 4\sqrt{\gamma_1^+\gamma_1^-} + 4\sqrt{\gamma_1^+\gamma_3^-} + 4\sqrt{\gamma_1^-\gamma_3^+} \qquad (2.5)$$

2.2.2. Simulation description

Since one set of the contact angles of three different solvents can generate a set of surface tension parameters (STPs) according to Eqn. 2.1, a library of STPs that the polymeric membranes are able to feature can be proposed if a pool of contact angles that the membranes can have with the test solvents is defined. Defining the realistic ranges of contact angles of the test liquids on the possible membranes is equal to characterizing the boundary conditions of contact angles of the test liquids and may be conducted with the help of the literature survey. However, defining directly the boundary conditions of contact angles is indeed limited because each study utilizes a slightly different set of test solvents as shown in Table 2.1.

The reverse process that define the boundary conditions of contact angles using the literature values of STPs of membranes may overcome the issue of utilization of the different set of test solvents. Majority of research have adopted the reference values of the water STPs proposed by van Oss and showed that the polar STPs have certain limits such as $\gamma_s^+ < 1$ and $\gamma_s^- < 50$. Moreover, because van Oss theory uses the square roots of components, each

component should be positive. Therefore, the available ranges of polar properties can be defined as

$$0 < \gamma_s^+ < 1 \tag{2.6}$$

$$0 < \gamma_s^- < 50 \tag{2.7}$$

Eqn. 2.6 and Eqn. 2.7 provide a basis of the boundary conditions of contact angles of given test liquids when reversely interpreting these equations with Eqn. 2.1 and van Oss' reference values of solvents components, which all of the membrane-characterizing literatures have adopted (Table 2.1).

Table 2.1. Physicochemical properties of polymeric membranes

Membrane	Contact angle of liquid (°)			Surface tension parameter* (mJ/m^2)			*Ref.*
	Polar 1	*Polar 2*	*Apolar*	γ^{LW}	$\gamma+$	$\gamma-$	
PVDF	59.1 (DI)	50.5 (GL)	26.4 (DM)	45.6	0.44	16.0	25
	59.9 (DI)	50.5 (GL)	34.8 (DM)	42.1	0.77	15.6	26
	59.6 (DI)	52.3 (GL)	22.0 (DM)	47.2	0.21	16.4	27
	57.9 (DI)	54.4 (GL)	19.0 (DM)	48.1	0.03	19.8	28
	79.7 (DI)	53.0 (FA)	47.5 (DM)	35.7	0.95	4.0	29
	83.1 (DI)	52.8 (FA)	27.0 (DM)	45.4	0.12	2.2	30
	58.4 (DI)	50.8 (GL)	20.8 (DM)	47.6	0.27	16.7	31
	66.8 (DI)	49.7 (EG)	44.8 (DM)	37.1	0.01	18.5	This study
PES	49.8 (DI)	29.0 (EG)	17.7 (DM)	48.4	0.00	29.5	This study
	80.9 (DI)	54.6 (FA)	36.8 (DM)	41.2	0.19	3.9	30
	58.5 (DI)	42.4 (FA)	18.9 (DM)	48.1	0.00	20.4	32
PAN	57.0 (DI)	49.0 (GL)	6.0 (α-B)	44.2	0.61	17.7	3
	49.5 (DI)	40.0 (FA)	41.3 (DM)	38.9	0.39	30.2	29
	40.6 (DI)	22.9 (EG)	25.6 (DM)	45.9	0.02	39.5	This study

Table 2.1. Continued

PVC	75.4 (DI)	59.3 (GL)	39.1 (DM)	40.1	0.85	5.1	33
	74.3 (DI)	54.9 (FA)	34.1 (DM)	42.4	0.00	9.5	29
PP	98.1 (DI)	87.0 (GL)	68.0 (DM)	24.0	0.11	1.8	26
	94.0 (DI)	83.0 (GL)	42.0 (α-B)	33.7	0.01	2.1	3
CA	67.9 (DI)	10.6 (FA)	19.0 (DM)	48.1	3.47	2.7	30
	59.0 (DI)	54.0 (GL)	26.0 (α-B)	40.0	0.48	19.2	3
PANi	57.0 (DI)	36.0 (EG)	35.0 (DM)	42.0	0.06	23.9	34
	41.0 (DI)	19.0 (EG)	36.0 (DM)	41.6	0.25	38.4	34
PTFE	117.0 (DI)	112.0 (GL)	93.0 (α-B)	10.0	0.01	1.2	3
PC	78.0 (DI)	66.0 (GL)	12.0 (α-B)	43.4	0.06	5.6	3
PSf	82.0 (DI)	67.0 (GL)	14.0 (α-B)	43.1	0.13	3.19	3

The reverse interpretation of Eqn. 2.6 and Eqn. 2.7 with Eqn. 2.1 can start with determination of the dispersive component (γ_s^{LW}). For an apolar liquid, which has $\gamma_s^+ = \gamma_s^- = 0$, Eqn. 2.1 provides

$$\gamma_s^{LW} = \frac{1}{\gamma_{apolar}^{LW}} \cdot \left[\frac{\left(1+\cos\theta_{apolar}\right)\gamma_{apolar}^{TOT}}{2} \right]^2 \tag{2.8}$$

For the water and another polar liquid (polar 2), Eqn. 2.1 results in, respectively,

$$\frac{\left(1+\cos\theta_{water}\right)\gamma_{water}^{TOT}}{2}-\sqrt{\gamma_s^{LW}\gamma_{water}^{LW}}=\sqrt{\gamma_s^{+}\gamma_{water}^{-}}+\sqrt{\gamma_s^{-}\gamma_{water}^{+}}=A_{water} \tag{2.9}$$

$$\frac{\left(1+\cos\theta_{polar2}\right)\gamma_{polar2}^{TOT}}{2}-\sqrt{\gamma_s^{LW}\gamma_{polar2}^{LW}}=\sqrt{\gamma_s^{+}\gamma_{polar2}^{-}}+\sqrt{\gamma_s^{-}\gamma_{polar2}^{+}}=A_{polar2} \tag{2.10}$$

Integration of Eqn. 2.9 and Eqn. 2.10 generates

$$A_{polar2}\sqrt{\gamma_{water}^{+}}-A_{water}\sqrt{\gamma_{polar2}^{+}}=\sqrt{\gamma_s^{+}}\left(\sqrt{\gamma_{water}^{+}\gamma_{polar2}^{-}}-\sqrt{\gamma_{water}^{-}\gamma_{polar2}^{+}}\right) \tag{2.11}$$

and

$$A_{polar2}\sqrt{\gamma_{water}^{-}}-A_{water}\sqrt{\gamma_{polar2}^{-}}=\sqrt{\gamma_s^{-}}\left(\sqrt{\gamma_{water}^{-}\gamma_{polar2}^{+}}-\sqrt{\gamma_{water}^{+}\gamma_{polar2}^{-}}\right) \tag{2.12}$$

Since $\gamma_{water}^{+}=\gamma_{water}^{-}$ according to van Oss' reference values, Eqn. 2.11 and Eqn. 2.12 can be simplified and rearranged to

$$\sqrt{\gamma_s^{+}}=\frac{A_{polar2}-A_{water}\sqrt{\gamma_{polar2}^{+}/\gamma_{water}^{+}}}{\sqrt{\gamma_{polar2}^{-}}-\sqrt{\gamma_{polar2}^{+}}} \tag{2.13}$$

$$\sqrt{\gamma_s^{-}}=\frac{A_{polar2}-A_{water}\sqrt{\gamma_{polar2}^{-}/\gamma_{water}^{-}}}{\sqrt{\gamma_{polar2}^{+}}-\sqrt{\gamma_{polar2}^{-}}} \tag{2.14}$$

Now it is ready to interpret Eqn. 2.6 and Eqn. 2.7; their corresponding substitution into Eqn. 2.13 and Eqn. 2.14 leads to

$$A_{water}\sqrt{\frac{\gamma_{polar2}^{+}}{\gamma_{water}^{+}}}<A_{polar2}<A_{water}\sqrt{\frac{\gamma_{polar2}^{+}}{\gamma_{water}^{+}}}+\sqrt{\gamma_{polar2}^{-}}-\sqrt{\gamma_{polar2}^{+}} \tag{2.15}$$

and

$$A_{polar2}\sqrt{\frac{\gamma_{water}^{-}}{\gamma_{polar2}^{-}}}<A_{water}<A_{polar2}\sqrt{\frac{\gamma_{water}^{-}}{\gamma_{polar2}^{-}}}+\sqrt{50\gamma_{water}^{-}}\left(1-\sqrt{\frac{\gamma_{polar2}^{+}}{\gamma_{polar2}^{-}}}\right) \tag{2.16}$$

Definition of A_{water} and A_{polor2} by Eqn. 2.9 and Eqn. 2.10 develop Eqn. 2.15 and Eqn. 2.16 in terms of the contact angle of the test solvent such as

$$\frac{2}{\gamma_{polar2}^{Total}}\left[A_{water}\sqrt{\frac{\gamma_{polar2}^{+}}{\gamma_{water}^{+}}}+\sqrt{\gamma_s^{LW}\gamma_{polar2}^{LW}}\right]-1<\cos\theta_{polor2}$$
$$<\frac{2}{\gamma_{polar2}^{Total}}\left[A_{water}\sqrt{\frac{\gamma_{polar2}^{+}}{\gamma_{water}^{+}}}+\sqrt{\gamma_{polar2}^{-}}-\sqrt{\gamma_{polar2}^{+}}+\sqrt{\gamma_s^{LW}\gamma_{polar2}^{LW}}\right]-1 \quad (2.17)$$

and

$$\frac{2}{\gamma_{water}^{Total}}\left[A_{polar2}\sqrt{\frac{\gamma_{water}^{-}}{\gamma_{polar2}^{-}}}+\sqrt{\gamma_s^{LW}\gamma_{water}^{LW}}\right]-1<\cos\theta_{water}$$
$$<\frac{2}{\gamma_{water}^{Total}}\left[A_{polar2}\sqrt{\frac{\gamma_{water}^{-}}{\gamma_{polar2}^{-}}}+\sqrt{50\gamma_{water}^{-}}\left(1-\sqrt{\frac{\gamma_{polar2}^{+}}{\gamma_{polar2}^{-}}}\right)+\sqrt{\gamma_s^{LW}\gamma_{water}^{LW}}\right]-1 \quad (2.18)$$

Note that Eqn. 2.17 defines the boundary conditions of θ_{polar2} based on the limits of γ_s^+ while Eqn. 2.18 does so for θ_{water} with the value limits of γ_s^-. The boundary conditions of θ_{water} and θ_{polar2} are dependent on γ_s^{LW} and thus the range of θ_{apolar} determines the scope of the available θ_{water} and θ_{polar2}. This study defines the boundary conditions of θ_{water} and θ_{polar2} by the range of θ_{apolar} between 10° and 90°. An example of the boundary conditions of contact angles simulated is illustrated in Figure 2.1.

2.2.3. Parameter values of the test solvents

Contact angles information with at least three different liquids (two polar liquids and one apolar liquid) is necessary to determine the STPs of membrane surfaces. van Oss recommended to utilize the solvents that have high surface free energy and high values of STPs such as α-bromonaphthalene, diiodomethane, water, glycerol and ethyleneglycol.[16] Therefore, this study adopted diiodomethane, water and ethylene glycol as the model liquids. van Oss characterized the STPs of these model liquids based on the assumption that the polar properties ratio of water

is unity. Lee and Volpe suggested different reference values of the water STPs and thus ones of other solvents as shown in Table 2.2.

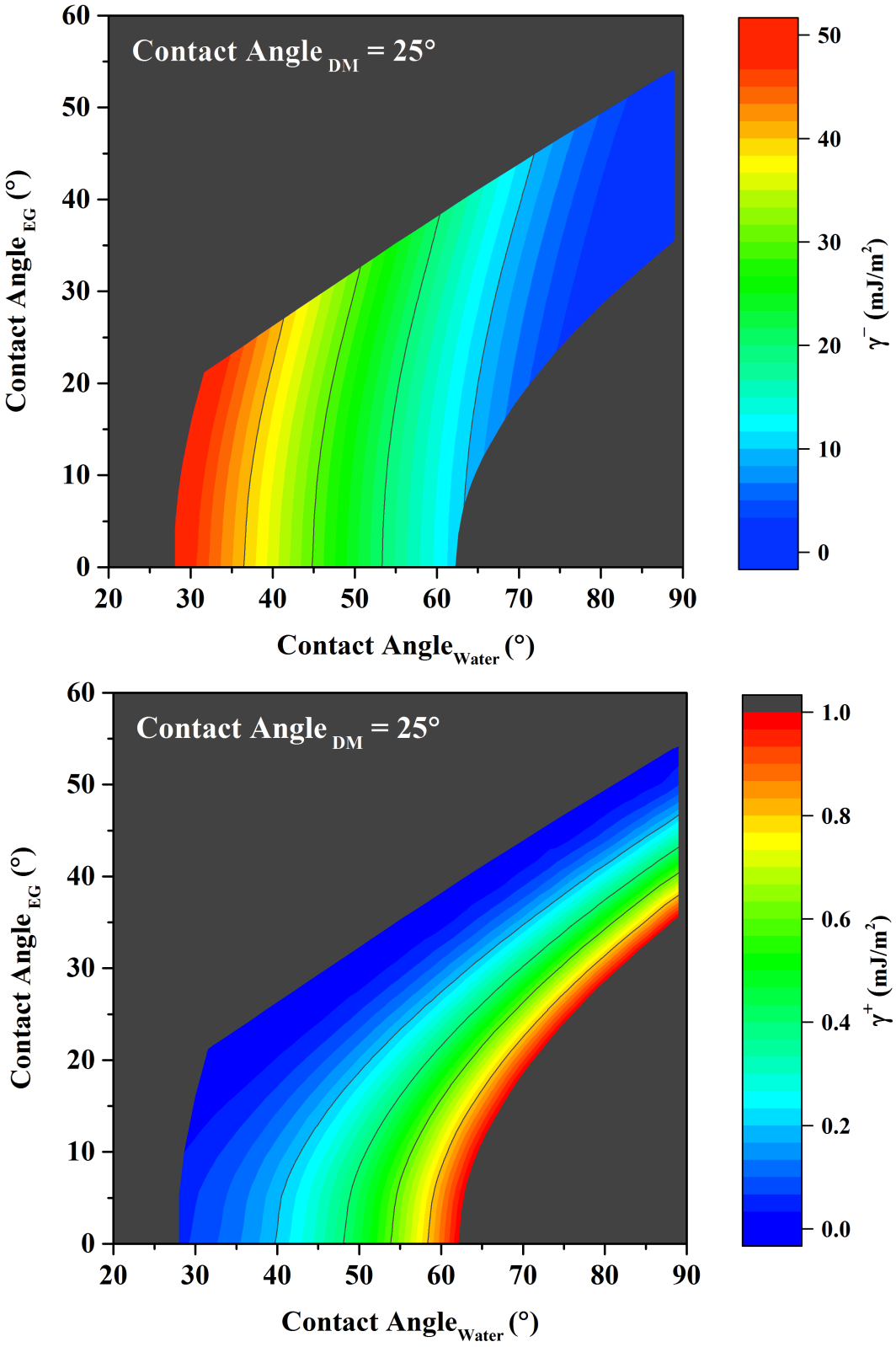

Figure 2.1. An example set of the simulated surface tension parameters under the boundary condition of contact angles defined by Eqn. 2.17 and Eqn. 2.18

Table 2.2. Surface tension parameters of the test solvents

		γ^{LW} (mJ/m^2)	$\gamma+$ (mJ/m^2)	$\gamma-$ (mJ/m^2)	γ^{AB} (mJ/m^2)	γ^{tot} (mJ/m^2)
Water	van Oss	21.8	25.5	25.5	51	72.8
	Lee	21.8	34.2	19.0	51	72.8
	Volpe	26.2	48.6	11.2	46.6	72.8
Ethylene glycol	van Oss	29.0	1.9	47.0	19.0	48.0
	Lee	29.0	2.6	34.8	19.0	48.0
	Volpe	33.9	1.0	51.6	14.1	48.0
Diiodomethane	van Oss	50.8	0	0	0	50.8
	Lee	50.8	0	0	0	50.8
	Volpe	50.8	0	0	0	50.8

2.3. Results and discussion

2.3.1. Effects of the reference values on simulated STPs of membranes

Different reference basis of the water STPs affects the calculation of Eqn. 2.1 and results in different set of STPs of membrane. When the reference value set with a polar properties ratio (γ_l^+/γ_l^-) higher than unity is applied to the test liquids, theoretically Eqn. 2.1 produces the STPs of a solid with an elevated γ_s^+ and a lowered γ_s^- compared to those calculated with van Oss' reference values of liquids.[17,20,22] This general fact is observed at the simulated library of the membrane STPs as depicted in Figure 2.2. Since all of van Oss, Lee and Volpe adopted the same reference STP value of diiodomethane ($\gamma_s^{LW} = 50.8\,mJ/m^2$), the dispersive component, γ_s^{LW} , has the exactly same value ranges of 12.7~50.3 mJ/m^2 according to Eqn. 2.8. However, the values of γ_s^- at the simulated libraries based on Lee and Volpe's reference values present lower levels in

contrast to their increased values of γ_s^+. As a simulated library accepts higher polar properties ratio, which means the greater Lewis acidity over Lewis basicity of water, the membrane surface is characterized to have the enhanced electron-accepting potential and the depressed electron-donating one.

Unlike the altered ranges of STPs of membranes, each simulated library demonstrates similar distribution pattern of polar STPs of membranes. Although the Lee-based and Volpe-based simulations have shorter ranges of γ_s^-, both of the simulations present well-balanced γ_s^- distributions comparable to the van Oss-based simulation's results. By contrast, distribution of γ_s^+ is heavily weighted on the small scales in all of simulated libraries: the elevated ranges of γ_s^+ in Lee-based and Volpe-based libraries have little impact on the highly unbalanced γ_s^+ distribution. Distribution patterns statistically describe the possibilities of each value-scope in which a test membrane may fit. Therefore, the unbalanced distribution patterns of γ_s^+ even in the Lee-based and Volpe-based libraries, which inherently intend to generate the elevated Lewis acidity of the test membrane, imply the limited probability of meeting the membrane that has a high γ_s^+ level. These statistical results of unbalanced γ_s^+ distribution may offer a dilemma to the original purpose of Lee's and Volpe's modified reference values of the solvent STPs.

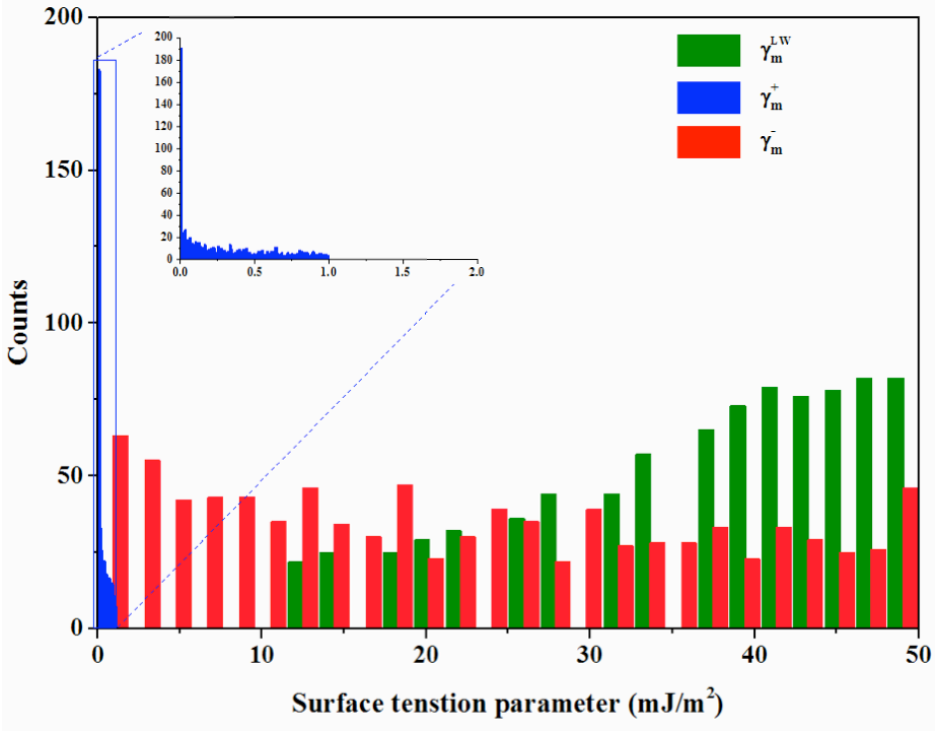
Counts
Surface tenstion parameter (mJ/m²)
γ_m^LW
γ_m^+
γ_m^-

(a)

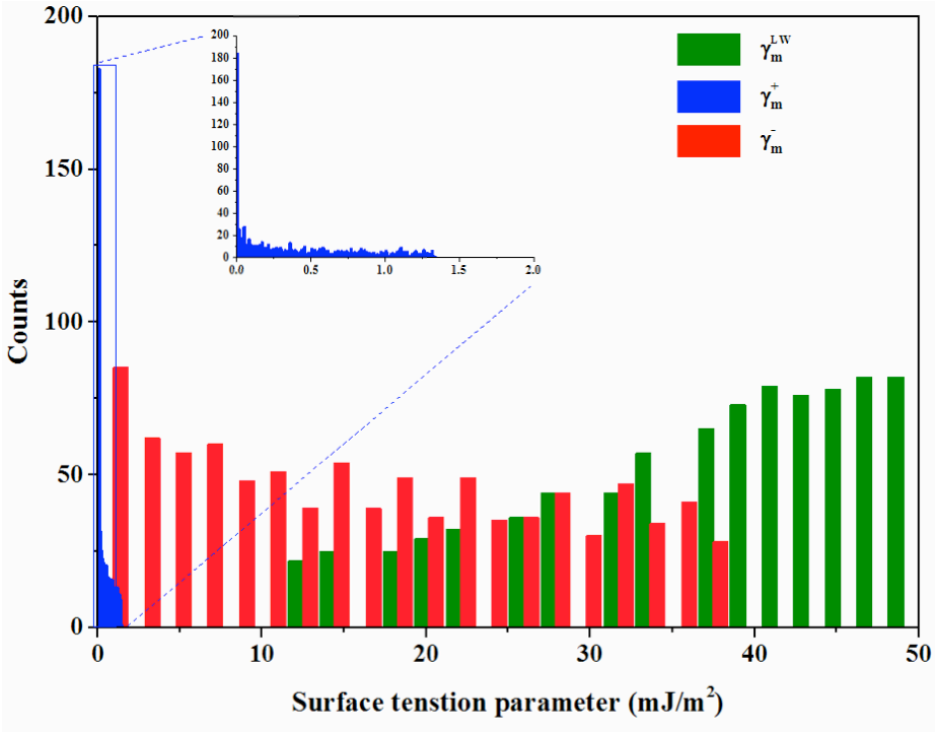
Counts
Surface tenstion parameter (mJ/m²)
γ_m^LW
γ_m^+
γ_m^-

(b)

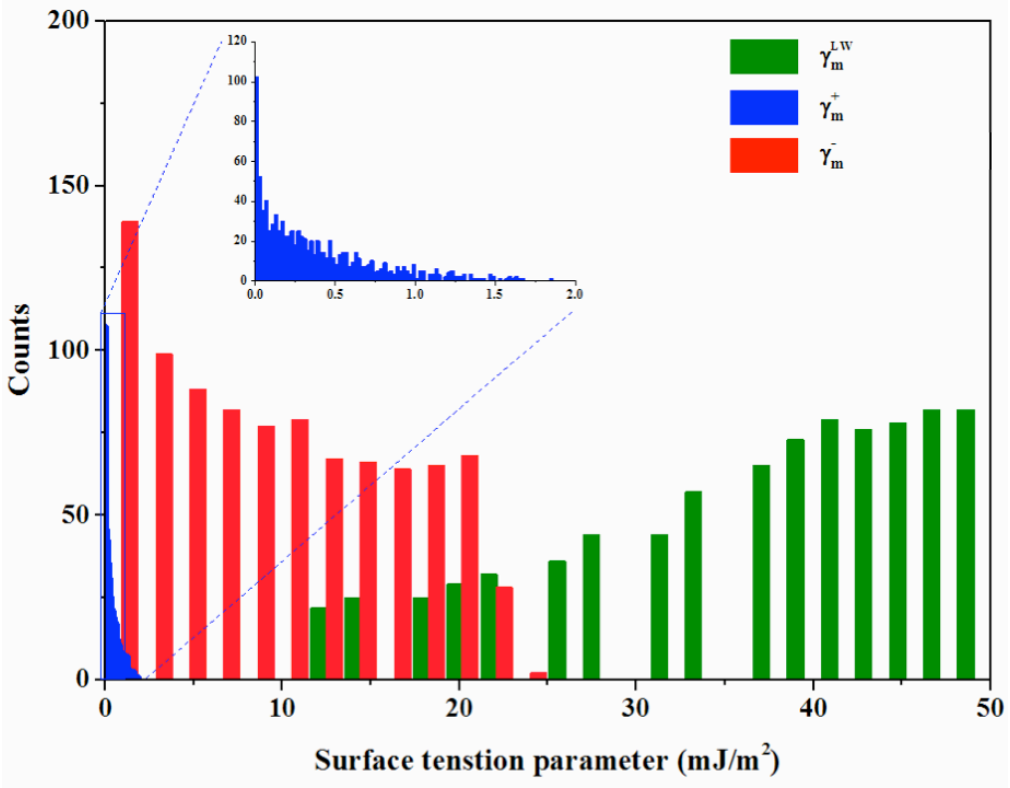

(c)

Figure 2.2. Distribution of the STPs of simulated membrane chemistries with the reference values of the test liquids suggested by van Oss (a), Lee (b) and Volpe (c).

2.3.2. Effects of the reference values on the mono-polarity of membrane surface

Monopolarity is designated for the surface where one kind of polar property dominates over the other kind.[35] Monopolar electron-donating surfaces are more commonly found in Nature than monopolar electron-accepting surfaces.[36] If a membrane surface is a strong electron-donor (γ_m^-) but has close-to-zero electron-accepticity (γ_m^+), the surface's monopolarity hardly contribute the acid-base cohesion component (γ_m^{AB}) in Eqn. 2.4 and Eqn. 2.5. However, the surface is still able to interact with a bipolar liquid or solid, which has electron-accepting and electron-donating potentials at appreciable levels, because the electron-donating sites of the membrane surface can

react with the electron-acceptors of the bipolar substance. Monopolarity may be one of key features determining how the membrane to interact with the water molecules and biopolymers in contact because several studies have reported the close-to-monopolar or semi-monopolar properties of the polymeric membranes as already shown in Table. 2.1. However, the results in Table. 2.1 were calculated with the reference values suggested by van Oss so that the monopolarity of the test membranes may be over-evaluated because of their lower γ_m^+ and elevated γ_m^- compared to those polar properties predicted with Lee's and Volpe's reference values.

Figure 2.3 compares the monopolar tendencies of the three different libraries in terms of γ_m^+/γ_m^-. As shown in Figure 2.3 (a), van Oss-based simulation demonstrates 90% and 75% of data within γ_m^+/γ_m^- of 0.11 and 0.03, respectively, implying the highly semi-monopolar membrane surfaces as expected. This non-uniform distribution of γ_m^+/γ_m^- presents a clear contrast to the well-balanced distribution of γ_m^-. These distribution patterns of γ_m^+/γ_m^- and γ_m^- mostly maintain their tendencies even at Lee-based and Volpe-based libraries. Both of Lee-based and Volpe-based libraries reveal the well-spread distribution of γ_m^- even though the slightly higher count numbers of data exist at the lower levels of γ_m^-. Regarding the monopolarity, Lee-based and Volpe-based reference values cause the membrane surfaces to be characterized less monopolar. Lee-based simulation generates 90% and 75% of data within 0.20 and 0.06 of γ_m^+/γ_m^-, which are nearly twice extended ranges than those of van Oss-based calculation. Volpe-based computation also extends these ranges such as 0.15 and 0.08 of γ_m^+/γ_m^- for 90% and 75% of data as depicted in Figure 2.4. However, the simulation libraries based on Lee's and Volpe's

reference values still have predominance of the γ_m^- close-to-monopolar or semi-monopolar membrane surfaces because of the exceedingly higher values of γ_m^- than γ_m^+.

All of the three simulation libraries expose overall inverse relationships between γ_m^- and γ_m^+/γ_m^-; greater electron-donating potentials on the membrane surfaces clearly tend to have stronger electron-donating monopolarity. The inverse relation occurs because of not only the existence of γ_m^- in the denominator of γ_m^+/γ_m^- but also the inherent link between γ_m^- and γ_m^+/γ_m^- as determined in Eqn. 2.9. Rearrangement of the right sides of Eqn. 2.9 leads to

$$\frac{A_{water}}{\sqrt{\gamma_{water}^-}} = \sqrt{\gamma_s^+} + \sqrt{\gamma_s^-}\sqrt{\frac{\gamma_{water}^+}{\gamma_{water}^-}} = \sqrt{\gamma_s^-}\left(\sqrt{\frac{\gamma_{water}^+}{\gamma_{water}^-}} + \sqrt{\frac{\gamma_s^+}{\gamma_s^-}}\right) \tag{2.19}$$

For instance, van Oss' reference value set of the water specifies Eqn. 2.19 as

$$\frac{A_{water}}{5.05} = \sqrt{\gamma_s^-}\cdot\left(1+\sqrt{\frac{\gamma_s^+}{\gamma_s^-}}\right) \tag{2.20}$$

Eqn. 2.19 theoretically explains the concealed reason for the inverse relationship between γ_m^- and γ_m^+/γ_m^- as well as γ_m^- and γ_m^+. Moreover, because A_{water} can be calculated with one apolar and one polar liquid (herein, water and diiodomethane), Eqn. 2.19 suggests the possibility of calculating STPs of a test membrane even with two different liquids instead of three solvents if the value of γ_m^+/γ_m^- is reasonably presumed This finding will be used to evaluate the empirical validity of the simulated γ_m^+/γ_m^- in Section 2.3.6.

2.3.3. Effects of the reference values on the ΔG_{131}^{tot} and ΔG_{132}^{tot} of membrane surface

ΔG_{131}^{tot} represents the interfacial interaction between two identical substances (1) immersed in a liquid (3). When the substance and the liquid have polar properties, ΔG_{131}^{tot}

comprises five different free energy components as presented in Eqn. 2.5. The first term reflects the Lifshitz-van der Waals interaction energy between 1 and 3. The second term and third term describe the polar free energies of cohesion of 1 and 3, respectively. The forth term and fifth term characterize the polar free energies of adhesion between 1 and 3. In the case that solids with high electron-donating potentials are submerged in aqueous media, the fifth term is known frequently more dominant than the forth term because of the high Lewis acidity of water.[37,38]

Figure 2.5 compares the values of ΔG_{131}^{tot} calculated with van Oss' reference values with those with Lee's and Volpe's reference values. Lee's reference value sets of the test solvents have no impact on the values of ΔG_{131}^{tot}, compared to those with van Oss' reference value sets (Figure 2.5a). ΔG_{131}^{tot} keeps an absolute value because Lee basically followed van Oss' underlying rules that preserve $\gamma_w^{AB} = 2\sqrt{\gamma_w^+ \gamma_w^-} = 51\ mJ/m^2$ and determine a solvent's polar STPs as relative to those of water. Lee's compliance to van Oss' rules induces each energy component of ΔG_{131}^{tot} to maintain the exactly same values as shown in Figure 2.6a. Volpe's reference values of the test liquids calculate ΔG_{131}^{tot} in a bit different output; in general, the values of ΔG_{131}^{tot} with Volpe's reference values are slightly smaller than those with van Oss' reference values as depicted in Figure 2.5b. Because Volpe applied a bit different rule to determine the STPs of the test liquids (i.e. $\gamma_w^{AB} = 46.6\ mJ/m^2$, a matrix-based regression with multi-probes more than three liquids), Volpe-based library composes a somehow different structure to the energy component composition of ΔG_{131}^{tot} (Figure 2.6.b). The lower value of γ_w^{AB} at the Volpe-based library directly causes the hydrogen-bonding driven cohesion energy (2nd term) to be less cohesively attractive between the water molecules, supplying an enhanced hydrophilic basis (+8.9 mJ/m^2) to the membrane surface character. However, the two polar free energies provoked by the hydration of

the membrane (4th and 5th terms) lose their hydration intensity (-1.9 and -8.8 mJ/m^2, respectively) as much as fails to save the elevated hydrophilic credit given by the altered value in 2nd term.

No matter which reference value set is applied, ΔG_{131}^{tot} is critically quantified by the polar adhesion energy between the electron-donating moiety of a membrane and electron-accepting moiety of water (5th term). This polar energy component has the most positive potential on average (+79.6~88.4 mJ/m^2), which significantly introduces the hydrophilic repulsion to ΔG_{131}^{tot}. Furthermore, the extent of the 5th term is highly variable alongside the membrane chemistries and ΔG_{131}^{tot} closely follows this variation of the 5th term. The qualitatively and quantitatively high dependency of ΔG_{131}^{tot} on the 5th term may shed light on the key interfacial interaction mechanism between a membrane and water as will be discussed in the following section.

2.3.4. Mechanism of AB interaction for membrane in aqueous media

The attractive polar free energy of cohesion between water molecules is always present even when a net hydrophilic repulsion ($\Delta G_{131}^{tot} > 0$) happens; a hydrophilic membrane surface demands the hydrophilic repulsion quantitatively stronger than the strong hydrophobic attraction between water molecules exerted by their inherently strong hydrogen-bonding. As shown in Figure 2.6, the polar adhesion energies between a polar moiety of a membrane surface and the polar moiety of the opposite sign of water (4th term and 5th term) dominate the hydrophilic repulsion by their hydration energies and, especially, the 5th term spearhead the strong hydration of the membrane surface in aqueous media.

The two major momentums of empowering the 5th term are the strong Lewis acidity of water and the prevailing Lewis donicities of membrane surfaces. Figure 2.7 illustrates how these

two factors manipulate the interfacial interaction between a membrane surface and water. Water is known one of the strongest Lewis acids because of its hydrogen atoms, electrons of which are highly partitioned to the oxygen atoms and thus have enough rooms of accepting the negative electrostatic potential from the third entity (herein, a membrane surface). Consequently, the strong Lewis acidity of water emphasizes the role of electron-donating potential of a solid in contact; water molecules easily orient their dipoles to compensate the electron-donating potentials of the adjoining molecules and the water molecules are quickly forming a hydration cells around the solid without significant enthalpy gain. Moreover, the majority of membrane surfaces appear to have predominant electron-donicity, which is an excellent electrostatic potential for the water molecules to carry the adjacent electron-donating energy into their electron-accepting sites, reaching more stable enthalpy status. The strong interaction between the electron-donor of a membrane surface and the electron-acceptor of water cause the Lee-based and Volpe-based calculation to have the same or little different ΔG_{131}^{tot} than van Oss-based ΔG_{131}^{tot}. Because Lee and Volpe did not intend to differentiate the final interfacial free energies such as ΔG_{131}^{tot} but originally to generate more reasonable values of polar STPs of a solid, the same or similar values of ΔG_{131}^{tot} with van Oss', Lee's and Volpe's different reference values may be a satisfactory result to ones who consider to adopt Lee's or Volpe's approach.

2.3.5. Implication of monopolarity on hydrophilicity and wettability of membrane

The fact that the high Lewis acidity of water and the prevailing electron-donor semi-monopolar surfaces of most membranes emphasize the role of the electron-donating potential of a membrane surface in its interfacial interaction with water molecules results in a strong relationship between γ_m^- and the membrane hydrophilicity as depicted in Figure 2.8. The scatter

plotting matrix in Figure 2.8 describes the impact of each surface tension component of membrane on ΔG_{131}^{tot}. The dispersive component, γ_m^{LW}, is found to little contribute to the membrane hydrophilicity. Mathematically, γ_m^{LW} can influence ΔG_{131}^{tot} according to Eqn. 2.5, which quantifies the dispersive term (1st term) by the basis on the "difference" between the square roots of γ_m^{LW} and γ_{water}^{LW} and thus suppresses the effect of γ_m^{LW} compared to the polar properties of applying the product rules (2nd~5th terms). This mathematical result is theoretically inevitable because van Oss theory adopted Fowkes' geometric-mean combing approach for the Lifshitz-van der Waals component in contrast to the acid-base component with Small's combing rule.

In the above theoretical background, γ_m^+ is capable to deeply manipulate the membrane hydrophilicities due to its multiplying combination with the basicity of water; however in reality γ_m^+ fails to occupy its original influence on ΔG_{131}^{tot} because of the prevailing electron-donicity of the membrane (γ_m^-) as shown in Figure 2.8. Even in Lee-based and Volpe-based simulation, γ_m^+ does not overcome the overwhelming influence of γ_m^- on ΔG_{131}^{tot} and presents little correlation with ΔG_{131}^{tot} although Lee-based and Volpe-based calculations successfully forced γ_m^+ to be exalted and γ_m^- depressed. Contrary to γ_m^{LW} and γ_m^+, γ_m^- shows a crystal clear impact on the membrane hydrophilicity. As the membrane surface has the enhanced electron-donor property, the superior hydrophilicity (higher ΔG_{131}^{tot}) is detected on the membrane surface.

The electron-donor-dominant semi-monopolarity of membrane may affect the mechanism of determining the wettability of membrane. Since the wetting is also a part of thermodynamic phenomena, the wettability of membrane can be quantified by the solid-water interfacial free energy (ΔG_{13}^{tot}). According to the Young-Dupré equation (Eqn. 2.1), the solid-water interfacial

free energy can be readily calculated with the contact angle of water on membrane and the larger value of $-\Delta G_{13}^{tot}$ indicates the better tendency of membrane to be wetted to a liquid (herein, water).[39] The Young-Dupré equation follows the Dupré-proposed basis that defines the work of adhesion ($W_{13}^{a} = -\Delta G_{13}^{tot}$) as the reversible work per unit area, required to *separate* a column of two different entities (herein, membrane and water) from their interface. The Dupré-proposed definition writes the work of adhesion in terms of surface tension as

$$-\Delta G_{13}^{tot} = W_{13}^{a} = \gamma_1 + \gamma_3 - \gamma_{13} \tag{2.21}$$

Eqn. 2.21 reveals that a greater surface free energy (higher γ_1) of membrane and its higher favorable interaction with water (lower γ_{13}) have the membrane surface more water-wettable.

Figure 2.9 illustrates how the electron-donating potential of membrane alters the membrane wettability and its two major components, γ_1 and γ_{13}. It might be expected that the surface free energy of the membrane could change closely alongside the value of γ_m^- because the electron-donating component is one of major surface tension parameters of a solid. However, because the contribution of γ_m^- to γ_1 depends on γ_m^+ as $2\sqrt{\gamma_m^+\gamma_m^-}$, the electron-donor semi-monopolarity of most membranes and, reversely saying, their little quantities of γ_m^+ suppress the contribution of γ_m^- to γ_1. However, the other major wetting component, γ_{13}, has the polar adhesion term ($-4\sqrt{\gamma_1^-\gamma_3^+}$) that can be independently controlled by the level of electron-donating property of membrane. Consequently, increase of γ_m^- leads to nearly proportional reduction of γ_{13}, which implies less free energy demanded to enlarge the membrane-water interface due to the presence of stronger hydrogen-bonding intensity. Overall, the less γ_{13} by the enhanced γ_m^- results in the increment of $-\Delta G_{13}^{tot}$ and thus better membrane wettability.

2.3.6. Validity assessment of monopolarity of simulated membranes

As discussed in Section 2.3.2, all of the simulation results through different reference values of the solvents indicate the close-to-monopolar surface of most membranes. Because these simulations applied extensive ranges of combinatorial contact angle sets and some of these sets might contain impractical classes, it is necessary to compare the monopolar level of simulated membranes to experimental data that can be found in references. For instance, the contact angle set of $\theta_w = 87°, \theta_{EG} = 30°$ *and* $\theta_{DM} = 10°$ at van Oss-based, Lee-based, and Volpe-based calculation leads correspondingly to γ_m^+/γ_m^- of 122, 256, and 67, which may be considered unrealistic values.

In the simulated libraries, the level of γ_m^+/γ_m^- greatly varies with the given contact angle information so that this study calculates the average of γ_m^+/γ_m^- in each simulated library. As the distribution of γ_m^+/γ_m^- is very imbalanced to the smaller scale, the average γ_m^+/γ_m^- also becomes differentiated according to the scope of the selected data. In order to statistically exclude improbable data sets, we chose the data scopes that include 75% and 97.7% of existing data and apply their average values of γ_m^+/γ_m^- into Eqn. 2.19 to calculate the membrane STPs with the contact angles of two probe solvents (water and diiodomethane) and then the ΔG_{131}^{tot} with the two-solvent-based STPs. The average values of γ_m^+/γ_m^- in each simulated library are illustrated in Figure 2.10.

Figure 2.11 compared the two-solvent-based ΔG_{131}^{tot} and three-solvent-based one. Application of the two-solvent-based STPs with the cumulative γ_m^+/γ_m^- average at 97.7% level appeared to underestimate high-level ΔG_{131}^{tot} values ($\Delta G_{131}^{tot} > -20\, mJ/m^2$) in van Oss-based

calculation (Figure 2.11a) and Lee-based one (Figure 2.11b) while Volpe-based calculation kept a considerable consistency even at the high level of ΔG_{131}^{tot}. However, the cumulative average of γ_m^+/γ_m^- at 75% level caused the two-solvent-based ΔG_{131}^{tot} to be better concordance with the three-solvent-based ΔG_{131}^{tot} of a whole range in all of simulation libraries. This result confirms that the representative level of monopolarity of membrane can be derived from the lower scale of γ_m^+/γ_m^- and van Oss's theory tends to characterize the membrane surface as γ_m^- dominant monopolarity no matter of which reference values of solvents are introduced in this theory.

2.4. Summary

The thermodynamic mechanisms of determining hydrophilicity and wettability of a membrane were theoretically examined using an extended DLVO theory that van Oss developed. This study simulated the surface tension parameters (STPs) of membranes by manually altering the wetting conditions (contact angle values) of the test solvents. The simulated libraries of STPs revealed that polymeric porous membranes highly tend to fall into a category of electron-donor monopolar or semi-monopolar solids. Although Lee-based and Volpe-based reference values of the test solvents succeeded to characterize the membrane surface with an enhanced electron-accepticity, the majority of the simulated membranes still hardly escaped their low levels of the γ_m^+/γ_m^- extents. The high electron-accepticity of water emphasized the role of γ^- of a membrane in the interfacial interaction between a membrane and water (ΔG_{131}^{tot}) and caused the polar adhesion between electron-donor sites of a membrane and electron-acceptor sites of water to be a major interaction component in ΔG_{131}^{tot} than other components. Because Lee-based and Volpe-based simulations adopted the higher Lewis acidity of water, which augments the interaction

with the electron-donicity of the membrane, the lower electron-donicities of the membranes found in those simulations barely differentiated the free energy quantity such as ΔG_{131}^{tot} compared to its value in van Oss-based simulation. The high Lewis acidity of water highlighted the role of γ^- of a membrane in its wettability as well. A higher electron-donicity of a membrane has little impact on the total surface tension of the membrane surface (γ_1), but successfully favors the electron-acceptor sites of water forming a significantly lower surface tension of the water-membrane interface (γ_{13}) and thus a greater affinity between the membrane and water ($-\Delta G_{13}^{tot}$).

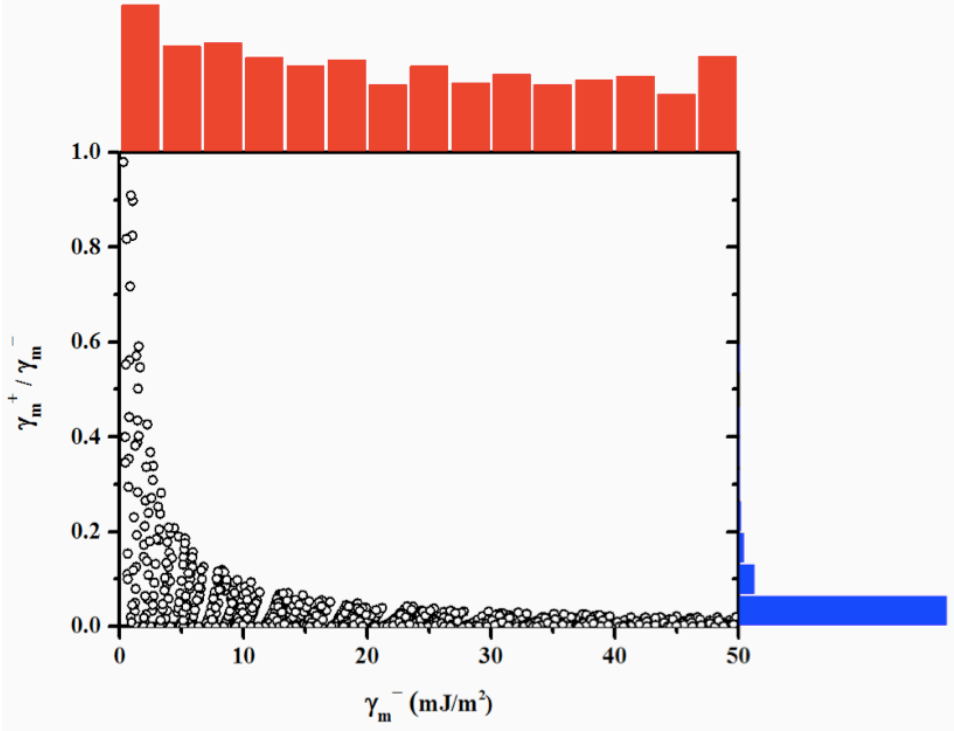
1.0
0.8
0.6
0.4
0.2
0.0
γ_m^+ / γ_m^-
0
10
20
30
40
50
γ_m^- (mJ/m^2)

(a)

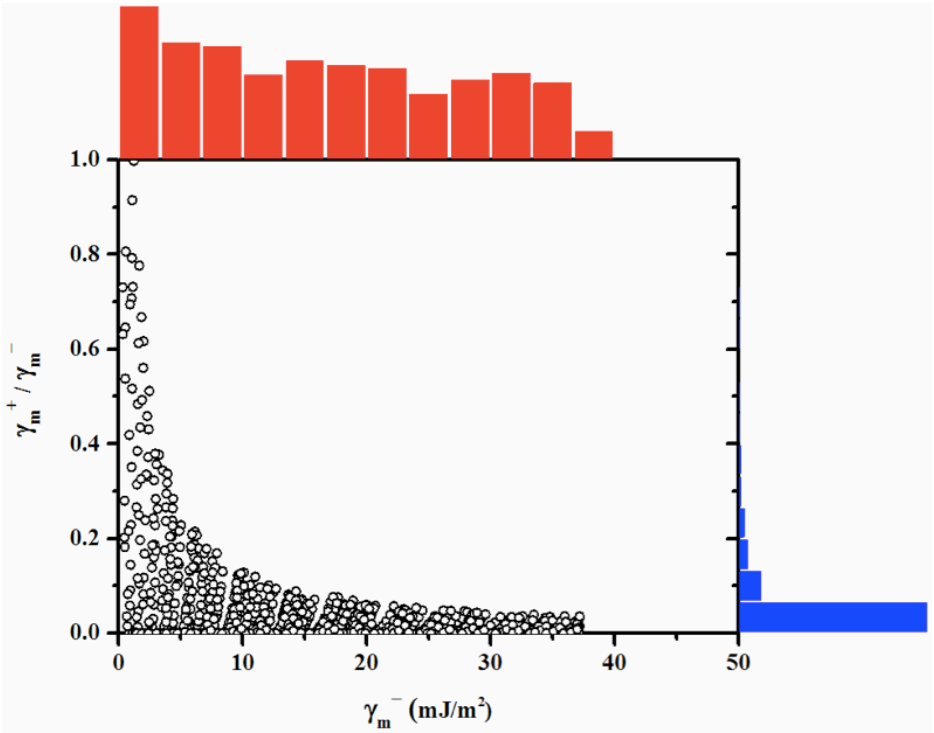
1.0
0.8
0.6
0.4
0.2
0.0
γ_m^+ / γ_m^-
0
10
20
30
40
50
γ_m^- (mJ/m^2)

(b)

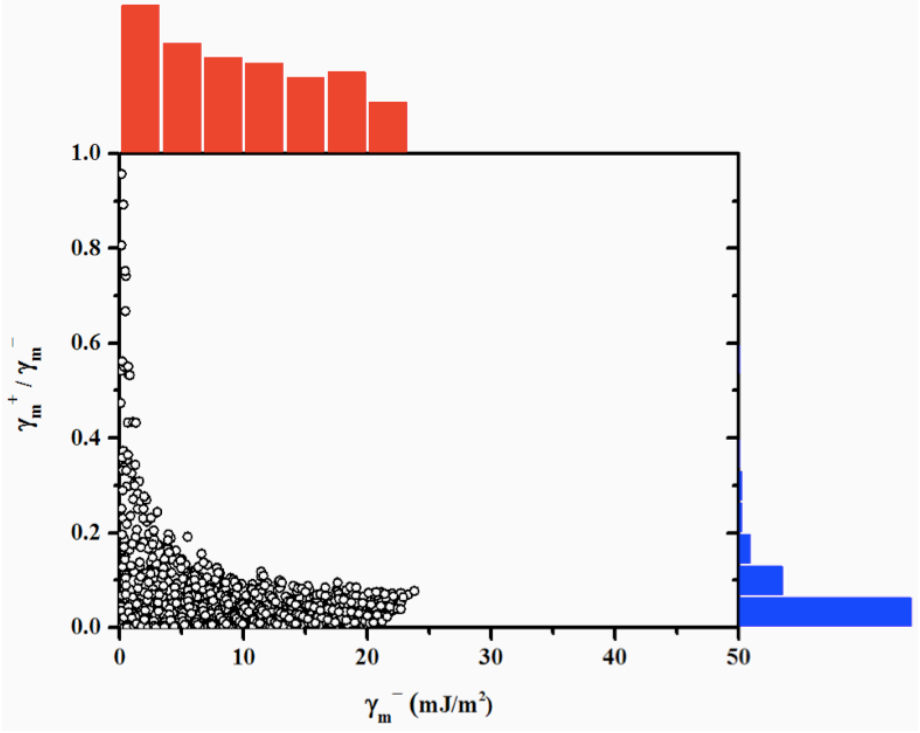

(c)

Figure 2.3. Monopolarities of membranes in (a) van Oss-based, (b) Lee-based and (c) Volpe-based libraries.

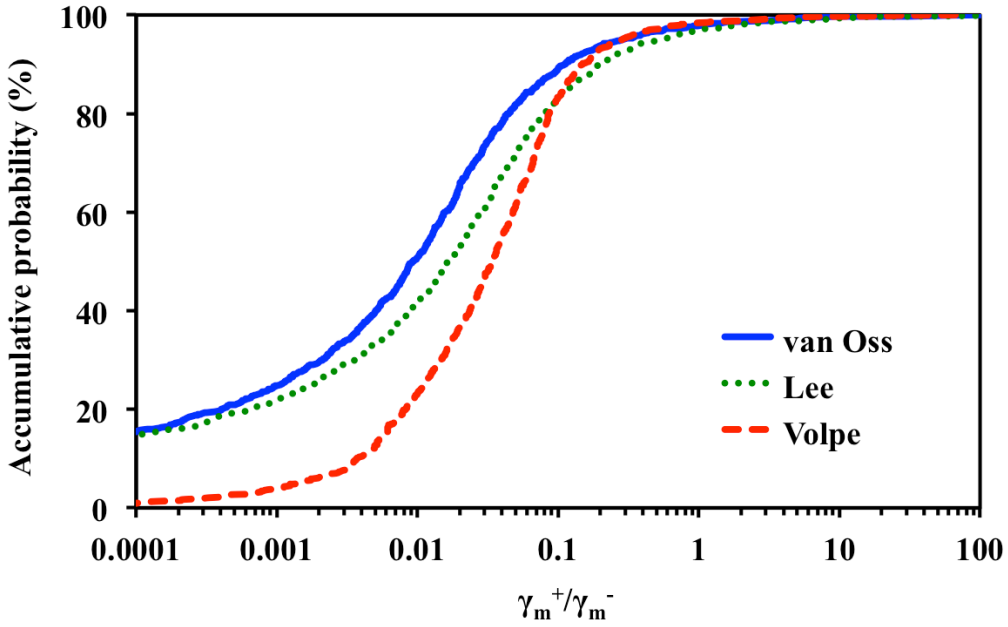

Figure 2.4. Distributions of γ_m^+/γ_m^- in the simulated libraries

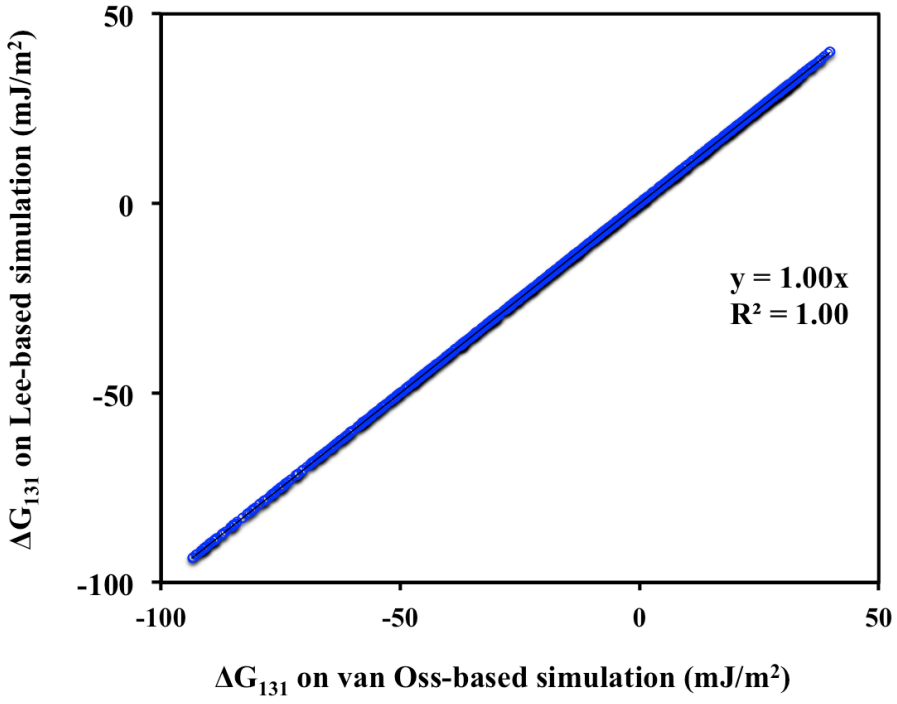

(a)

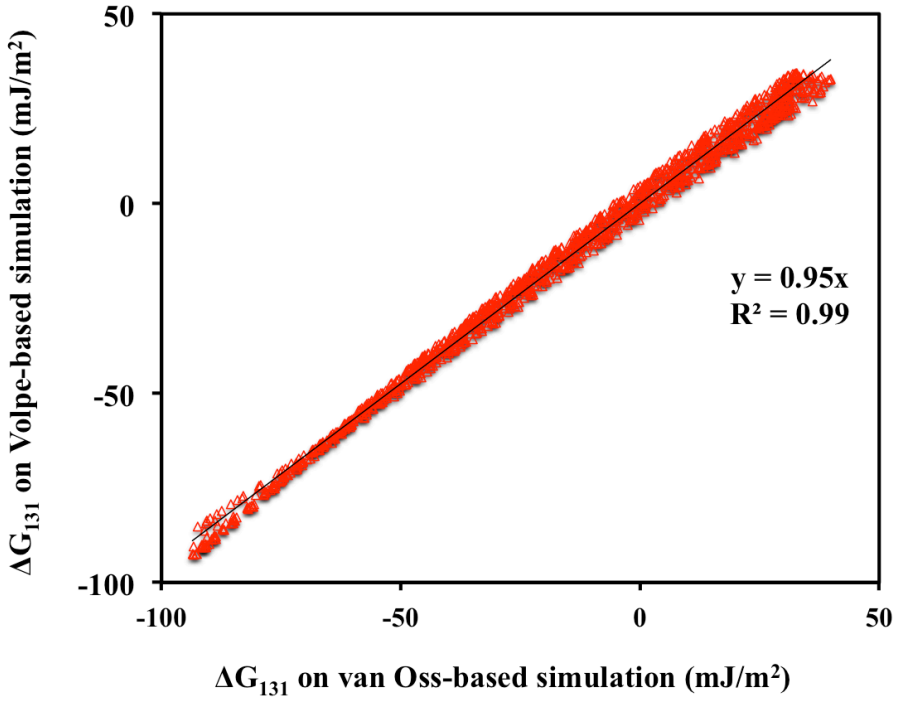

Figure 2.5. ΔG_{131} **consistency comparison between van Oss-based and Lee-based (a) and Volpe-based simulations (b)**

$$\Delta G_{131}^{tot} = \underbrace{-2\left(\sqrt{\gamma_1^{LW}}-\sqrt{\gamma_3^{LW}}\right)^2}_{\text{LW attraction between 1 and water}} \underbrace{-4\sqrt{\gamma_3^+\gamma_3^-}}_{\text{Polar cohesion of water}} \underbrace{-4\sqrt{\gamma_1^+\gamma_1^-}}_{\text{Polar cohesion of 1}} \underbrace{+4\sqrt{\gamma_1^+\gamma_3^-}}_{\text{Polar adhesion between e-acceptor of 1 and e-donor of water}} \underbrace{+4\sqrt{\gamma_1^-\gamma_3^+}}_{\text{Polar adhesion between e-donor of 1 and e-acceptor of water}}$$

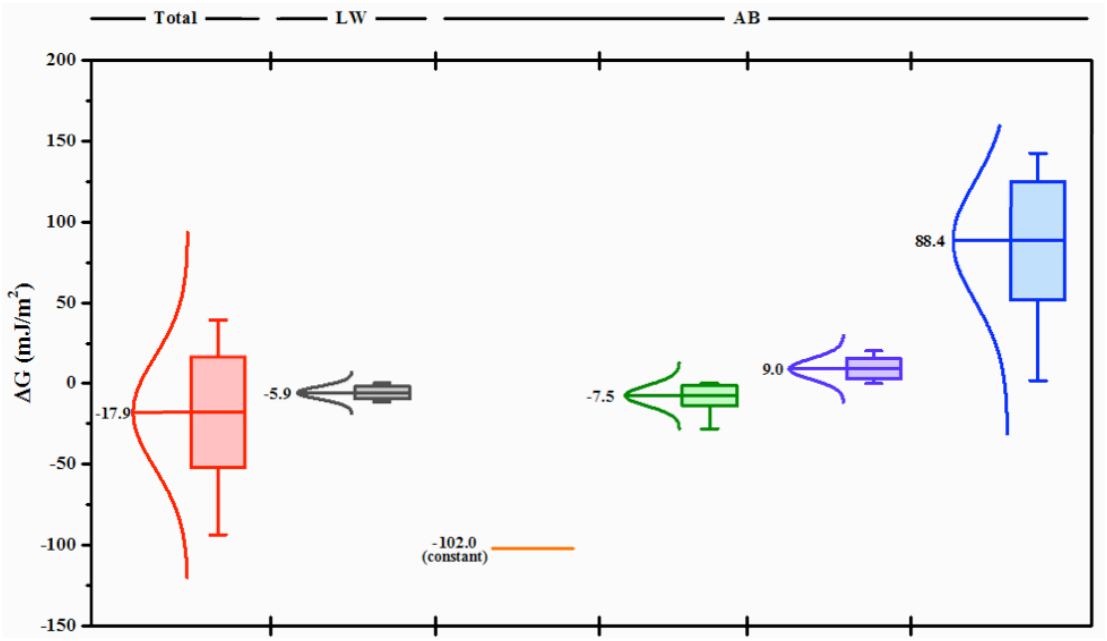

(a)

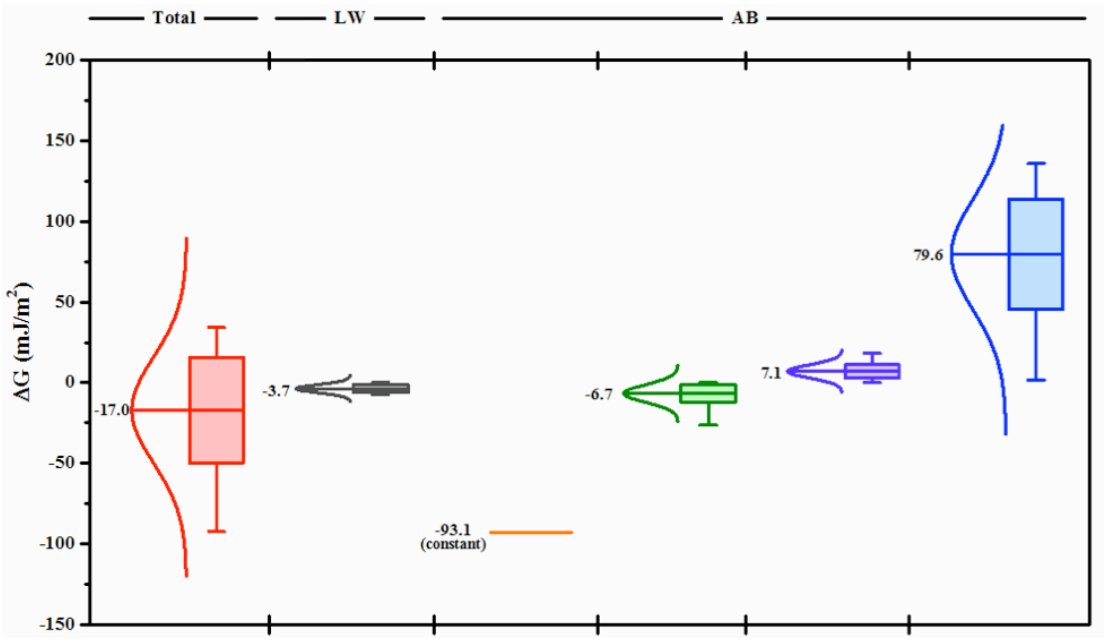

(b)

Figure 2.6. Influence of each interaction component in ΔG_{131}^{tot}
(a: van Oss-based and Lee-based simulation, b: Volpe-based simulation)

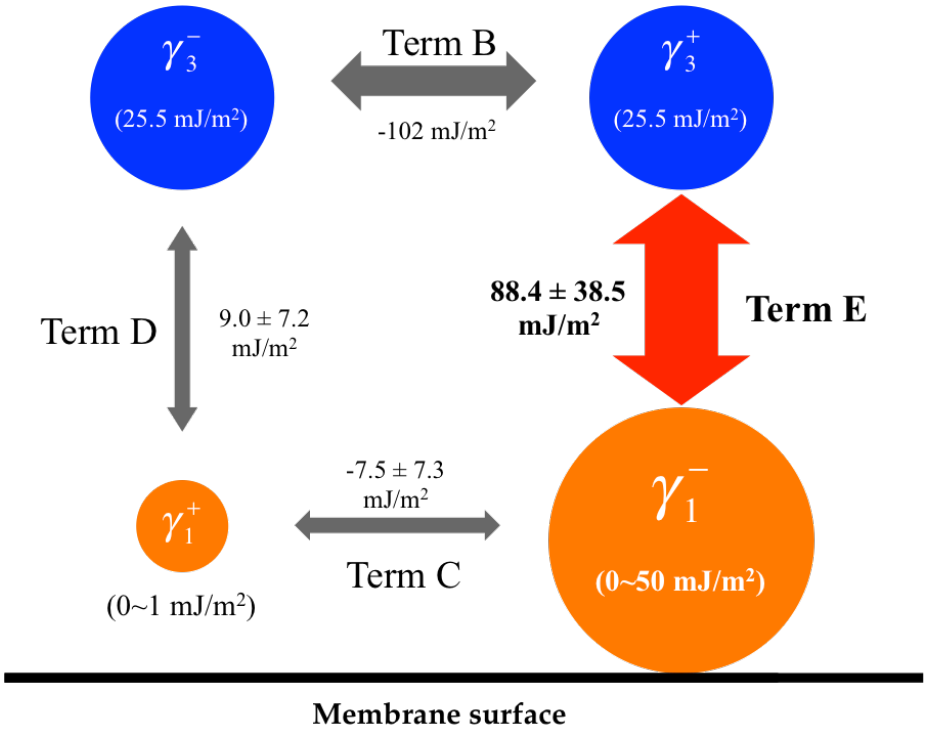

(a)

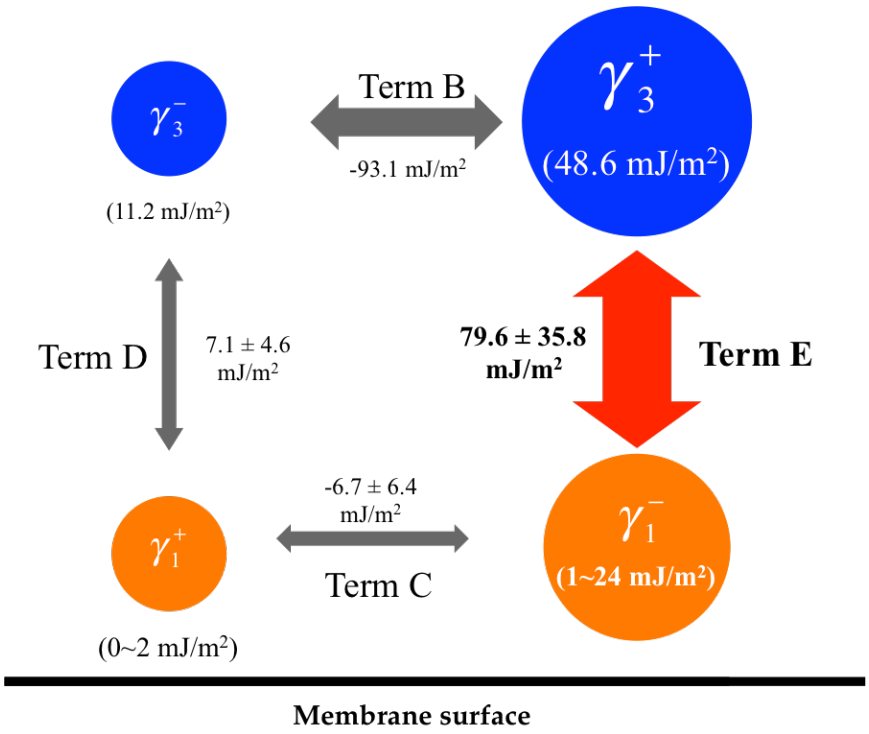

(b)

Figure 2.7. Schematic description of acid-base interaction mechanism for van Oss-simulation (a) and Volpe-based simulation (b)

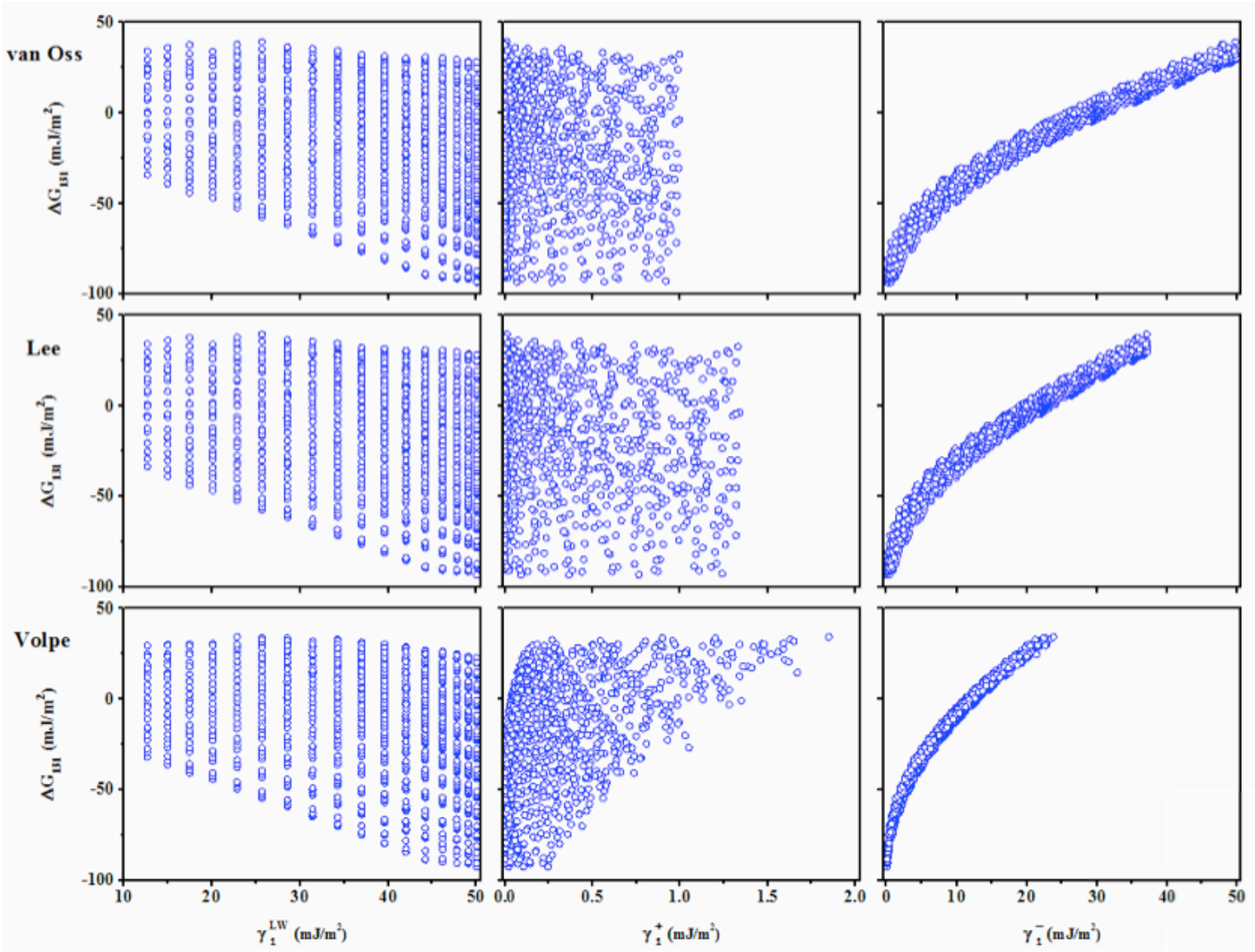

Figure 2.8. Correlation of each surface tension parameter with ΔG_{131}

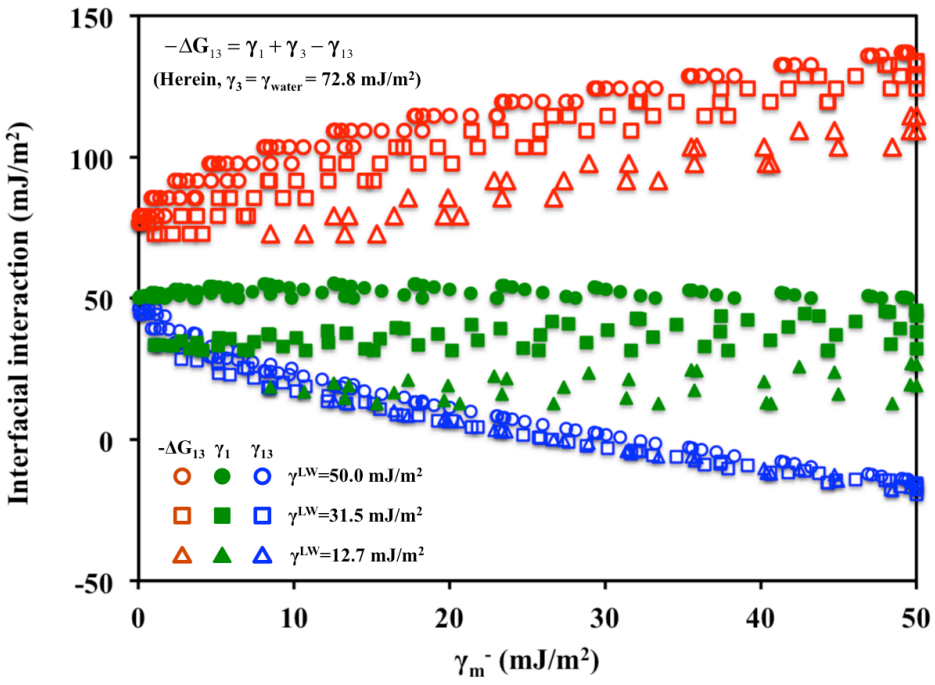

(a)

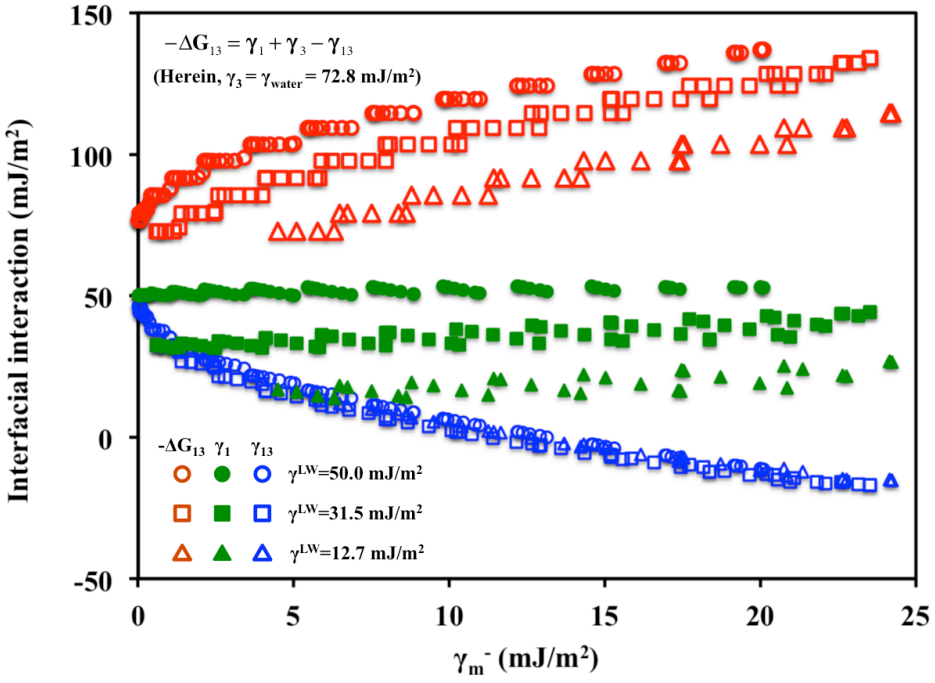

(b)

Figure 2.9. Influence of γ_m^- on γ_1, γ_{13} and $-\Delta G_{13}$
(a: van Oss-based, b: Volpe-based simulation)

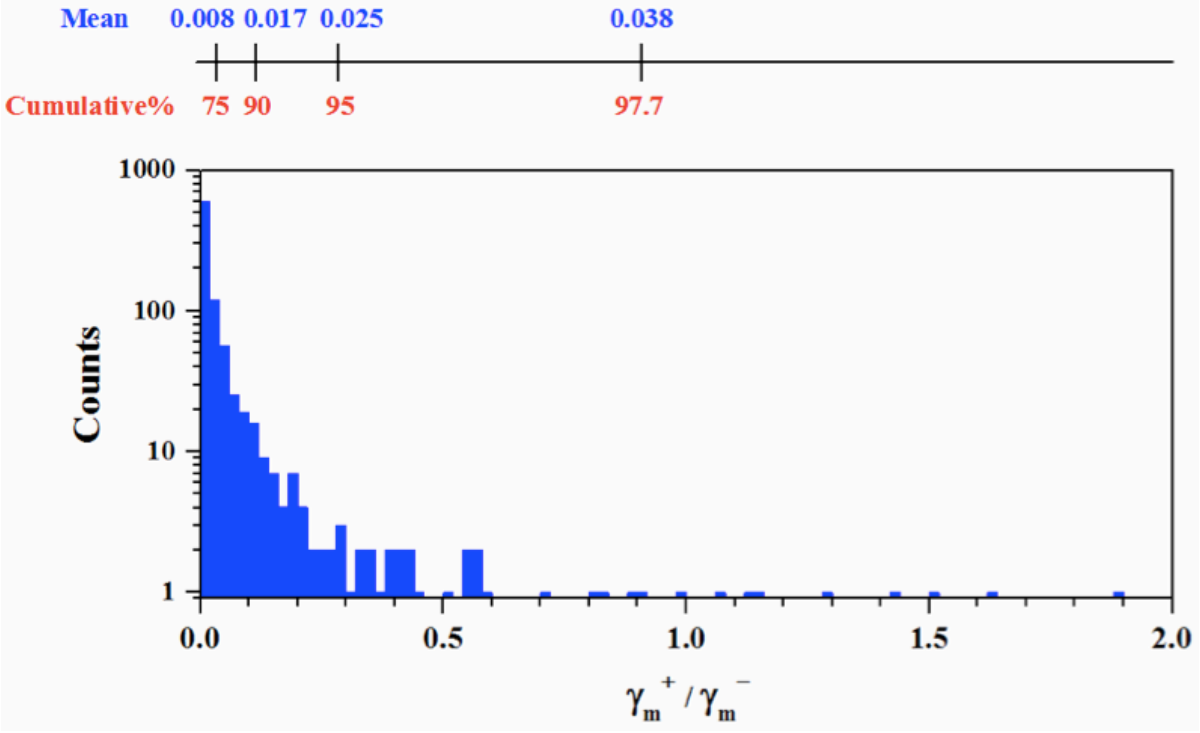
Mean
0.008
0.017
0.025
0.038
Cumulative%
75
90
95
97.7
1000
100
10
1
Counts
0.0
0.5
1.0
1.5
2.0
γ_m^+ / γ_m^-

(a)

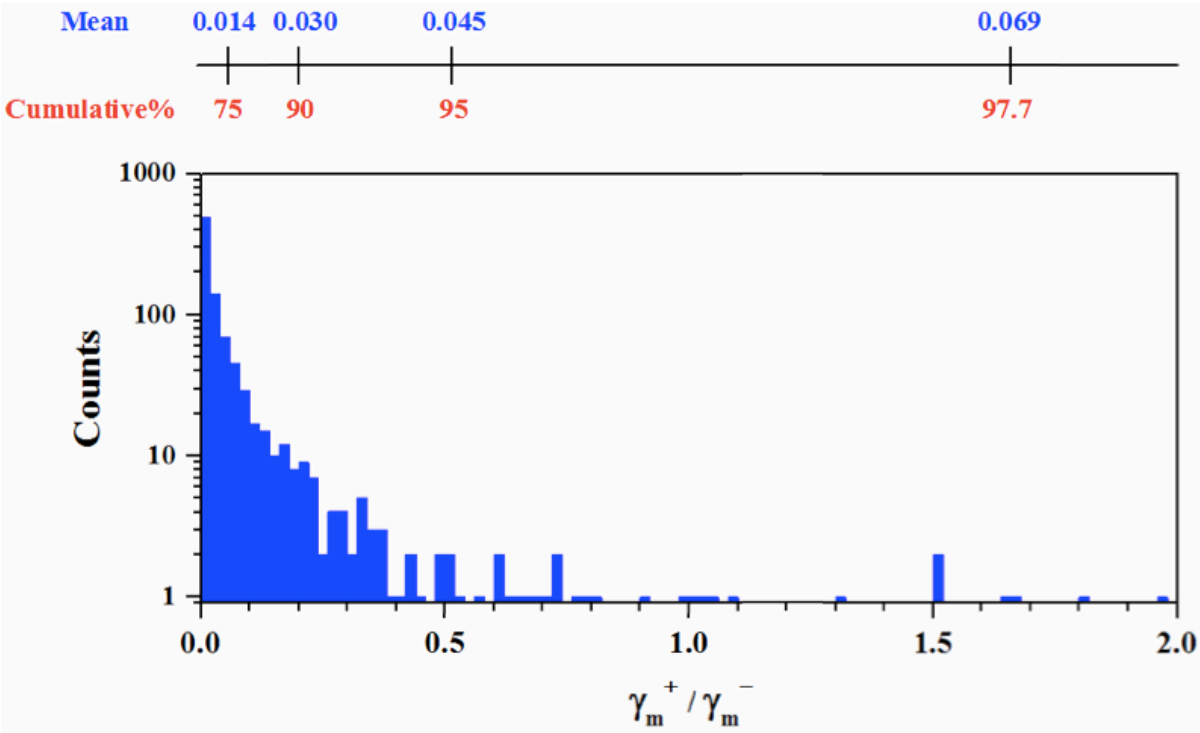
Mean
0.014
0.030
0.045
0.069
Cumulative%
75
90
95
97.7
1000
100
10
1
Counts
0.0
0.5
1.0
1.5
2.0
γ_m^+ / γ_m^-

(b)

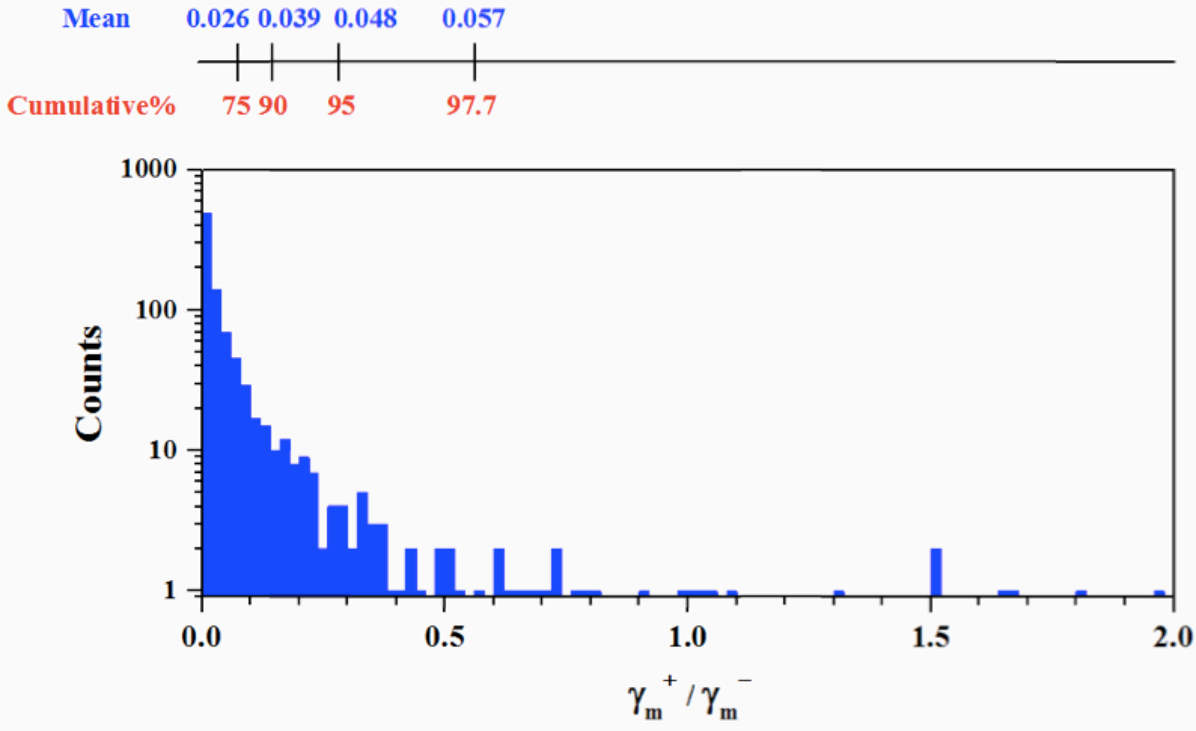

(c)

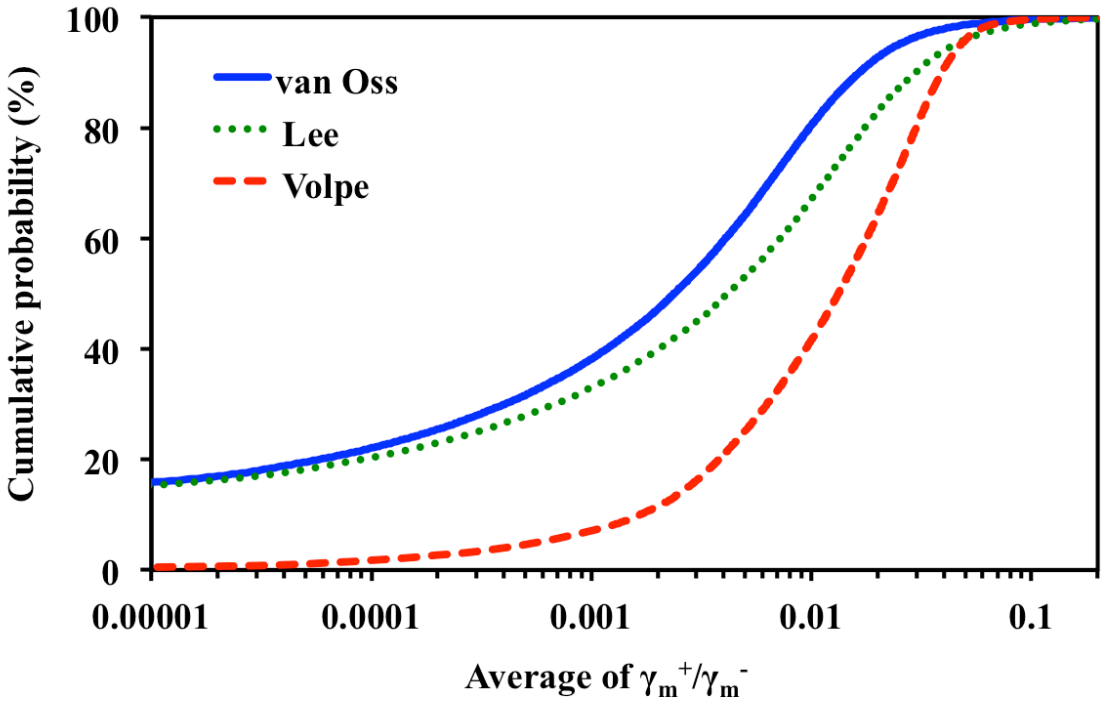

(d)

Figure 2.10. Histogram of γ_m^+ / γ_m^- in van Oss-based (a), Lee-based (b), and Volpe-based simulation (c) and the overall distributions of average γ_m^+ / γ_m^-

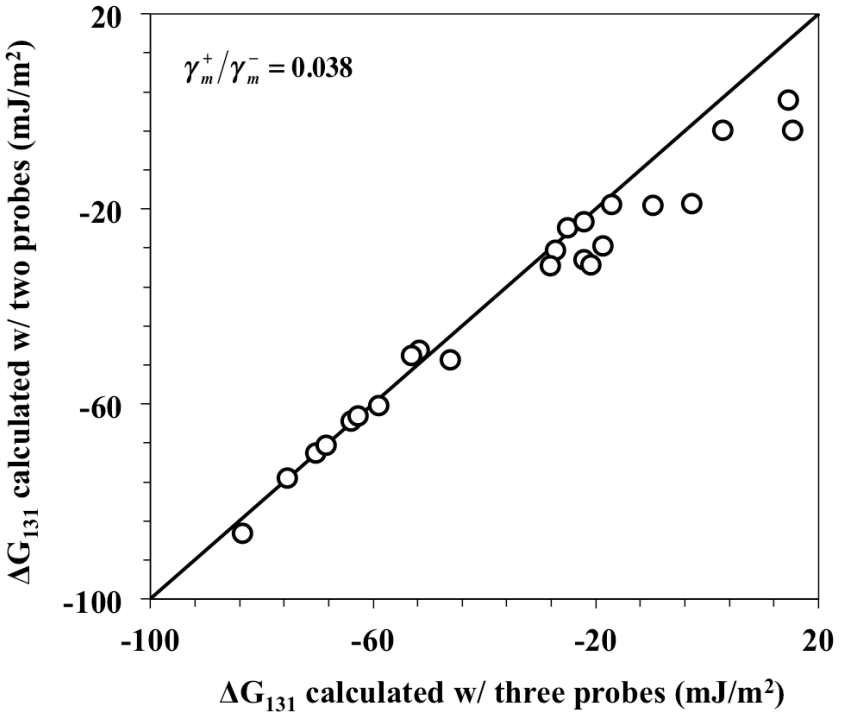

(a) In van Oss-based simulation w/ average of γ_m^+ / γ_m^- for 97.7% of data

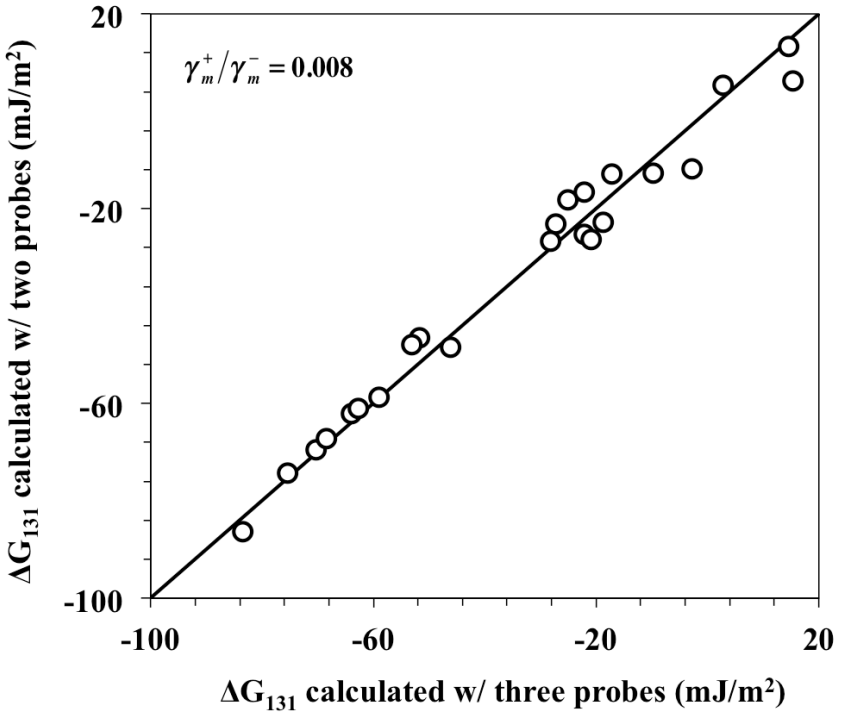

(b) In van Oss-based simulation w/ average of γ_m^+ / γ_m^- for 75% of data

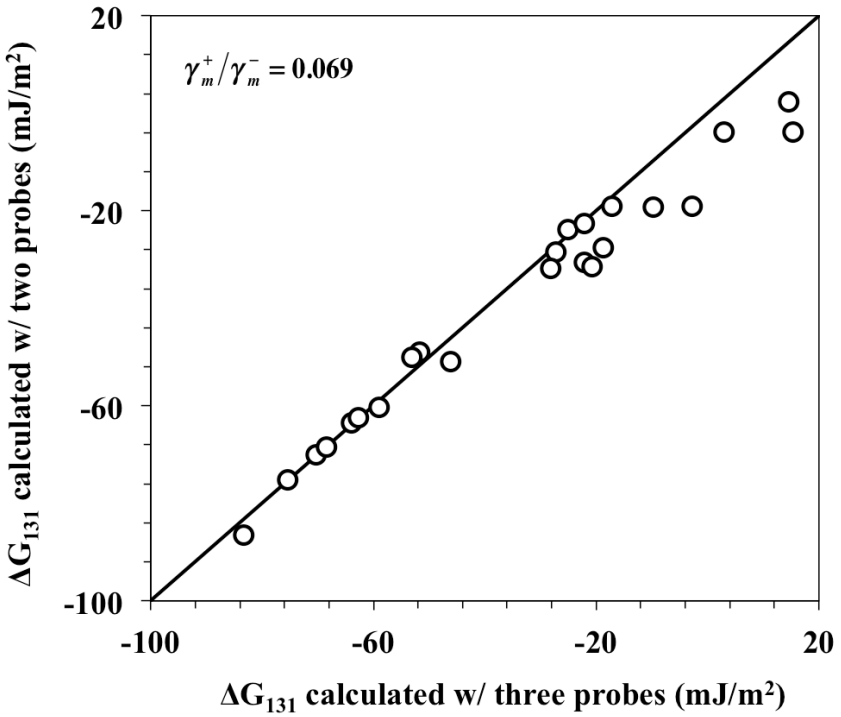

(c) In Lee-based simulation w/ average of γ_m^+ / γ_m^- for 97.7% of data

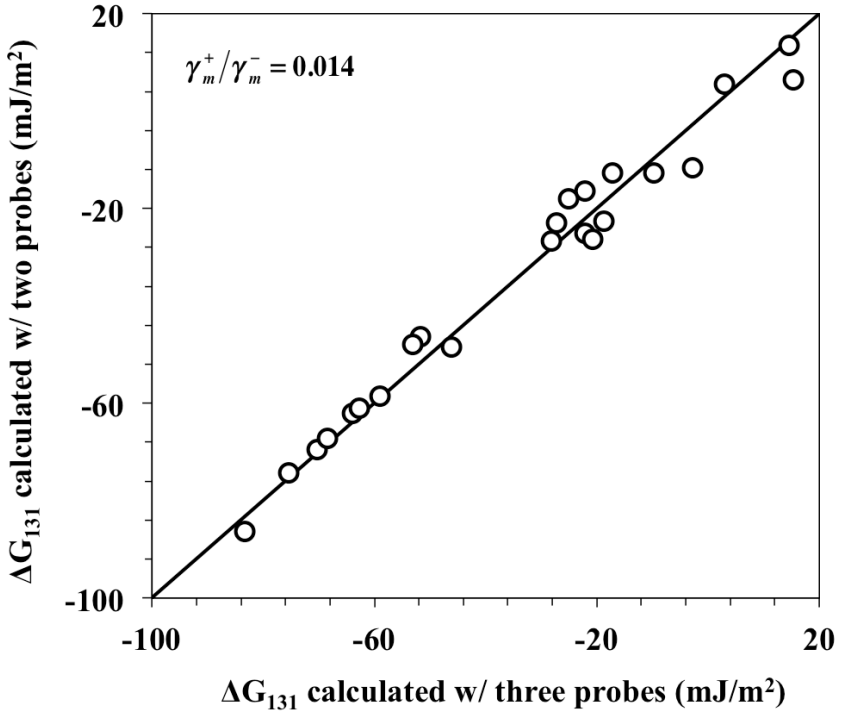

(d) In Lee-based simulation w/ average of γ_m^+ / γ_m^- for 75% of data

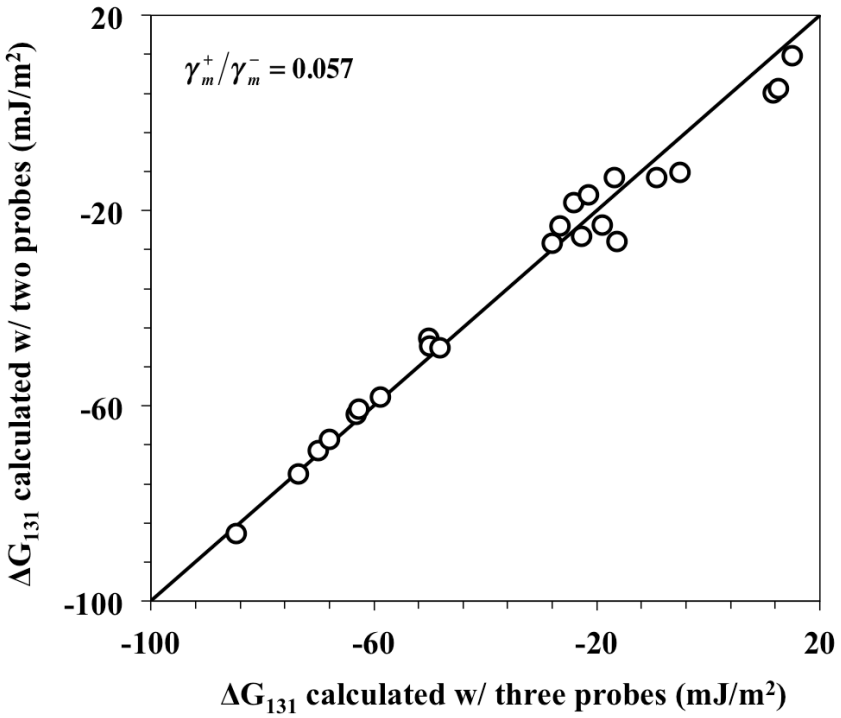

(e) In Volpe-based simulation w/ average of γ_m^+/γ_m^- for 97.7% of data

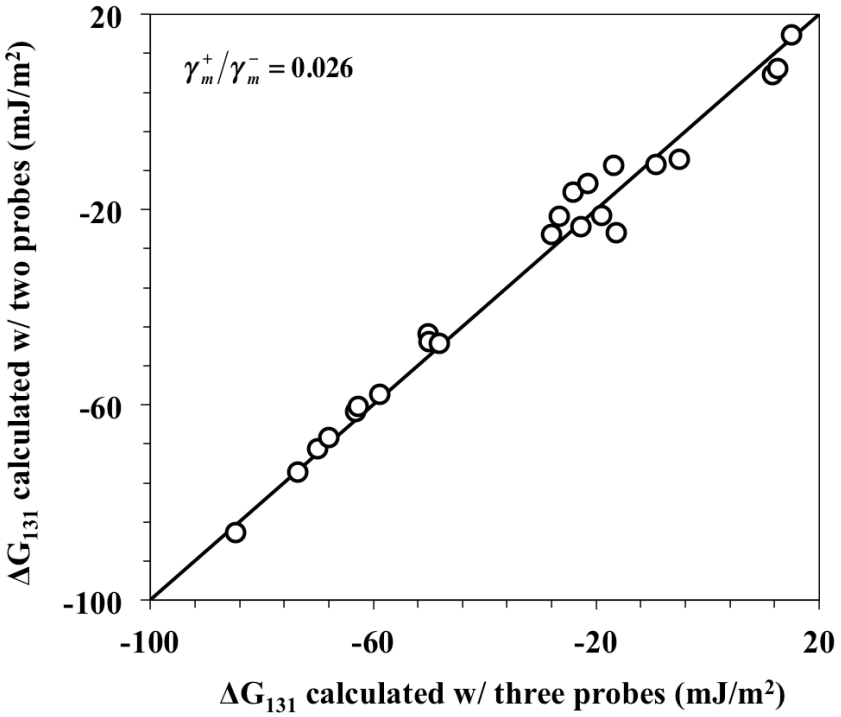

(f) In Volpe-based simulation w/ average of γ_m^+/γ_m^- for 75% of data

Figure 2.11. ΔG_{131} comparison between three-probe and two-probe wetting method

References

(1) Tiraferri, A.; Kang, Y.; Giannelis, E. P.; Elimelech, M. Superhydrophilic thin-film composite forward osmosis membranes for organic fouling control: fouling behavior and antifouling mechanisms. *Environ. Sci. Technol.* **2012**, *46* (20), 11135–11144.

(2) Subramani, A.; Hoek, E. M. V. Direct observation of initial microbial deposition onto reverse osmosis and nanofiltration membranes. *Journal of Membrane Science* **2008**.

(3) Cornelissen, E. R.; van den Boomgaard, T.; Strathmann, H. Physicochemical aspects of polymer selection for ultrafiltration and microfiltration membranes. *Colloids and Surfaces A: Physicochemical and Engineering Aspects* **1998**, *138*, 283–289.

(4) Brant, J. A.; Childress, A. E. Assessing short-range membrane–colloid interactions using surface energetics. *Journal of Membrane Science* **2002**.

(5) Kim, S.; Marion, M.; Jeong, B.-H.; Hoek, E. M. V. Crossflow membrane filtration of interacting nanoparticle suspensions. *Journal of Membrane Science* **2006**, *284* (1-2), 361–372.

(6) Kim, S.; Hoek, E. M. V. Interactions controlling biopolymer fouling of reverse osmosis membranes. *Desalination* **2007**, *202* (1-3), 333–342.

(7) Jin, X.; Huang, X.; Hoek, E. M. V. Role of Specific Ion Interactions in Seawater RO Membrane Fouling by Alginic Acid. *Environ. Sci. Technol.* **2009**, *43* (10), 3580–3587.

(8) Subramani, A.; Hoek, E. M. V. Biofilm formation, cleaning, re-formation on polyamide composite membranes. *Desalination* **2010**, *257* (1-3), 73–79.

(9) Wang, Q.; Wang, Z.; Zhu, C.; Mei, X.; Wu, Z. Assessment of SMP fouling by foulant–membrane interaction energy analysis. *Journal of Membrane Science* **2013**, *446* (C), 154–163.

(10) Wang, J.; Mo, Y.; Mahendra, S.; Hoek, E. M. V. Effects of water chemistry on structure and performance of polyamide composite membranes. *Journal of Membrane Science* **2014**, *452* (C), 415–425.

(11) Elimelech, M.; Jia, X.; Gregory, J.; Williams, R. *Particle Deposition and Aggregation*; Butterworth-Heinemann: Oxford, 1998.

(12) Subramani, A. Microbial adhesion mechanisms in reverse osmosis and nanofiltration, 2007, pp 1–215.

(13) Grasso, D.; Subramaniam, K.; Butkus, M.; Strevett, K.; Bergendahl, J. A review of non-DLVO interactions in environmental colloidal systems. *Rev Environ Sci Biotechnol* **2002**, *1* (1), 17–38.

(14) van Oss, C. J.; Good, R. J.; Chaudhury, M. K. The role of van der Waals forces and hydrogen bonds in “hydrophobic interactions” between biopolymers and low energy surfaces. *Journal of Colloid and Interface Science* **1986**, *111* (2), 378–390.

(15) van Oss, C. J.; Good, R. J.; Chaudhury, M. K. Determination of the Hydrophobia Interaction Energy-Application to Separation Processes. *Separation Science and Technology* **1987**, *22* (1), 1–24.

(16) van Oss, C. J.; Chaudhury, M. K.; Good, R. J. Interfacial Lifshitz-van der Waals and polar interactions in macroscopic systems. *Chemical Reviews* **1988**, *88* (6), 927–941.

(17) Volpe, Della, C.; Siboni, S. Acid–base surface free energies of solids and the definition of scales in the Good–van Oss–Chaudhury theory. *Journal of Adhesion Science and Technology* **2000**, *14* (2), 235–272.

(18) Morra, M. On the molecular basis of fouling resistance. *Journal of Biomaterials Science, Polymer Edition* **2000**, *11* (6), 547–569.
(19) van Oss, C. J. Acid—base interfacial interactions in aqueous media. *Colloids and Surfaces A: Physicochemical and Engineering Aspects* **1993**, *78*, 1–49.
(20) Volpe, C. D.; Siboni, S. Some Reflections on Acid–Base Solid Surface Free Energy Theories. *Journal of Colloid and Interface Science* **1997**, *195* (1), 121–136.
(21) Morra, M. Some Reflection on the Evaluation of the Lewis Acid–Base Properties of Polymer Surfaces by Wetting Measurements. *Journal of Colloid and Interface Science* **1996**, *182* (1), 312–314.
(22) Lee, L.-H. Adhesion and Surface-Hydrogen-Bond Components for Polymers and Biomaterials. *The Journal of Adhesion* **1998**, *67* (1-4), 1–18.
(23) Volpe, Della, C.; Maniglio, D.; Brugnara, M.; Siboni, S.; Morra, M. The solid surface free energy calculation. *Journal of Colloid and Interface Science* **2004**, *271* (2), 434–453.
(24) van Oss, C. J. Development and applications of the interfacial tension between water and organic or biological surfaces. *Colloids and Surfaces B: Biointerfaces* **2007**, *54* (1), 2–9.
(25) Hong, H.; Peng, W.; Zhang, M.; Chen, J.; He, Y.; Wang, F.; Weng, X.; Yu, H.; Lin, H. Thermodynamic analysis of membrane fouling in a submerged membrane bioreactor and its implications. *Bioresource Technology* **2013**, *146* (C), 7–14.
(26) Feng, L.; Li, X.; Du, G.; Chen, J. Adsorption and fouling characterization of Klebsiella oxytoca to microfiltration membranes. *Process Biochemistry* **2009**, *44* (11), 1289–1292.
(27) Lin, H.; Zhang, M.; Mei, R.; Chen, J.; Hong, H. A novel approach for quantitative evaluation of the physicochemical interactions between rough membrane surface and sludge foulants in a submerged membrane bioreactor. *Bioresource Technology* **2014**, *171* (C), 247–252.
(28) Hong, H.; Zhang, M.; He, Y.; Chen, J.; Lin, H. Fouling mechanisms of gel layer in a submerged membrane bioreactor. *Bioresource Technology* **2014**, *166* (C), 295–302.
(29) Wang, Q.; Wang, Z.; Zhu, C.; Mei, X.; Wu, Z. Assessment of SMP fouling by foulant–membrane interaction energy analysis. *Journal of Membrane Science* **2013**, *446* (C), 154–163.
(30) Chen, L.; Tian, Y.; Cao, C.-Q.; Zhang, J.; Li, Z.-N. Interaction energy evaluation of soluble microbial products (SMP) on different membrane surfaces: Role of the reconstructed membrane topology. *Water Research* **2012**, *46* (8), 2693–2704.
(31) Chen, J.; Shen, L.; Zhang, M.; Hong, H.; He, Y.; Liao, B.-Q.; Lin, H. Thermodynamic analysis of effects of contact angle on interfacial interactions and its implications for membrane fouling control. *Bioresource Technology* **2016**, *201*, 245–252.
(32) Lee, S.; Kim, S.; Cho, J.; Hoek, E. M. V. Natural organic matter fouling due to foulant–membrane physicochemical interactions. *Desalination* **2007**, *202* (1-3), 377–384.
(33) Lin, T.; Lu, Z.; Chen, W. Interaction mechanisms and predictions on membrane fouling in an ultrafiltration system, using the XDLVO approach. *Journal of Membrane Science* **2014**, *461* (C), 49–58.
(34) Guillen, G. R.; McVerry, B. T.; Kaner, R. B.; Hoek, E. M. V. Tuning the properties of polyaniline-based ultrafiltration membranes with chemical post-treatment. *Journal of Membrane Science*.
(35) van Oss, C. J.; Chaudhury, M. K.; Good, R. J. Monopolar surfaces. *Advances in Colloid and Interface Science* **1987**, *28* (1), 35–64.

(36) van Oss, C. J. *The properties of water and their role in colloidal and biological systems*; Academic Press, 2008.
(37) van Oss, C. J.; Giese, R. F. Role of the Polar Properties of Water in Separation Methods. *Separation & Purification Reviews* **2011**, *40* (3), 163–208.
(38) van Oss, C. J.; Giese, R. F. Role of the Properties and Structure of Liquid Water in Colloidal and Interfacial Systems. *Journal of Dispersion Science and Technology* **2008**, *25* (5), 631–655.
(39) Ghosh, A. K.; Jeong, B.-H.; Huang, X.; Hoek, E. M. V. Impacts of reaction and curing conditions on polyamide composite reverse osmosis membrane properties. *Journal of Membrane Science* **2008**, *311* (1-2), 34–45.

Chapter 3

IMPLICATION OF ELECTRON-DONOCITY OF MEMBRANE SURFACE ON BIOFOULING MECHANISM

3.1. Introduction

Transport of foulants is regulated by convection force toward the membrane surface and the back-transport force imposed on the particles. Shear-induced diffusion with a cross-flow of a feed solution or aeration is known very effective to enhance the back transport of suspended solids. However, because the detachment of small substances generally requires a high level of shear intensity, it often demands considerable energy to control the back transport of small colloids and solutes only by enhancing cross-flow velocity or aeration intensity.[1,2] Recent research has focused on developing new membrane materials that resist/reduce the rate of fouling. [3-14] Anti-biofouling materials that repel foulants will inherently foul less and become easier to clean with milder cleaning treatments.

Because the majority of biofouling occurs on the surface of the polymeric membranes, key interfacial interactions between a membrane surface and a biofoulant play a pivotal role in biofouling phenomena. [15,16] Physicochemical basis of the solid-liquid interface such as surface tension has been a significant concept for researchers to interpret the interfacial interactions between a membrane surface and a biofoulant. In thermodynamic perspective, biofouling can be interpreted as adhesion of two different entities, a biofoulant and a membrane, through a media, (herein, water), to be a combined column. Therefore, adhesion accompanies the structural change of interfaces existing in the aqueous system (i.e. from two interfaces of biofoulant-water and membrane-water to a interface of biofoulant-membrane). This interface-transitive nature of biofouling phenomena leads that surface tension-based theories are adopted in the fundamental understanding of the membrane biofouling. Among those theories, the van Oss approach has been considered prominent because of its satisfactory prediction for experimental results of biofouling tests either in dense membranes (NF/RO) and porous membranes (MF/UF). [17-24]

van Oss theory added Lewis acid-base interaction to conventional Derjaguin-Landau-Verwey-Overbeek (DLVO) theory and the theory has been recognized as an extended DLVO theory. According to van Oss approach, in aqueous media, Lewis acid-base interaction occurs between the electron-acceptor in hydrogen atoms of water and lone pairs of atoms of a solid, basically having an analogous concept with hydrogen-bonding. The membrane surface with high electron-donating potential is able to hold water molecules (as discussed in Chapter 2) and form a hydration cell layer on its surface, which may impede the access of biofoulant to the membrane surface. Because the biofoulant also has the electron-donating and accepting potentials, other interfacial interactions also occur in biofoulant-water and biofoulant–membrane surface. Therefore, better thermodynamic understanding on the biofouling phenomena need a perspective that ponders the three different but deeply interconnected interfacial interactions existing in membrane surface-water, water-biofoulant and biofoulant-membrane surface.

This chapter investigates the thermodynamic mechanism of biofouling based on van Oss approach. The interfacial interaction energies between biofoulants and membrane surface are dissected into each free energy components and their correlations with surface tension components are examined. The thermodynamic analysis is reviewed with experimental results of biofouling tests. Especially, this study evaluates the electron-donicity as an indicator for anti-biofouling property of a membrane by three different methods: microbial adhesion test, biopolymer fouling test, and fouling test in bench-scale MBR. Furthermore, based on the previous modeling results and reference survey results, this chapter simplifies the theory of van Oss to have it suggest a standard of physicochemical properties of membranes for biofouling resistance.

3.2. Theory

3.2.1. Basics of van Oss theory

In order to calculate the interfacial free energies (ΔG_{132}^{LW} , ΔG_{132}^{AB} , ΔG_{132}^{Tot}) the surface tensions (γ^{LW} , γ^{+} , γ^{-}) of membranes and particles should be determined with contact angles (θ) measured by using three different probe liquids, surface tensions of which are already known. The surface tensions are calculated by the extended Young-Dupré equation,[25]

$$-\Delta G_{sl} = (1+\cos\theta)\gamma_l^{tot} = 2\left(\sqrt{\gamma_s^{LW}\gamma_l^{LW}} + \sqrt{\gamma_s^{+}\gamma_l^{-}} + \sqrt{\gamma_s^{-}\gamma_l^{+}}\right) \tag{3.1}$$

where θ is the ideal contact angle formed between a droplet of liquid L and the smooth membrane surface, γ_S^{LW} and γ_L^{LW} are the apolar (Lifshitz-van der Waals) components of the surface tension of solid S (here, membrane or particle) and liquid L, γ_S^{+} , γ_L^{+} , γ_S^{-} , and γ_L^{-} are the polar (electron-acceptor and electro donor) components of the surface tension of solid S and liquid L, respectively.

The interfacial free energy at contact, ΔG_{132}^{tot} , an thermodynamic value of indicating the inherent affinity of a solid material (1) interacting through a liquid media (*3*) with another solid material (2). ΔG_{132}^{tot} can be determined as,

$$\Delta G_{132}^{tot} = \Delta G_{132}^{LW} + \Delta G_{132}^{AB} \tag{3.2}$$

ΔG_{132}^{LW} and ΔG_{132}^{AB} are the Lifshitz–van der Waals and Lewis acid–base interfacial free energies, respectively and they can be calculated from, [26]

$$\Delta G_{132}^{LW} = 2\left(\sqrt{\gamma_3^{LW}} - \sqrt{\gamma_1^{LW}}\right)\left(\sqrt{\gamma_2^{LW}} - \sqrt{\gamma_3^{LW}}\right) \tag{3.3}$$

$$\Delta G_{132}^{AB} = 2\sqrt{\gamma_3^{-}}\left(\sqrt{\gamma_1^{+}} + \sqrt{\gamma_2^{+}} - \sqrt{\gamma_3^{+}}\right) + 2\sqrt{\gamma_3^{+}}\left(\sqrt{\gamma_1^{-}} + \sqrt{\gamma_2^{-}} - \sqrt{\gamma_3^{-}}\right) - 2\left(\sqrt{\gamma_1^{+}\gamma_2^{-}} + \sqrt{\gamma_1^{-}\gamma_2^{+}}\right) \tag{3.4}$$

3.2.2. Simplification of van Oss theory for aqueous condition

Eqn. 3.4 can be rearranged in terms of each electron-donor component of three entities with the help of $\gamma_3^{AB} = 2\sqrt{\gamma_3^+\gamma_3^-}$ such as

$$\Delta G_{132}^{AB} = 2\sqrt{\gamma_1^-}\left(\sqrt{\gamma_3^+} - \sqrt{\gamma_2^+}\right) + 2\sqrt{\gamma_2^-}\left(\sqrt{\gamma_3^+} - \sqrt{\gamma_1^+}\right) + 2\sqrt{\gamma_3^-}\left(\sqrt{\gamma_1^+} + \sqrt{\gamma_2^+}\right) - 2\gamma_3^{AB} \qquad (3.5)$$

Eqn. 3.5 underlines how each electron-donor component of each entity contributes to ΔG_{132}^{AB}. The first term reveals that the electron-donor sites of membrane surface (1) cause competition between the electron-acceptors of water and biofoulant to occupy those electron-donating sites in membrane surface. The second term exhibits that the electron-acceptors of water and membrane surface compete to capture the electron-donor sites of biofoulant. However, as described in the third term, the electron-donor sites of water experience no conflict between the electron-acceptors of the other entities because water plays a role as an interfacing media between those entities.

The previous study theoretically and semi-empirically approved that the electron-donor monopolarity dominates most polymeric membrane surfaces and that the semi-empirical average of γ_m^+/γ_m^- of most polymeric membranes is close to 0.008 in case of applying the reference values of the test solvents that van Oss proposed. The electron-acceptor parameters of most biofoulants are also known highly lower than their own electron-donor parameters. This finding simplifies Eqn. 3.5 as

$$\Delta G_{132}^{AB} = 2\sqrt{\gamma_1^-}\left(\sqrt{\gamma_3^+} - \sqrt{\gamma_2^+}\right) + 2\sqrt{\gamma_2^-}\left(\sqrt{\gamma_3^+} - \sqrt{\gamma_1^+}\right) - 2\gamma_3^{AB} \qquad (3.6)$$

As described in Chapter 2, water is considered one of prominent Lewis acids and its electron-accepting potential of water is generally much greater than the one of solids ($\gamma_3^+ \gg \gamma_1^+, \gamma_3^+ \gg \gamma_2^+$). Therefore, Eqn. 3.6 can reduce to

$$\Delta G_{132}^{AB} = 2\sqrt{\gamma_3^+}\left(\sqrt{\gamma_1^-} + \sqrt{\gamma_2^-}\right) - 2\gamma_3^{AB} \tag{3.7}$$

Finally, Eqn. 3.7 expresses the simplest formula of ΔG_{132}^{AB}, which clearly emphasizes the role of the high Lewis-accepticity of water and thus its counter-polar properties of membrane (γ_1^-) and biofoulant (γ_2^-). Note that Eqn. 3.6 assumes the electron-donor dominant surfaces of solids (low γ_1^+ and γ_2^+) while Eqn. 3.7 additionally reflects the high electron-accepticity of water (high γ_3^+).

3.3. Materials and Methods

3.3.1. Surface tension parameters of membrane and biofoulant

Deionized water contact angles were measured using a goniometer (DSA10, KRŰSS GmbH). Surface tensions of polyvinylidene fluoride (PVDF), polyethersulfone (PES), and polyacrylonitrile (PAN) membranes were determined by measuring sessile drop contact angles of deionized water, ethylene glycol, glycerol, and diiodomethane on membrane samples mounted on glass slides with double-sided tape. At least twelve equilibrium contact angles were measured for each sample obtained directly for this study, where the equilibrium angle was determined from the average of right and left angles. The highest and lowest values were discarded before taking the average and standard deviation.

Numerous studies have been conducted to study the apolar and polar surface tension parameters of polymers, bacterial surfaces, and biofilms. In order to compare thermodynamic

surface characteristics of major membrane materials and biofoulants, datasets of their surface tension components was collected from several research references as presented in Table 3.1.

3.3.2. Cross-flow biofouling test

In order to evaluate the fouling resistance of the modified membranes, a lab-built cross-flow apparatus was used to monitor the dynamic change of trans-membrane pressure (TMP) in the presence of sodium alginate solution. 19 cm^2 cutout of the membranes were compacted first using DI water at 15 psi for three hours. A weight balance connecting to a computer was used to record and calculate the active flux. Once stable, permeate flux was then adjusted manually to 100 LMH using a peristaltic pump. After 30 min of stable flux at 100 LMH, the feed was switched to 200 ppm sodium alginate solution while maintaining the same flux. Pressure gauges were placed at both the feed side and the permeate side and connected to the computer. TMP was calculated automatically throughout the cross-flow fouling test via Eqn.3.8:

$$TMP = \frac{(P_{in} - P_{ret})}{2} - P_{perm} \tag{3.8}$$

where P_{in} is the inlet pressure and P_{ret} are the pressure at the feed side and the retentate side of the membrane, respectively, and P_{perm} is the pressure on the permeate side of the film.

3.3.3. Biofouling test in a membrane bioreactor (MBR)

A laboratory-scale MBR with a working volume of 2 L is fabricated with a submerged type of membrane module. The membrane module is able to equip a commercial flat sheet membrane. The feature of easy disassembly and assembly of the membrane module allows us to readily evaluate any commercial flat sheet membrane that this research aims to test. The

membrane module comprises a flow channel, a spacer, two permeate outlets, two support plates, four standing legs, and sealing parts as described in Figure 3.1 and provides the membrane the total contact area of 155 cm^2.

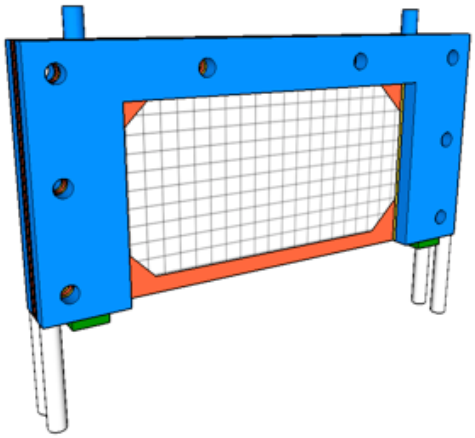

Figure 3.1. Flat sheet type of membrane module

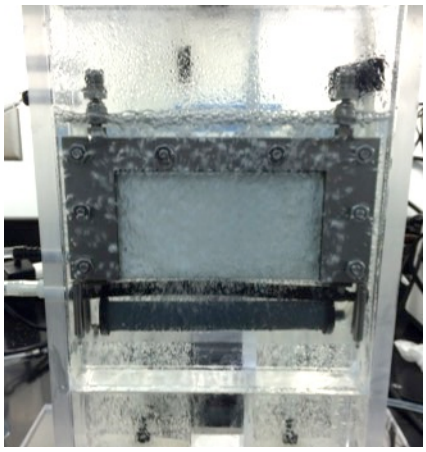

Figure 3.2. Membrane module submerged in bioreator

The membrane module is placed inside MBR. An aeration diffuser connected with a pure oxygen container is installed immediately below the membrane module and at the base of the reactor as shown in Figure 3.2. To maintain a constant-flux filtration, a peristaltic pump is used on the permeate stream. Independent pressure transducers and digital flow meter records feed, retentate, and permeate pressures and permeate flow, and streams data to a laboratory PC in real time for data extraction as presented in Figure 3.3.

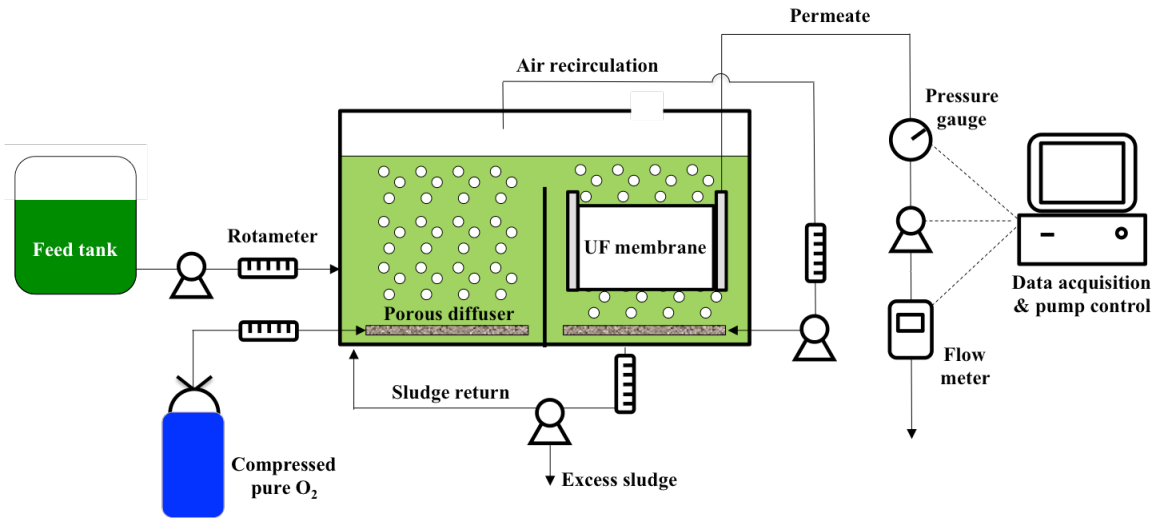

Figure 3.3. Schematic diagram of bench-scale MBR

The bioreactor was inoculated with an activated sludge from a municipal wastewater treatment plant that utilizes the pure oxygen for aeration (Joint Water Pollution Control Plant in the city of Carson). Mixed liquor suspended solid (MLSS) is analyzed according to the standard methods (APHA, 1995) to monitor the microbial sludge concentration and MLSS 7,000 mg/L is maintained by control of sludge retention time (SRT).

For acclimatization of microbial sludge, the bioreactor is supplied with a synthetic sewage recipe following a recipe adapted from OECD guideline (2001) as presented in Table 3.1. This synthetic sewage yields a mean chemical oxygen demand (COD) of 700 mg COD/L and total nitrogen (TN) of 90 mg N/L. The synthetic sewage is fed with the organic loading rate of 0.4 g COD/g MLSS/day.

Table 3.1. Physicochemical properties of polymeric membranes

Membrane	γ^{LW}	γ^{+}	γ^{-}	γ^{AB}	γ^{tot}	*Ref.*
PVDF	45.6	0.44	16.0	5.3	50.9	[27]
	42.1	0.77	15.6	6.9	49.0	[28]
	47.2	0.21	16.4	3.7	50.9	[29]
	48.1	0.03	19.8	1.5	49.6	[30]
	35.7	0.95	4.0	3.9	39.6	[31]
	45.4	0.12	2.2	1.0	46.4	[32]
	47.6	0.27	16.7	4.2	51.8	[33]
	42.3	0.23	3.7	1.8	44.1	[34]
	36.7	0.23	13.9	3.6	40.3	[35]
	48.4	0.06	18.3	2.2	50.5	[36]
	37.1	0.01	18.5	0.9	38.0	This study
PES	41.2	0.19	3.9	1.7	42.9	[32]
	35.7	0.05	27.6	2.3	38.0	[35]
	48.1	0.00	20.4	0.0	48.1	[37]
	48.4	0.00	29.5	0.0	48.4	This study
PAN	44.2	0.61	17.7	6.6	50.8	[17]
	38.9	0.39	30.2	6.9	45.8	[31]
	45.9	0.02	39.5	1.8	47.7	This study

Table 3.1. Continued

Membrane	γ^{LW}	γ^{+}	γ^{-}	γ^{AB}	γ^{tot}	*Ref.*
PVC	40.1	0.85	5.1	4.2	44.3	[34]
	43.7	0.08	0.2	0.3	44.0	[31]
	42.4	0.00	9.5	0.0	42.4	[31]
PP	24.0	0.11	1.8	0.9	24.9	[28]
	33.7	0.01	2.1	0.3	34.0	[17]
CA	48.1	3.47	2.7	6.1	54.2	[32]
	40.0	0.48	19.2	6.1	46.1	[17]
PANi	42.0	0.06	23.9	2.4	44.4	[38]
	41.6	0.25	38.4	6.2	47.8	[38]
PC	43.4	0.06	5.6	1.2	44.6	[17]
PSf	43.1	0.13	3.19	1.3	44.4	[17]

(PVDF, Polyvinylidene fluoride; PES, Polyethersulfone; PAN, Polyacrylonitrile; PVC, Polyvinyl chloride; PP, Polypropylene; CA, Cellulose acetate; PANi, Polyaniline; PC, Polycarbonate; PSf, Polysulfone)

Table 3.2. Synthetic sewage recipe

Constituent	Peptone	Meat extract	Urea	$CaCl_2 \cdot 2H_2O$	K_2HPO_4	$MgSO_4 \cdot 7H_2O$	NaCl	$NaHCO_3$
Conc. (g/L)	0.755	0.519	0.071	0.019	0.132	0.009	0.033	0.944

3.3.4. Microbial adhesion test

Microbial adhesion test was conducted with three different membrane materials: PVDF (250 kDa), PAN (250kDa) and PES (300 kDa). *Escherichia coli* was used as the model bacteria and the overall test procedure including the microbial suspension and membrane incubation in the microbial suspension followed the protocol proposed by Yang et al. (2011).[39] After incubating the membrane samples in the bacterial suspension for 24 hr at 25 rpm and 35ºC, the samples were soaked in a dye solution (SYTO 9 live/dead Kit L13152, Molecular Probes) for 15 min. After staining the bacteria deposited on membranes, the membrane surface was viewed with a microscope (Olympus BX51 microscope) equipped with a fluorescent lamp and green/red fluorescence filters and a 4x CCD camera attachment (FVIEW-II, Soft Imaging System, USA). ImageJ software was used to quantify the surface coverage and count number of deposited cells on membrane.

3.4. Results and Discussion

3.4.1. γ^{LW} and γ^- of different membrane chemistries

Figure 3.4a shows the γ^{LW} and γ^- of different membrane chemistries; the values of the same membrane materials were averaged. The dispersive component of each membrane presents similar level between 41~43 mJ/m^2 except the PP membrane, which is considered highly hydrophobic material. This result is consistent with van Oss' analysis that the γ^{LW} value of about 40 mJ/m^2 is common among hydrophilic organic polymers.[26,40] Because the dispersive component is the source for positive interfacial tension and negative free energy, hydrophilic membrane chemistry demands a certain magnitude of γ^- to compensate the hydrophobic contribution of γ^{LW}. van Oss theoretically calculated that $\gamma_s^- \geq 28.3 mJ/m^2$ is required to make the polymer with $\gamma^{LW} = 40 mJ/m^2$ hydrophilic and water-soluble.[26,40]

In contrast to γ^{LW}, γ^- of the membrane surface apparently varies with the given membrane chemistry as presented Figure 3.4b. PANi and PAN membranes, which are recognized highly hydrophilic, demonstrate the highest extent of electron-donicity while PVC, PSF and PP membranes, which are among the hydrophobic materials, do the lowest γ^- magnitude. The highly variable γ^- of different membrane chemistries may be contributed by the variety and complexity in physiochemical mechanism of shaping the Lewis acid-base nature of each material. Since the electron-donicity of a polymeric membrane is determined by the extent of accessible lone pairs in a polymer, chemical composition of the polymer in conjunction with its molecular structure may affect the electron-donor functionality of a membrane.[41]

3.4.2. Combinational impacts of γ^+_{water} *and* $\gamma^-_{membrane}$ *on* ΔG_{132}

As studied in Chapter 2, the high Lewis acidity of water emphasizes the role of the electron-donicity of a solid in the solid-water interfacial interaction. This principle is evaluated in terms of acid-base (AB) interaction and compared to Lifshiz-van der Waals (LW) interaction. Figure 3.5 illustrates how each surface tension component of membrane surface affect the AB interaction and LW interaction of membrane with sodium alginate (Figure 3.5a) and *E.coli* (Figure 3.5b) in aqueous media. Regardless of the biofoulant type, ΔG_{132} is enforced with higher electron-donor property of membrane while greater dispersive property depresses ΔG_{132}, as generally expected. Figure 3.5 apparently reveals another intriguing result that the absolute slopes of AB and LW interaction significantly different; the absolute slope of AB interaction is about 2.5 times greater than the one of LW interaction. The greater change of AB interaction with $\gamma^-_{membrane}$, which more markedly varies with membrane chemistry as discussed in the above section, offers the Lewis donicity of membrane a supreme governance over biofoulant-membrane interfacial interaction.

The original cause of the high influence of $\gamma^-_{membrane}$ on AB interaction can be semi-empirically explained by the elevated Lewis acidity of water compared to biofoulants. Differentiation of Eqn. 3.3 and Eqn. 3.4 with $\sqrt{\gamma_1^{LW}}$ and $\sqrt{\gamma_1^-}$ results in, respectively,

$$\frac{d\Delta G_{132}^{LW}}{d\sqrt{\gamma_1^{LW}}} = 2\left(\sqrt{\gamma_3^{LW}} - \sqrt{\gamma_2^{LW}}\right) \tag{3.9}$$

$$\frac{d\Delta G_{132}^{AB}}{d\sqrt{\gamma_1^-}} = 2\left(\sqrt{\gamma_3^+} - \sqrt{\gamma_2^+}\right) \tag{3.10}$$

Eqn. 3.9 describes that the varying degree of LW interfacial interaction component with $\gamma_{membrane}^{LW}$ is determined by the difference between the corresponding surface tension parameters of water (3) and a biofoulant (1). Because LW surface tension component of water (γ_3^{LW}) is 21.8 mJ/m^2 and its typical value of biofoulant (γ_2^{LW}) is about 40 mJ/m^2, the final solution of Eqn. 3.9 approximately lies in -3.3 mJ$^{0.5}$/m. In the similar approach, the AB interaction shifted by $\gamma_{membrane}^{-}$ is regulated by the different between the electron-accepticities of water and a biofoulant. Majority of biofoulants have electron-donor dominant monopolar surfaces and thus their Lewis acidities are commonly below 1.0 mJ/m^2 or negligible compared to the one of water. Therefore, the final answer of Eqn. 3.10 proximately exists between $2\left(\sqrt{\gamma_3^+}-1\right)$ and $2\sqrt{\gamma_3^+}$ (7.5~10.1 mJ$^{0.5}$/m), which are 2.3~3.1 times greater than the absolute value of Eqn. 3.9.

Understanding the role of the high Lewis acidity of water in the biofoulant-membrane interaction in aqueous media becomes more distinct if ΔG_{132} is analyzed in terms of interfacial tension following Dupré equation:

$$\Delta G_{132} = \gamma_{12} - \gamma_{13} - \gamma_{23} \tag{3.11}$$

Because the interfacial tension is a thermodynamically reverse term of affinity between two substances, Eqn. 3.11 explains that the free energy of adhesion (energy barrier to adhesion) is formed by the membrane-biofoulant-water inter-affinities. In principle, the lower membrane-biofoulant affinity (higher γ_{12}) and higher water-solids affinities (lower γ_{13} and γ_{23}) are able to form higher adhesion energy barrier (ΔG_{132}) to impede the access of biofoulant to membrane by the hydration layer.

Figure 3.6 depicts the interfacial tensions for the aqueous interactions of different membranes with two biofoulants, sodium alginate (a) and *E.coli* (b). The membranes with higher

γ^- clearly tend to have lower membrane-water and membrane-biofoulant interfacial tension, which implies their enhanced affinities to water as wells as biofoulant. Since AB interaction is always an attractive term, the electron-acceptor sites of water as well as biofoulants are leading to draw the electron-donating potentials of membranes and thus generate greater affinities with the membranes owning elevated γ^-. Although higher $\gamma^-_{membrane}$ results in more favorable biofoulant-membrane interaction (lower γ_{12}) and drives a biofoulant to adhere the membrane surface, much more enhanced affinity between water and the membrane (lower γ_{13}) tends to form a stronger hydration layer and aggressively prevent the access of the biofoulant to the membrane surface. The driving component that causes the water-membrane interaction (γ_{13}) to be more critical than the biofoulant-membrane interaction (γ_{12}) is the higher Lewis acidity of water than any other biofoulants; the greater electron-accepting functionality of water succeeds to prevailingly occupy the electron-donor sites of membranes than the biofoulant does.

The role of the elevated Lewis acidity of water in (ΔG_{132}) can be more highlighted when the membrane and the biofoulant are exposed to the warmer water. As the temperature of water increases, water equips more available unbound aqueous hydrogen atoms and gains a stronger electron-accepticity (Table 3.3).[42,43] The increased Lewis acidity of warmer water assists the water molecules to strongly favor the electron-donor sites of a contacting solid and generate a more tightly bound hydration layer, displacement of which can cause a considerable enthalpy gain. Because the electron-accepting sites of a biofoulant experiences a further inferior intensity compared to those of water, water molecules bound on the electron-donor sites of the membrane may be more hardly replaced by a biofoulant, causing higher ΔG_{132}. Figure 3.7 shows the effects of elevated Lewis acidity of warmer water on ΔG_{132}. In the interfacial interaction between the

membrane and alginate through water (Figure 3.7a), the warmer water enhances the energy barrier against adhesion by 8.4~13.3 mJ/m^2; the membranes with greater electron-donicity such as PANi and PAN earn more intensified ΔG_{132} than the ones with inferior electron-donicity (i.e. PVC, PP, and PSf). The interaction of the membrane with *E.coli* acquires a bit better advantage of high Lewis acidity of warmer water due to high electron-donicity of *E.coli*, demonstrating the increase of ΔG_{132} by 13.8~18.7 mJ/m^2. Since the electron-donicity of biofoulant also interact with the electron-basicity of water, the greater Lewis basicity of *E.coli* cooperates energetically with the higher Lewis acidity of warmer water and succeeds to improve ΔG_{132} further. This result reveals that Lewis acidity of water has duel impacts on ΔG_{132} by two separate but additive hydration energies on the membrane surface as well as the biofoulant surface, which will be discussed in the following section.

Table 3.3. Surface tension components of water at different temperatures [42,43]

Temperature (°C)	γ^{LW} (mJ/m^2)	$\gamma+$ (mJ/m^2)	$\gamma-$ (mJ/m^2)	γ^{AB} (mJ/m^2)	γ^{tot} (mJ/m^2)
0	22.8	19.0	37.0	53.0	75.8
20	21.8	25.5	25.5	51.0	72.8
38	21.0	32.4	18.5	49.0	70.0

3.4.3. Effects of $\gamma^-_{biofoulant}$ on ΔG_{132} and demand of $\gamma^-_{membrane}$ for anti-biofouling

As the high Lewis acidity of water leads the water-solid interaction to be a major driving component in ΔG_{132}, the Lewis donicity of a biofoulant also shall play a role as critical as the one of membrane. For instance, compared to sodium alginate, *E.coli* experiences higher energy

barrier because of its greater Lewis donicity and thus its higher water affinity as shown in Figure 3.7a and 3.7b. Figure 3.8 compares γ^- of various biofoulants that a membrane may intact during a separation process. The intensity of electron-donating potential of each biofoulant differs as apparently as the one of membranes already presented. BSA, alginate and SMP, which are considered "sticky" foulants forming irreversible fouling layers on the membrane surface, are among the biofoulants with the lowest γ^-.

The highly varying γ^- properties of different biofoulants induce the biofoulants to have different levels of interfacial interactions with membrane and, especially, water. Since the majority of membranes have trivial extents of γ^+, the high Lewis acidity of water mainly contributes to interfacial interaction of biofoulant with membrane in aqueous media by the biofoulant-water interaction (γ_{23}). The biofoulant with the lower electron-donating functionality can have less hydration cells around its surface due to its inferior water affinity and alleviate the hindrance of the hydration layer when approaching the membrane surface. Figure 3.9 illustrates how $\gamma^-_{biofoulant}$ impacts AB interaction between the membrane and the biofoulant in water. Repeatedly confirmed, as the biofoulants have lower Lewis-donicity, they experience lower AB energy barrier letting them have easier access to the membrane surface. In order to prevent the more favorable adhesion of the biofoulant with low electron-donicity, the contacting membrane surface will be required to have high electron-donicity and bind the water molecules on the surface enough to form as much hydration energy barrier as the biofoulants miss.

The theoretical mechanism that $\gamma^-_{biofoulant}$ controls ΔG^{AB}_{132} can be clearly explained by the simplest formula of ΔG^{AB}_{132} as suggested in Eqn. 3.7:

$$\Delta G^{AB}_{132} = 2\sqrt{\gamma^+_3}\left(\sqrt{\gamma^-_1} + \sqrt{\gamma^-_2}\right) - 2\gamma^{AB}_3 \tag{3.7}$$

The first term in Eqn. 3.7 indicates that the hydration energy formed in water-membrane and water-biofoulant is variable with electron-donicities of membrane and biofoulant and able to control AB interaction between membrane and biofoulant through aqueous media. Although if the biofoulant does not have sufficient electron-donor sites and fails to form the hydration cells, the electron-donor sites of the hydrophilic membrane are able to compensate the inferior hydration layer between the biofoulant and the membrane.

Consequently, Eqn. 3.7 suggests that each membrane separation process demands a specific level of $\gamma^-_{membrane}$ according to the interfacial tension property of the target biofoulant in order to maintain the positive degree of the adhesion energy barrier. This result leads to an idea of proposing an anti-biofouling map that advises the minimum $\gamma^-_{membrane}$ required to form a positive energy barrier to a given biofoulant. Under an assumption that $\gamma^+_{membrane}$ is negligible compared to $\gamma^-_{membrane}$, recalling Eqn. 3.2, Eqn. 3.3 and Eqn. 3.4 with the condition of $\Delta G^{tot}_{132} \geq 0$ results in:

$$2\sqrt{\gamma_m^-}\left(\sqrt{\gamma_l^+}-\sqrt{\gamma_s^+}\right) \geq -\Delta G^{LW}_{mls} - 2\left(\sqrt{\gamma_l^+\gamma_s^-}+\sqrt{\gamma_l^-\gamma_s^+}\right)+2\gamma_l^{AB} \qquad (3.12)$$

Since water has $\gamma_3^+ = \gamma_3^-$, Eqn 3.12 reduces to

$$2\sqrt{\gamma_1^-}\left(1-\sqrt{\gamma_2^+/\gamma_3^+}\right) \geq -\Delta G^{LW}_{132}\Big/\sqrt{\gamma_3^+} - 2\left(\sqrt{\gamma_2^-}+\sqrt{\gamma_2^+}\right)+4\sqrt{\gamma_3^+} \qquad (3.13)$$

Eqn. 3.13 can be more simplified as with assumptions of $\gamma_2^+ \ll \gamma_3^+$ and $\gamma_2^+ \ll \gamma_2^-$

$$\sqrt{\gamma_1^-} \geq -\Delta G^{LW}_{132}\Big/2\sqrt{\gamma_3^+} - \sqrt{\gamma_2^-}+2\sqrt{\gamma_3^+} \qquad (3.14)$$

The insertion of $\gamma_3^{LW} = 21.8\,mJ/m^2$ and $\gamma_3^+ = 25.5\,mJ/m^2$ with approximation of $\gamma_1^{LW} \approx 40 mJ/m^2$ into Eqn. 3.14 leads to

$$\sqrt{\gamma_1^-} \geq 0.33\sqrt{\gamma_2^{LW}} - \sqrt{\gamma_2^-}+8.57 \qquad (3.15)$$

Finally, Eqn. 3.15 supplies an approximate basis determining the minimum γ^- of membrane necessary to establish a repulsive free energy between a given biofoulant and the membrane surface. Figure 3.10 demonstrates Eqn. 3.15 and plots several examples with various biofoulants. It should be noted that the high degree of γ^- of a membrane is able to satisfy the anti-biofouling potential against the biofoulants owning the high γ^{LW} and low γ^-.

3.4.4. Microbial adhesion test

Figure 3.11 shows the fluorescent microscope images of three different membranes (PAN, PES, and PVDF) that contacted the microbial solution. Among tested membranes, PVDF membrane presented largest quantities of attached *E. coli*, indicating that the surface of PVDF is highly favorable to deposition of *E. coli*. In clearly contrast to PVDF, PAN membranes were able to prevent the membrane surface from serious deposition of *E. coli* so that the attached microbes hardly were observed on the surface of PAN membrane. Under the same hydrodynamic condition, the microbial deposition on the membrane surface can be affected by several factors such as surface roughness, heterogeneity of membrane surface, existence of a concentration layer by rejected ions and surface chemistry (hydrophobicity).[22,44] Unlike the dense membranes (NF/RO), the tested porous membranes are considered to have as smooth surfaces as their surface morphologies may have little impact on microbial adhesion. Also the test protocol does not contain any separation process that may cause formation of a concentration layer on the tested membranes. Therefore, the surface chemistry is considered to be a main factor to control the microbial adhesion on the membrane surface.

Figure 3.12 shows the electron-donicities of the test membranes and analyzes their interfacial interactions with *E.coli* through water. As the membrane has higher electron-donating

functionality, greater affinity with *E.coli* in direct contact is found (lower γ_{12}). However, the greater γ^- of membrane also leads to elevated hydration energy (lower γ_{13}) and results in higher free energy barrier against the *E.coli* surface (ΔG_{132}). Although a quantitative consistency is not exactly found in the relationship between the extent of microbial deposition and γ^- and ΔG_{132} of membrane, the order of microbial deposition on membrane surfaces reversely follows the order of γ^- and ΔG_{132} of membrane implying that the thermodynamic analysis on the affinity between the membranes and *E.coli* can qualitatively predict the microbial adhesion tendencies of membranes.

3.4.5. Biofouling test

Figure 3.13 shows the fouling behaviors of the three membranes during cross-flow filtration of the alginate solution with a constant flux of 100 LMH. Different fouling rates are observed at the different membrane chemistries: PVDF membrane suffered the rapidest TMP increase due to cake formation and concentration polarization and PES membrane exhibited the next fastest fouling rate followed by PAN membrane. The order of fouling rates of membranes reversely corresponds to the order of the free energy barriers of adhesion as illustrated in Figure 3.14. The PAN membrane, which performed the lowest biofouling with alginate solution, is characterized with the highest interaction energy barrier ($\Delta G_{132} = -7.2\, mJ/m^2$) while the most favorable interaction with alginate particles is found at the surface of PVDF membrane ($\Delta G_{132} = -20.1\, mJ/m^2$) being most vulnerable to biofouling of alginate solution. There are several research studies that tested different materials of porous membranes with a synthetic biofoulant solution such as alginate, BSA, actual SMPs, and NOM and they reported the similar

consistent relationship between the interaction energy calculated by the thermodynamic theory and the experimental biofouling with a synthetic biofoulant solution. [32,34,37,45,46] It should be noted that the extent of interaction energy barriers in those studies as well as this study is attributed to the intensity of electron-donicities of the test membranes as already shown in Figure 3.5 and Figure 3.6.

Biofouling tests of the three membranes were conducted in the continuously operated MBR, which is a complex biological system that contains the mixture of various microbial species and their exopolymers and aggregated flocs, and feed organic solution. The MBR was operated with the finest conditions such as 99% of COD removal, 95% of nitrification efficiency, large floc size over 100 um, no excessive filamentous bacteria, and low SMP concentrations (less than 15 mg Protein/L). With the help of an exemplary microbiological status of the MBR, the bioreactor caused exceedingly low biofouling to PVDF and PES membranes as depicted Figure 3.15. However, PAN membrane suffered from a suddenly deteriorated bioreactor possibly due to the biodegradation of the membrane surface and its toxic effects on the microbial community and experienced severe biofouling after 40 hours. Excluding the period that PAN membrane encountered deterioration of the MBR, the biofouling tendencies of the test membranes followed their thermodynamic biofoulant-affinities, which are originally determined by the degrees of γ^- of the membrane surfaces as shown in Figure 3.16. The biofouling tests of Li (2013) and Zhang (2015) in their own accustomed MBRs also reveal the same results for the latent correlation between the experimental anti-biofouling property and γ^- of the membrane. [47,48]

Figure 3.17 summarizes the relationship between $\gamma^-_{membrane}$ and microbial adhesion and biofouling rates of the test membranes. Microbial adhesion decreased exponentially as $\gamma^-_{membrane}$ increased while biofouling rates either in the alginate cross-flow filtration and in the MBR

became abating almost linearly with $\gamma^-_{membrane}$. The inverse correlations of those biofouling tendencies with $\gamma^-_{membrane}$ reveal a reliable potential of $\gamma^-_{membrane}$ as a qualitative and quantitative indicator for the anti-biofouling property of a membrane. However, it should be emphasized that the impacts of $\gamma^-_{membrane}$ on biofouling can be depreciated by other membrane surface characteristics such as pore-size distribution and zeta potential so that the slight difference of $\gamma^-_{membrane}$ may fail to apparently differentiate the biofouling tendency.

3.5. Summary

The thermodynamic mechanism of biofouling was investigated using the surface-tension-based theory that van Oss proposed. The high electron-accepticity of water emphasized the importance of γ^- of a membrane and a biofoulant in their interfacial interaction through water and drove acid-base interaction to be a major interaction component in the interfacial interactions between membranes and a biofoulant (ΔG_{132}). Because polymeric porous membranes exhibit similar levels of dispersive properties but exceedingly various intensities of the electron-donicities, acid-base interaction than Lifshiz-van der Waals interaction seriously differentiated ΔG_{132}. The surfaces of various biofoulants are also characterized with highly variable electron-donicities and the biofoulant with lower electron donicity can be more vulnerable to biofouling due to the inferior hydration energy formed on the surface of the biofoulant and thus lower ΔG_{132}. The inferior hydration energy by a low electron-donicity of a biofoulant can be compensated by an enhanced electron-donicity of a membrane; this fact leads to propose a standard of an electron-donicity demand for a membrane to have a positive ΔG_{132} with a given biofoulant. Experimental results of a microbial adhesion test and biofouling tests qualitatively correlated well with tendencies of electron-donicities of the test membranes, proving an electron-donicity of a membrane to be a reasonable indicator for the anti-biofouling property of the membrane.

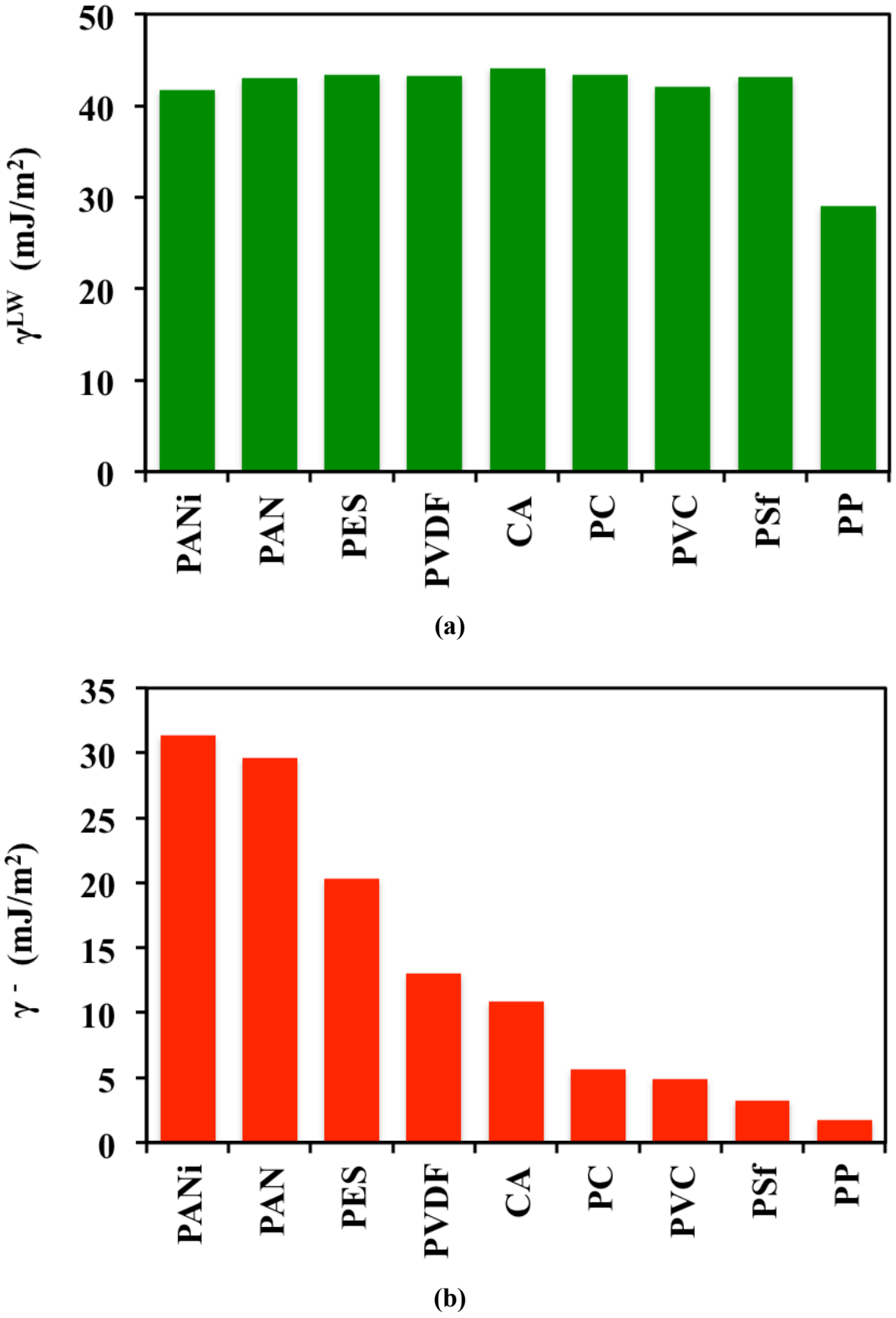

Figure 3.4. γ^{LW} (a) and γ^- (b) of different membrane chemistries. (Average values of data in Table 3.1 were employed)

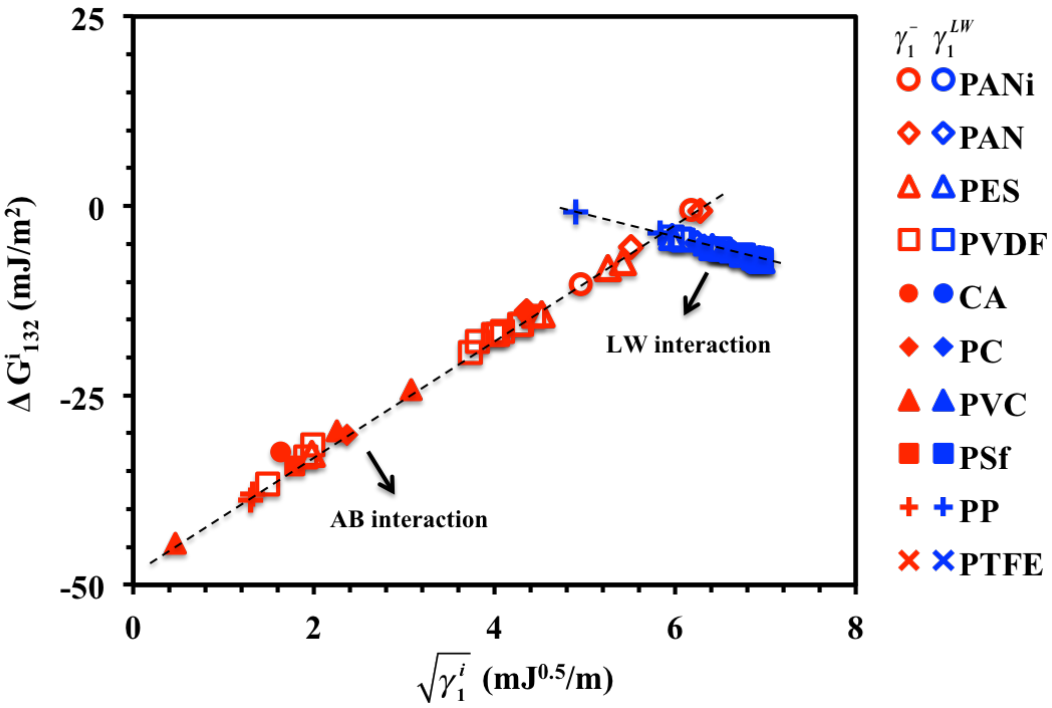

(a)

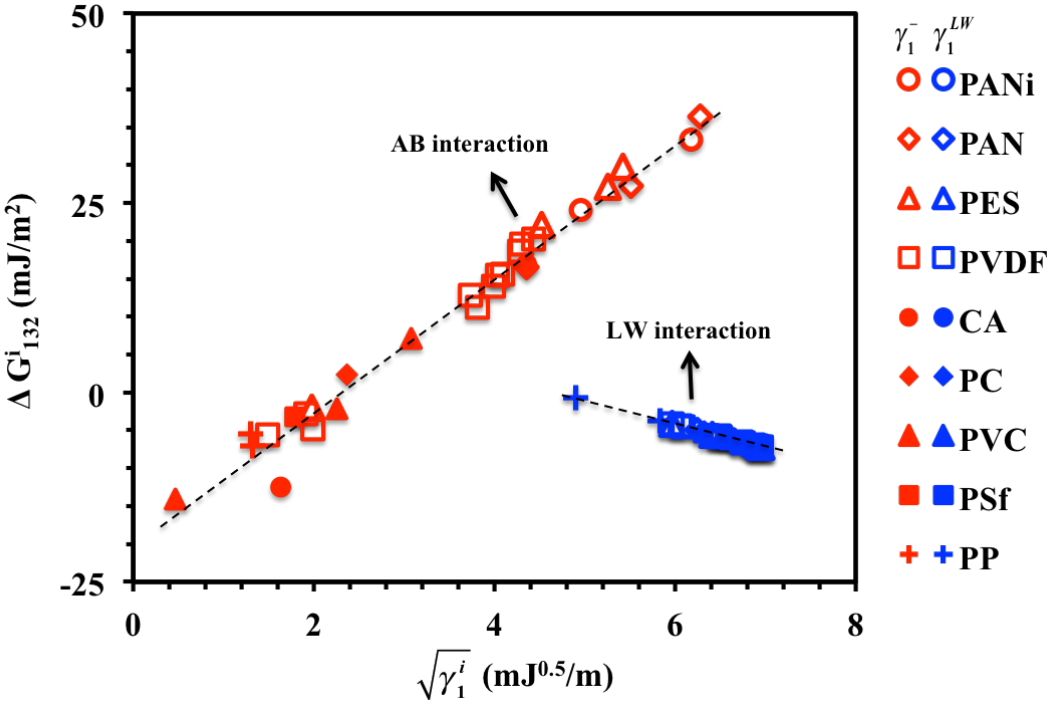

(b)

Figure 3.5 Impacts of γ^- and γ^{LW} of membrane on ΔG_{132} with sodium alginate (a) and *E.coli* (b). (Data in Table 3.1 were employed)

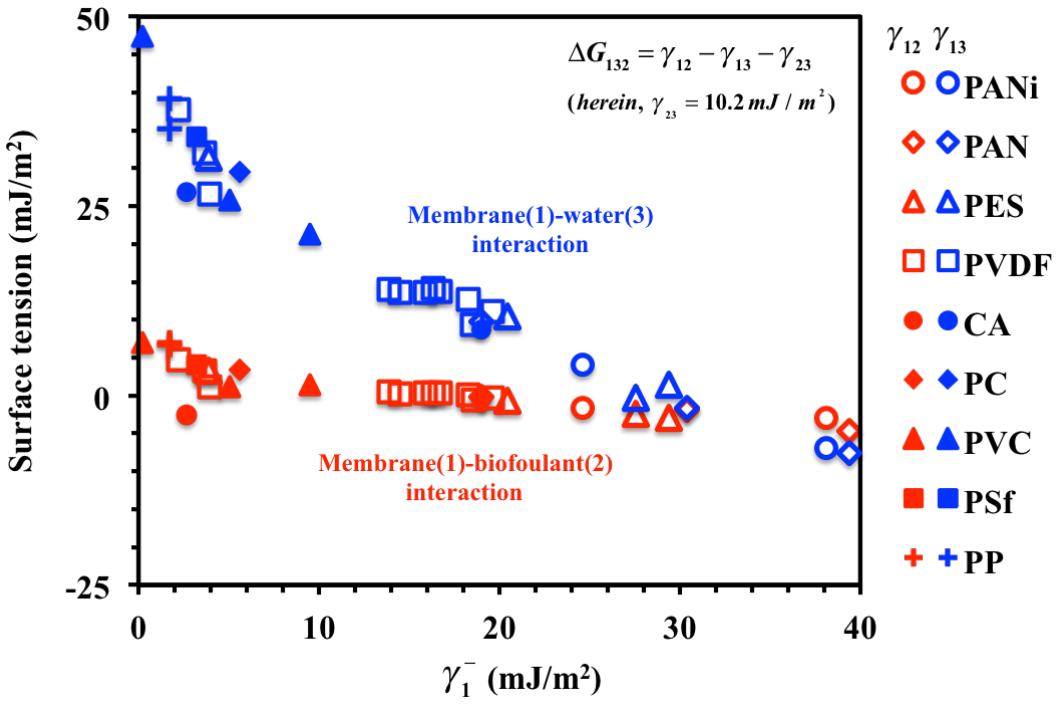

(a)

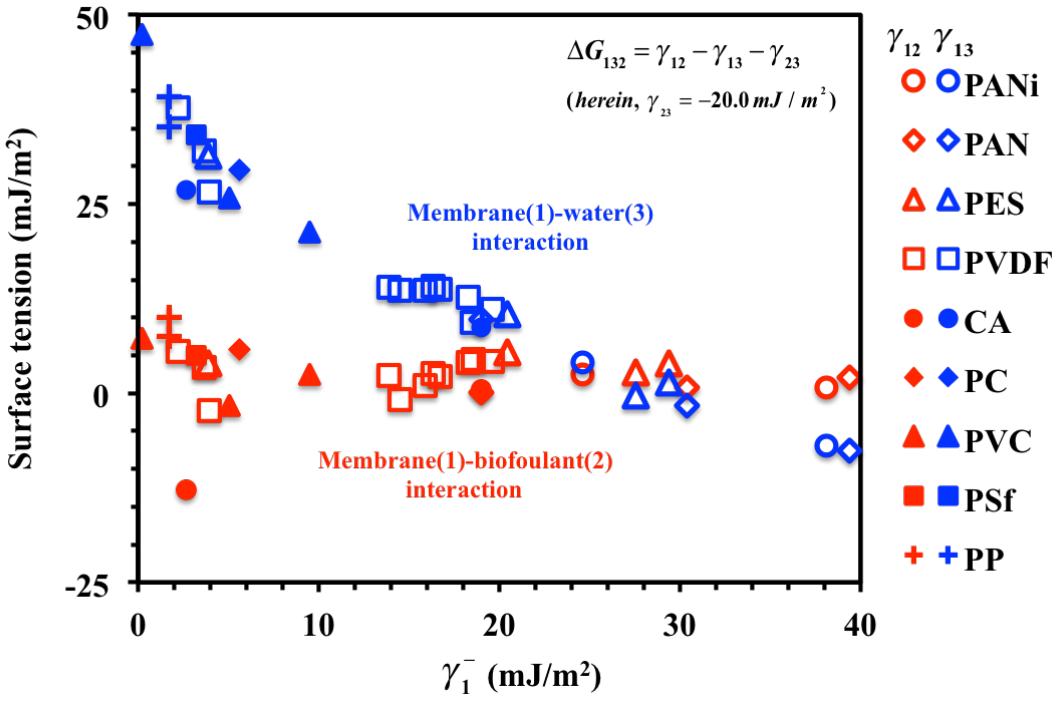

(b)

Figure 3.6. Impacts of γ^- of membrane on surface tension components in the interaction with alginate (a) and *E.coli* (b). (Data in Table 3.1 were employed)

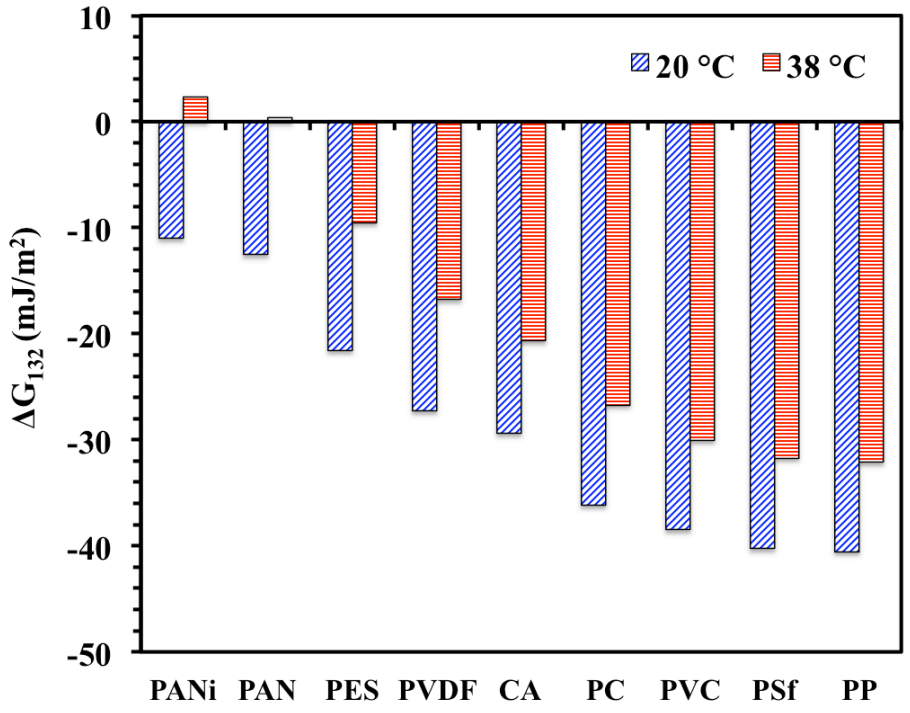

(a)

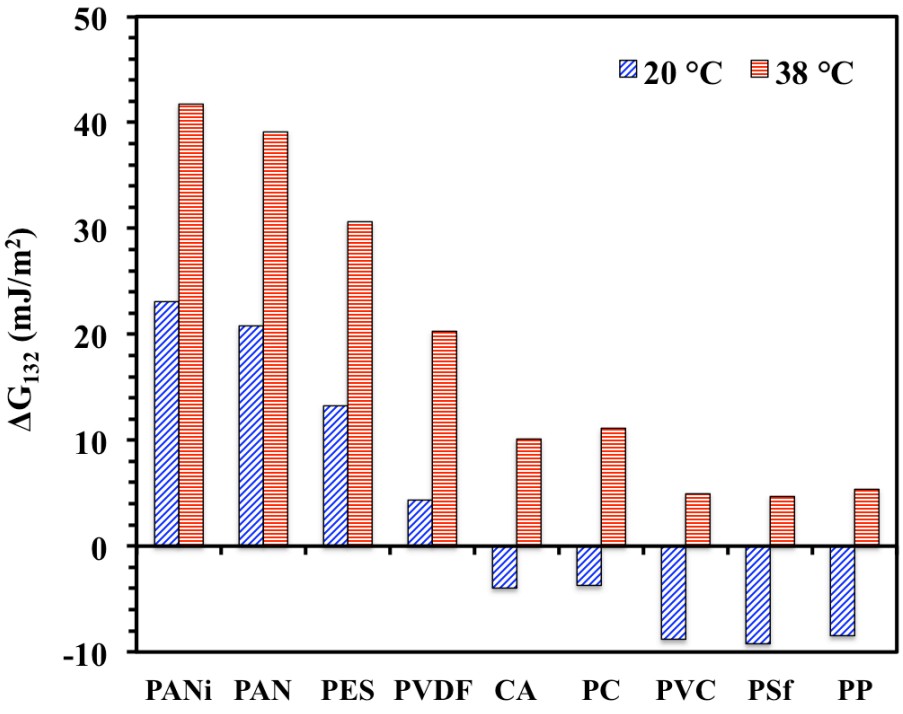

(b)

Figure 3.7. Effects of water temperature on ΔG_{132} with alginate (a) and *E.coli* (b). (Average values of Data in Table 3.1 were employed)

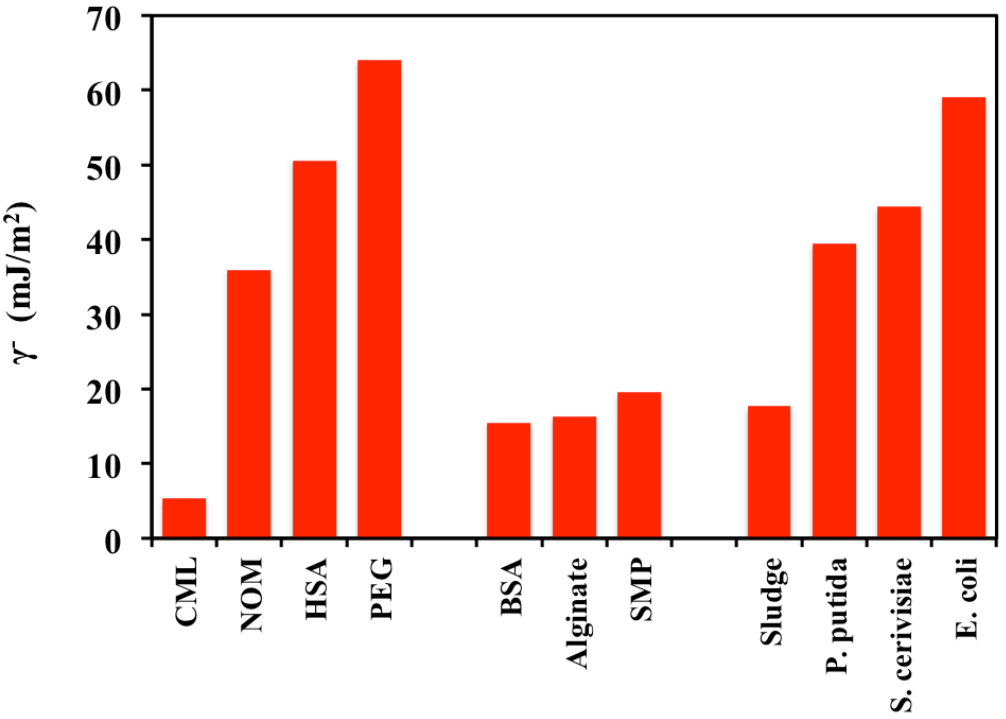

Figure 3.8. γ^- of different biofoulants

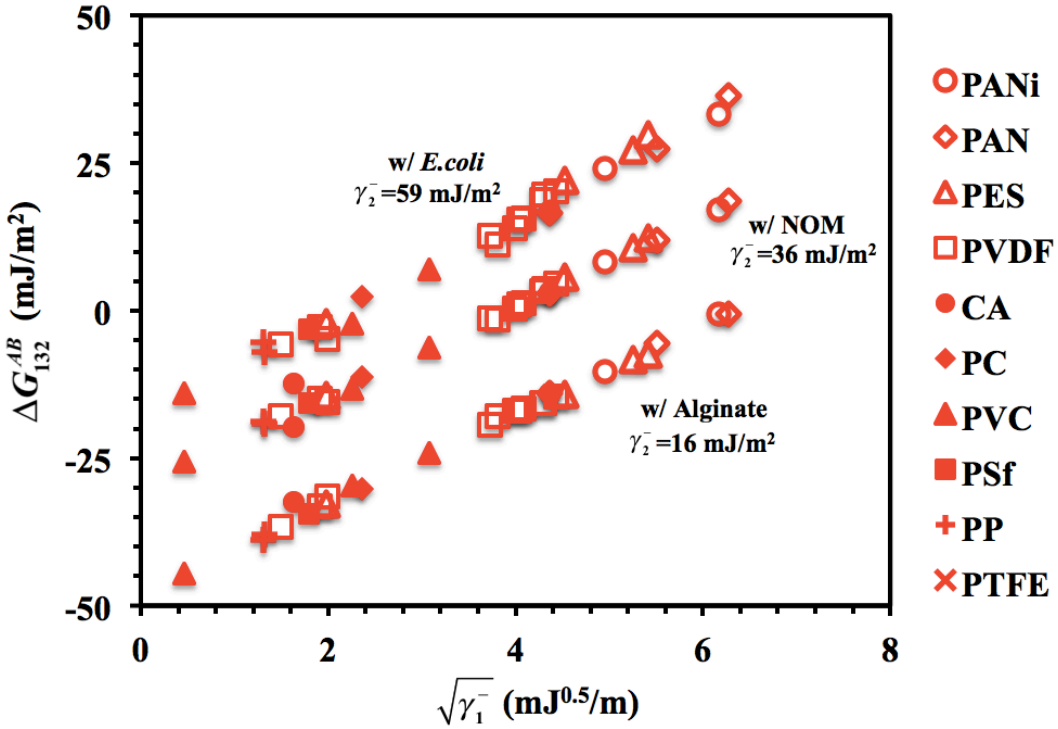

Figure 3.9. ΔG_{132}^{AB} of different biofoulants with varying γ_1^-
(Data in Table 3.1 were employed)

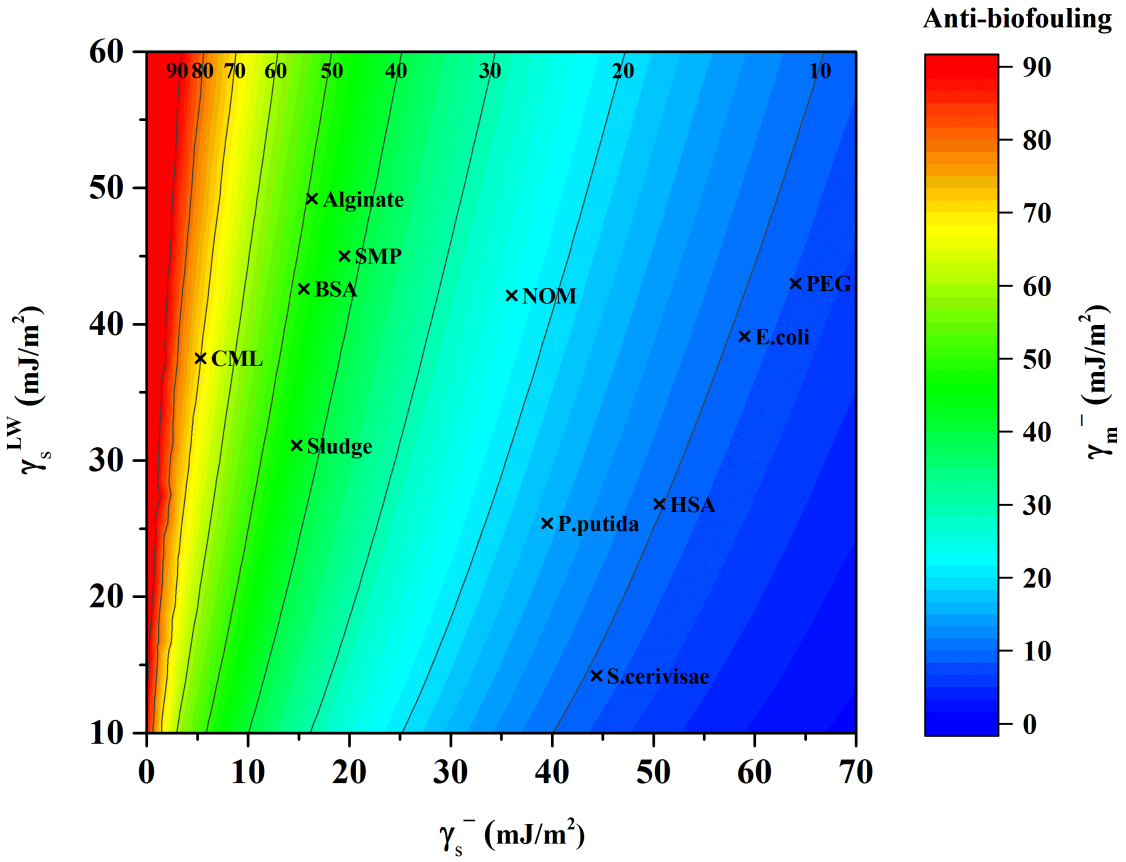

Figure 3.10. Anti-biofouling demand for the electron-donicity of membrane according to the surface chemistries of a given biofoulant

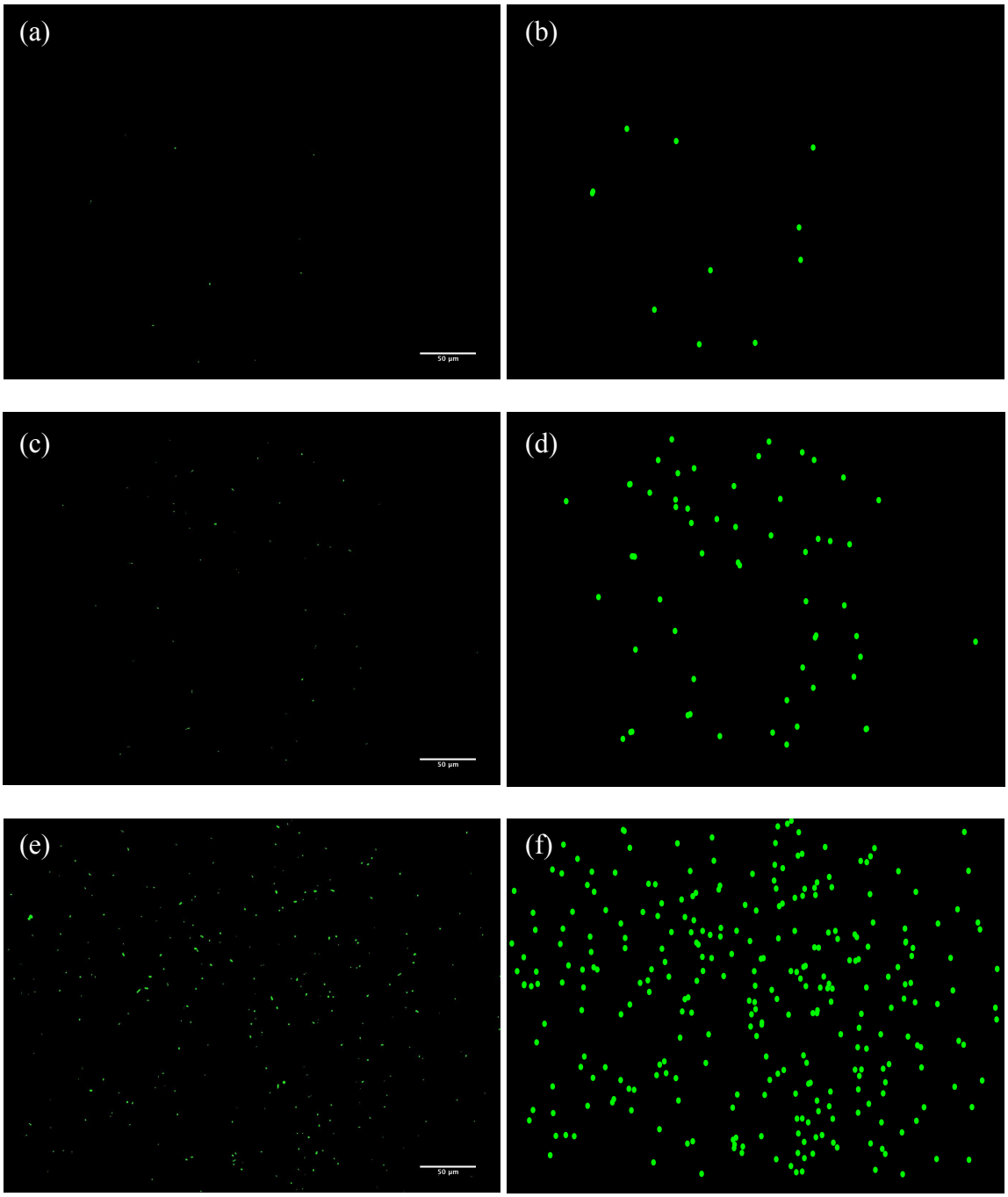

Figure 3.11. Microbial deposition on PAN (a,b), PES (c,d), and PVDF (e,f) membrane.
(Left column: raw images; Right column: clearly replotted images)

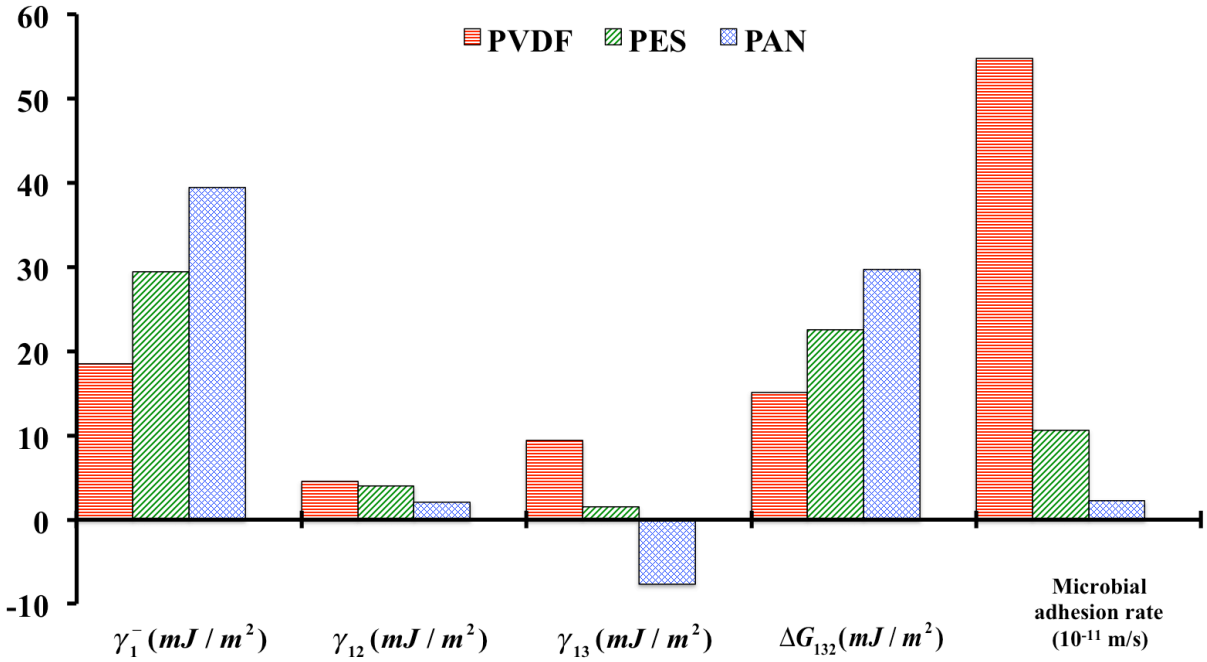

Figure 3.12. Microbial adhesion tendencies of test membranes and their thermodynamic properties

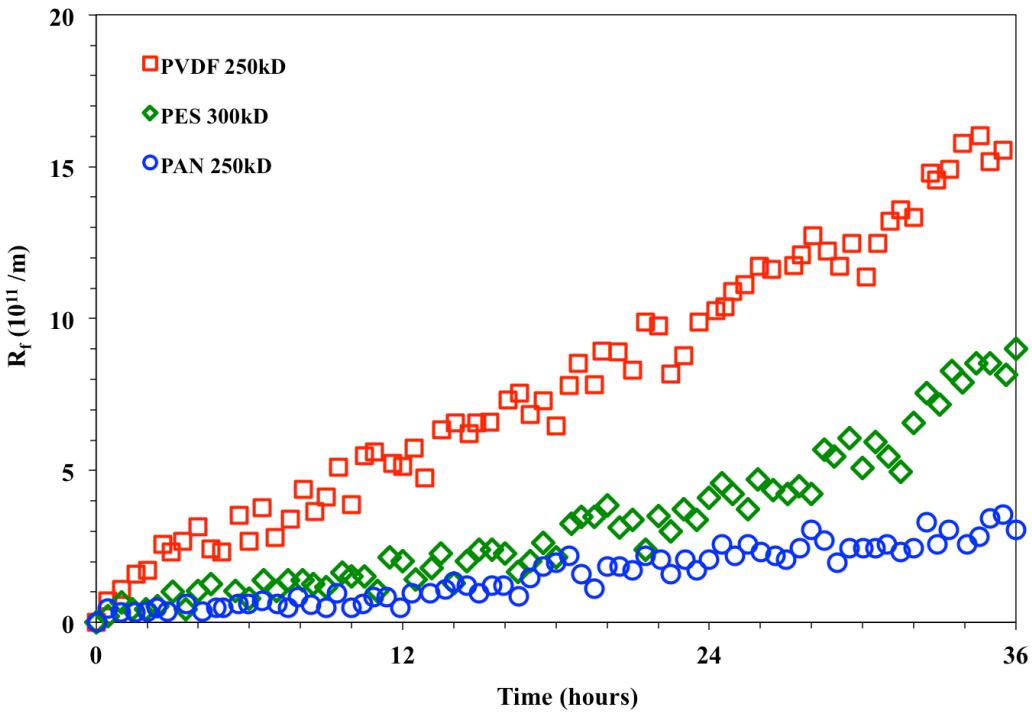

Figure 3.13. Biofouling behaviors of three membranes with alginate solution (200 mg/L sodium alginate, Flux=100 LMH, Re=100)

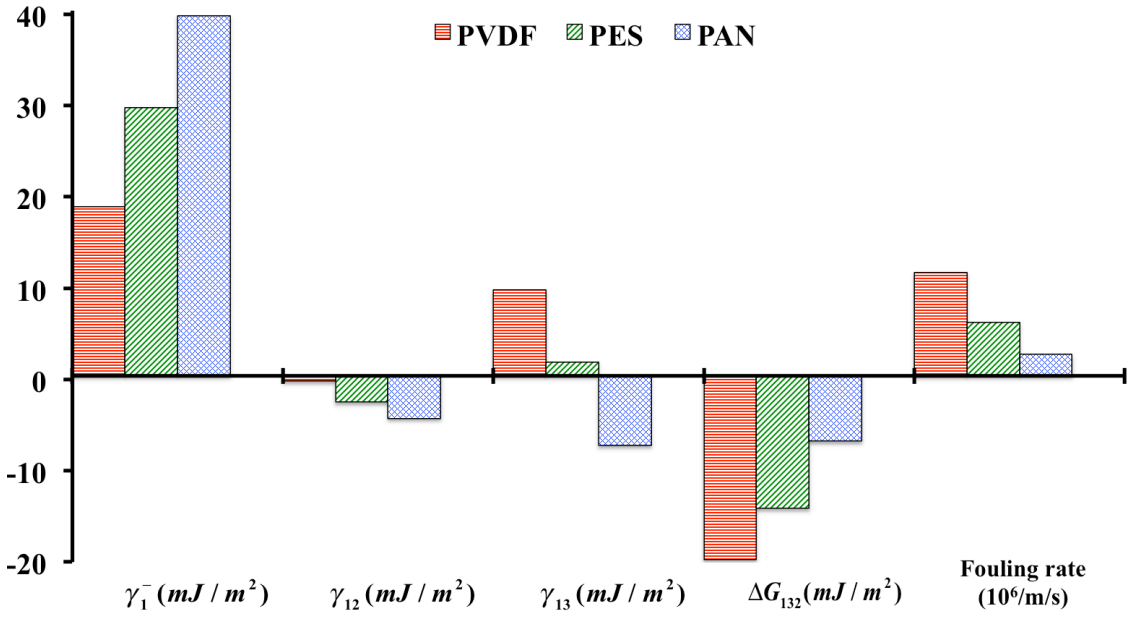

Figure 3.14. Biofouling tendencies of test membranes and their thermodynamic properties (Test biofoulant: alginate solution)

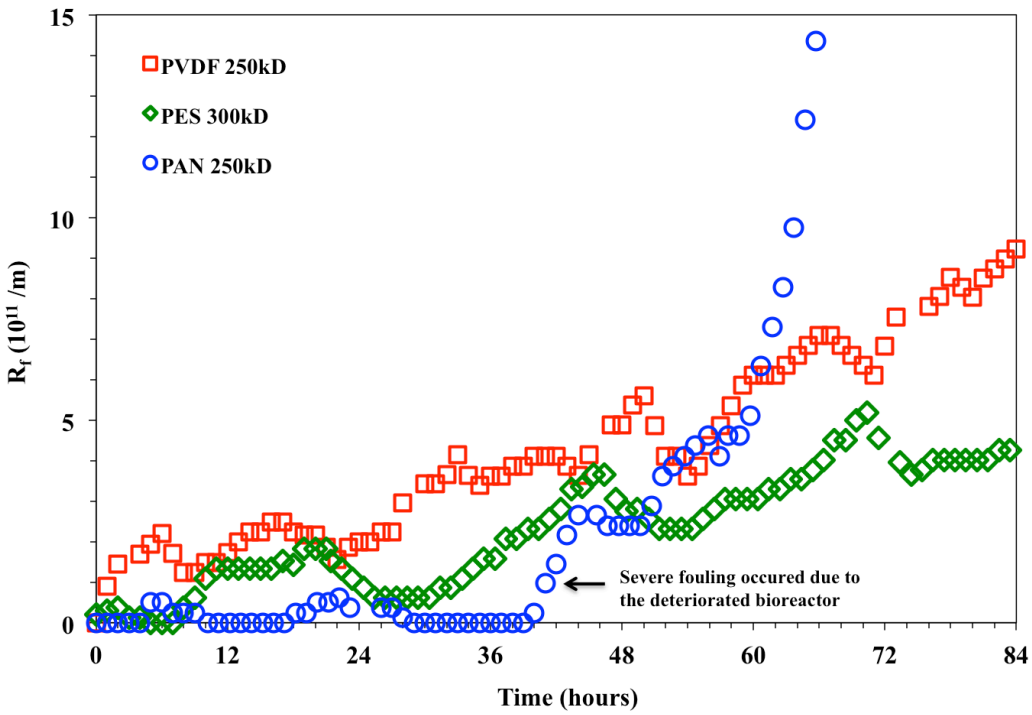

Figure 3.15. Biofouling behaviors of three membranes in a membrane bioreactor (Flux=24 LMH)

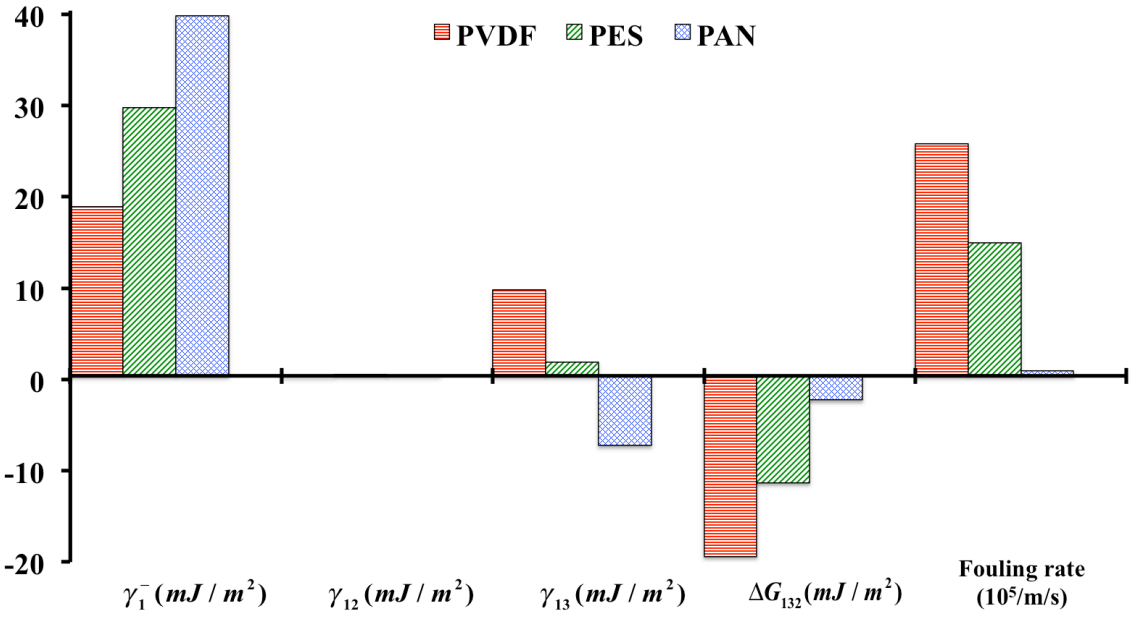

Figure 3.16. Biofouling tendencies of test membranes and their thermodynamic properties (Test system: a submerged type of membrane bioreactor)

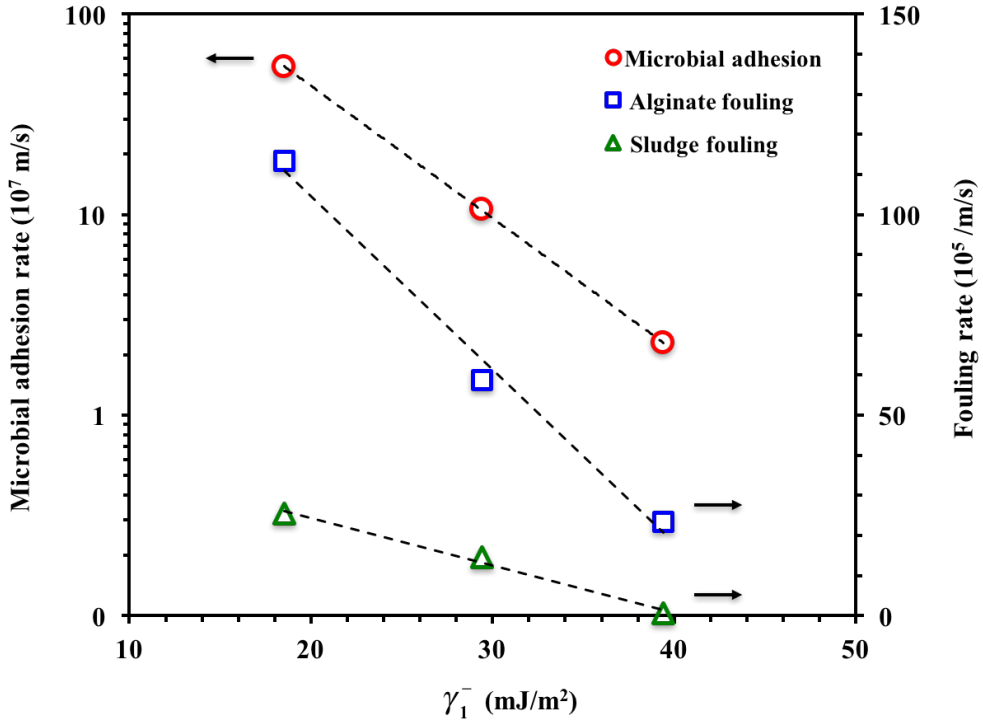

Figure 3.17. Correlation of γ_1^- with microbial deposition and biofouling rates

References

(1) Meng, F.; Zhang, H.; Yang, F.; Li, Y.; Xiao, J.; Zhang, X. Effect of filamentous bacteria on membrane fouling in submerged membrane bioreactor. *Journal of Membrane Science* **2006**, *272* (1-2), 161–168.

(2) Chang, I. S.; Le-Clech, P.; Jefferson, B. Membrane fouling in membrane bioreactors for wastewater treatment. *Journal of Environmental Engineering* **2002**.

(3) Guillen, G. R.; Pan, Y.; Li, M.; Hoek, E. M. V. Preparation and Characterization of Membranes Formed by Nonsolvent Induced Phase Separation: A Review. *Ind. Eng. Chem. Res.* **2011**, *50* (7), 3798–3817.

(4) Elimelech, M.; Phillip, W. A. The future of seawater desalination: energy, technology, and the environment. *Science* **2011**, *333* (6043), 712–717.

(5) Shannon, M. A.; Bohn, P. W.; Elimelech, M.; Georgiadis, J. G.; Mariñas, B. J.; Mayes, A. M. Science and technology for water purification in the coming decades. *Nature* **2008**, *452* (7185), 301–310.

(6) Montgomery, M. A.; Elimelech, M. Water and sanitation in developing countries: Including health in the equation. *Environ. Sci. Technol.* **2007**, *41* (1), 17–24.

(7) Kerry J Howe; Ashish Marwah; Kuang-Ping Chiu, A.; Adham, S. S. Effect of Coagulation on the Size of MF and UF Membrane Foulants. *Environ. Sci. Technol.* **2006**, *40* (24), 7908–7913.

(8) Meng, F.; Zhang, H.; Yang, F.; Li, Y.; Xiao, J.; Zhang, X. Effect of filamentous bacteria on membrane fouling in submerged membrane bioreactor. *Journal of Membrane Science* **2006**, *272* (1-2), 161–168.

(9) Lee, N.; Amy, G.; Croué, J.-P.; Buisson, H. Identification and understanding of fouling in low-pressure membrane (MF/UF) filtration by natural organic matter (NOM). *Water Research* **2004**, *38* (20), 4511–4523.

(10) Decarolis, J.; Hong, S. K.; Taylor, J. Fouling behavior of a pilot scale inside-out hollow fiber UF membrane during dead-end filtration of tertiary wastewater. *Journal of Membrane Science* **2001**, *191* (1-2), 165–178.

(11) Cho, J.; Amy, G.; Pellegrino, J. Membrane filtration of natural organic matter: factors and mechanisms affecting rejection and flux decline with charged ultrafiltration (UF) membrane. *Journal of Membrane Science* **2000**, *164* (1-2), 89–110.

(12) Baker, J. S.; Dudley, L. Y. Biofouling in membrane systems — A review. *Desalination* **1998**, *118* (1-3), 81–89.

(13) Zhu, X.; Elimelech, M. Colloidal fouling of reverse osmosis membranes: measurements and fouling mechanisms. *Environ. Sci. Technol.* **1997**.

(14) Choo, K. H.; Lee, C. H. Membrane fouling mechanisms in the membrane-coupled anaerobic bioreactor. *Water Research* **1996**, *30* (8), 1771–1780.

(15) Liu, F.; Du, C.-H.; Zhu, B.-K.; Xu, Y.-Y. Surface immobilization of polymer brushes onto porous poly(vinylidene fluoride) membrane by electron beam to improve the hydrophilicity and fouling resistance. *Polymer* **2007**, *48* (10), 2910–2918.

(16) Li Liu; Mark H Engelhard, A.; Mingdi Yan. *Surface and Interface Control on Photochemically Initiated Immobilization*; American Chemical Society, 2006; Vol. 128, pp 14067–14072.

(17) Cornelissen, E. R.; van den Boomgaard, T.; Strathmann, H. Physicochemical aspects of

polymer selection for ultrafiltration and microfiltration membranes. *Colloids and Surfaces A: Physicochemical and Engineering Aspects* **1998**, *138*, 283–289.
(18) Brant, J. A.; Childress, A. E. Assessing short-range membrane–colloid interactions using surface energetics. *Journal of Membrane Science* **2002**.
(19) Kim, S.; Marion, M.; Jeong, B.-H.; Hoek, E. M. V. Crossflow membrane filtration of interacting nanoparticle suspensions. *Journal of Membrane Science* **2006**, *284* (1-2), 361–372.
(20) Kim, S.; Hoek, E. M. V. Interactions controlling biopolymer fouling of reverse osmosis membranes. *Desalination* **2007**, *202* (1-3), 333–342.
(21) Jin, X.; Huang, X.; Hoek, E. M. V. Role of Specific Ion Interactions in Seawater RO Membrane Fouling by Alginic Acid. *Environ. Sci. Technol.* **2009**, *43* (10), 3580–3587.
(22) Subramani, A.; Hoek, E. M. V. Biofilm formation, cleaning, re-formation on polyamide composite membranes. *Desalination* **2010**, *257* (1-3), 73–79.
(23) Wang, Q.; Wang, Z.; Zhu, C.; Mei, X.; Wu, Z. Assessment of SMP fouling by foulant–membrane interaction energy analysis. *Journal of Membrane Science* **2013**, *446* (C), 154–163.
(24) Wang, J.; Mo, Y.; Mahendra, S.; Hoek, E. M. V. Effects of water chemistry on structure and performance of polyamide composite membranes. *Journal of Membrane Science* **2014**, *452* (C), 415–425.
(25) van Oss, C. J. Development and applications of the interfacial tension between water and organic or biological surfaces. *Colloids and Surfaces B: Biointerfaces* **2007**, *54* (1), 2–9.
(26) van Oss, C. J. Acid—base interfacial interactions in aqueous media. *Colloids and Surfaces A: Physicochemical and Engineering Aspects* **1993**, *78*, 1–49.
(27) Hong, H.; Peng, W.; Zhang, M.; Chen, J.; He, Y.; Wang, F.; Weng, X.; Yu, H.; Lin, H. Thermodynamic analysis of membrane fouling in a submerged membrane bioreactor and its implications. *Bioresource Technology* **2013**, *146* (C), 7–14.
(28) Feng, L.; Li, X.; Du, G.; Chen, J. Adsorption and fouling characterization of Klebsiella oxytoca to microfiltration membranes. *Process Biochemistry* **2009**, *44* (11), 1289–1292.
(29) Lin, H.; Zhang, M.; Mei, R.; Chen, J.; Hong, H. A novel approach for quantitative evaluation of the physicochemical interactions between rough membrane surface and sludge foulants in a submerged membrane bioreactor. *Bioresource Technology* **2014**, *171* (C), 247–252.
(30) Hong, H.; Zhang, M.; He, Y.; Chen, J.; Lin, H. Fouling mechanisms of gel layer in a submerged membrane bioreactor. *Bioresource Technology* **2014**, *166* (C), 295–302.
(31) Wang, Q.; Wang, Z.; Zhu, C.; Mei, X.; Wu, Z. Assessment of SMP fouling by foulant–membrane interaction energy analysis. *Journal of Membrane Science* **2013**, *446* (C), 154–163.
(32) Chen, L.; Tian, Y.; Cao, C.-Q.; Zhang, J.; Li, Z.-N. Interaction energy evaluation of soluble microbial products (SMP) on different membrane surfaces: Role of the reconstructed membrane topology. *Water Research* **2012**, *46* (8), 2693–2704.
(33) Chen, J.; Shen, L.; Zhang, M.; Hong, H.; He, Y.; Liao, B.-Q.; Lin, H. Thermodynamic analysis of effects of contact angle on interfacial interactions and its implications for membrane fouling control. *Bioresource Technology* **2016**, *201*, 245–252.
(34) Lin, T.; Lu, Z.; Chen, W. Interaction mechanisms and predictions on membrane fouling in an ultrafiltration system, using the XDLVO approach. *Journal of Membrane Science* **2014**, *461* (C), 49–58.

(35) Zhang, J.; Wang, Q.; Wang, Z.; Zhu, C.; Wu, Z. Modification of poly(vinylidene fluoride)/polyethersulfone blend membrane with polyvinyl alcohol for improving antifouling ability. *Journal of Membrane Science* **2014**, *466* (C), 293–301.
(36) Zhang, Y.; Zhang, M.; Wang, F.; Hong, H.; Wang, A.; Wang, J.; Weng, X.; Lin, H. Membrane fouling in a submerged membrane bioreactor: Effect of pH and its implications. *Bioresource Technology* **2014**, *152* (C), 7–14.
(37) Lee, S.; Kim, S.; Cho, J.; Hoek, E. M. V. Natural organic matter fouling due to foulant–membrane physicochemical interactions. *Desalination* **2007**, *202* (1-3), 377–384.
(38) Guillen, G. R.; McVerry, B. T.; Kaner, R. B.; Hoek, E. M. V. Tuning the properties of polyaniline-based ultrafiltration membranes with chemical post-treatment. *Journal of Membrane Science*.
(39) Yang, R.; Xu, J.; Ozaydin-Ince, G.; Wong, S. Y.; Gleason, K. K. Surface-Tethered Zwitterionic Ultrathin Antifouling Coatings on Reverse Osmosis Membranes by Initiated Chemical Vapor Deposition. *Chem. Mater.* **2011**, *23* (5), 1263–1272.
(40) van Oss, C. J.; Chaudhury, M. K.; Good, R. J. Monopolar surfaces. *Advances in Colloid and Interface Science* **1987**, *28* (1), 35–64.
(41) Morra, M. On the molecular basis of fouling resistance. *Journal of Biomaterials Science, Polymer Edition* **2000**, *11* (6), 547–569.
(42) van Oss, C. J.; Giese, R. F. Role of the Properties and Structure of Liquid Water in Colloidal and Interfacial Systems. *Journal of Dispersion Science and Technology* **2008**, *25* (5), 631–655.
(43) van Oss, C. J.; Giese, R. F. Role of the Polar Properties of Water in Separation Methods. *Separation & Purification Reviews* **2011**, *40* (3), 163–208.
(44) Hoek, E. M. V.; Bhattacharjee, S.; Elimelech, M. Effect of Membrane Surface Roughness on Colloid−Membrane DLVO Interactions. *Langmuir* **2003**, *19* (11), 4836–4847.
(45) Lin, T.; Shen, B.; Chen, W.; Zhang, X. Interaction mechanisms associated with organic colloid fouling of ultrafiltration membrane in a drinking water treatment system. *Desalination* **2014**, *332* (1), 100–108.
(46) Liang, S.; Kang, Y.; Tiraferri, A.; Giannelis, E. P.; Huang, X.; Elimelech, M. Highly hydrophilic polyvinylidene fluoride (PVDF) ultrafiltration membranes via postfabrication grafting of surface-tailored silica nanoparticles. *ACS Appl Mater Interfaces* **2013**, *5* (14), 6694–6703.
(47) Li, Z.; Tian, Y.; Ding, Y.; Chen, L.; Wang, H. Fouling potential evaluation of soluble microbial products (SMP) with different membrane surfaces in a hybrid membrane bioreactor using worm reactor for sludge reduction. *Bioresource Technology* **2013**, *140* (C), 111–119.
(48) Zhang, M.; Liao, B.-Q.; Zhou, X.; He, Y.; Hong, H.; Lin, H.; Chen, J. Effects of hydrophilicity/hydrophobicity of membrane on membrane fouling in a submerged membrane bioreactor. *Bioresource Technology* **2015**, *175* (C), 59–67.

Chapter 4

NOVEL, SMALL MOLECULE PERFLUOROPHENYLAZIDE COATINGS FOR SYNTHEIS OF BIOFOULING-RESISTANT MEMBRANE

4.1. Introduction

In the previous chapters, the simulation and experimental results demonstrated that the electron-donicity of a membrane suitably represents a biofouling-resistant property and hydrophilicity of a given membrane. These results motivate that improvement of electron-donor functionality of a given membrane may augment the anti-biofouling feature of a membrane if the membrane modification does not significantly alter other surface properties such as pore size, roughness, and dispersive component of surface tension. In order to achieve the above conditions, this study considers a grafting method using a polymer that contains several atoms where lone pairs of electron exist. The grafting method may coat the membrane surface with a shortly chained polymer at low surface density in order to avoid modifying the membrane surface morphology unnecessarily. Because hydrophilicity ($\Delta \boldsymbol{G}_{131}$) and biofouling-resistance ($\Delta \boldsymbol{G}_{132}$) are inherently correlated due to existence of the hydration energy barrier as discussed in Chapter 3, a polymer containing hydrophilic chains or groups can be considered as an appropriate candidate for anti-biofouling grafting.

Previously, McVerry et al. (2014) developed a grafting method that successfully modified the polymeric dense membranes using perfluorophenyl azide (PFPA) - a photoactive hydrophilic polymer.[1] The azide functionality of PFPA can be photo-activated to expel nitrogen gas (N_2) from nitrene, binding it with –NH- and C=C bonds of polymers in contact (herein, membrane surface). Since the terminal group of PFPA can be easily replaced by other target species of either long-chained or short-chained polymers, several hydrophilic PFPA derivatives with low molecular weights are synthesized and utilized to modify a commercial polymeric UF membrane. Surface tension properties of the unmodified and modified membranes are analyzed and correlated with the biofouling-resistant capabilities of the test membranes.

4.2. Theory

When a foulant contacts the membrane surface in solution, it experiences hydrodynamic forces and interfacial forces, which control the transport and deposition of the foulants. [2,3] With varying polymeric materials, interfacial forces determine the affinities of foulants to the polymer surface for the same foulants in solution, because hydrodynamic forces on these foulants are theoretically identical. Therefore, Kim et al. [4] defines the interfacial force as the sum of the Lifshitz-van der Waals force, the acid-base force and the electrostatic force, excluding any hydrodynamic forces. The mathematical expressions of these forces are summarized in Eqn. 4.1-4.3 as follows:[2,3]

Lifshitz–van der Waals force $$F_{LW} = 2\pi h_0^2 \Delta G_{132}^{LW} a_p \left(\frac{1}{h^2}\right)\left(1+\frac{5.32h}{\lambda_{LW}}\right)^{-1} \quad (4.1)$$

Acid-base force $$F_{AB} = 2\pi \Delta G_{132}^{AB} a_p \exp\left(-\frac{h_0 - h}{\lambda_{AB}}\right) \quad (4.2)$$

Electrostatic force $$F_{EL} = 4\pi\varepsilon\left(\frac{zF}{RT}\right)^2\left(\frac{\gamma_c\gamma_m}{\lambda_{EL}}\right)a_p \exp\left(-\frac{h}{\lambda_{EL}}\right) \quad (4.3)$$

where μ is the dynamic viscosity of the liquid, a_p is the radius of particle, v_w is the flow velocity, ϕ_H is the hydrodynamic correction factor (a function of membrane permeability, particle size and the particle separation distance), ρ_p is the particle density, ρ_l is the liquid density, h is the interfacial separation distance, h_0 is the minimum separation distance (0.157 nm), ΔG_{132}^{LW} and ΔG_{132}^{AB} the Lifshitz–van der Waals and Lewis acid–base interfacial free energies, λ_{LW} (= 100 nm), λ_{AB} ($\cong$ 0.6 nm), and λ_{EL} (= $[3.28\times10^9\sqrt{C_{NaCl}}]^{-1}$) are characteristic decay lengths for LW, AB, and EL interactions in water, ε the dielectric permittivity of water (= $78.5\times8.854\times10^{-12}CV^{-1}m^{-1}$), Υ_c and Υ_m are dimensionless surface (zeta) potentials $(\tanh[zF\zeta_{c/m}/4RT])$, and ζ_c and ζ_m are the

zeta potentials of particle and the membrane surface. ϕ_H can be reasonably be approximated by $\phi_H \cong (2/3 R_m a_p)^{1/2}$ if the particle is in contact with the membrane surface.[5]

In order to calculate the interfacial free energies (ΔG_{132}^{LW}, ΔG_{132}^{AB}, ΔG_{132}^{Tot}), the surface tension components of the foulants were obtained from previous studies,[6-8] while the surface tension components of the membranes were determined with contact angles (θ) measured by using three different probe liquids that have known values of surface tension components.[9] The extended Young-Dupré equation (Eqn. 4.4) was used to calculate the surface tension components:[10]

$$(1+\cos\theta)\gamma_l^{TOT} = 2\left(\sqrt{\gamma_s^{LW}\gamma_l^{LW}} + \sqrt{\gamma_s^{+}\gamma_l^{-}} + \sqrt{\gamma_s^{-}\gamma_l^{+}}\right) \quad (4.4)$$

where θ is the ideal contact angle formed between a droplet of liquid L and the smooth membrane surface, γ_S^{LW} and γ_L^{LW} are the apolar (Lifshitz-van der Waals) components of the surface tension of solid, S (membrane or particle) and liquid L, γ_S^{+}, γ_L^{+}, γ_S^{-}, and γ_L^{-} are the polar (electron-acceptor and electro donor) components of the surface tension of solid (*s*) and liquid (*l*), respectively.

The interfacial free energy at contact, ΔG_{132}^{Tot}, is a thermodynamic value indicating the inherent affinity of a solid foulant (1) interacting through a liquid media (*3*) with a solid membrane surface (2). ΔG_{132}^{Tot} can be determined from Eqn. 4.5:

$$\Delta G_{132}^{Tot} = \Delta G_{132}^{LW} + \Delta G_{132}^{AB} \quad (4.5)$$

where ΔG_{132}^{LW} and ΔG_{132}^{AB} are the Lifshitz–van der Waals and Lewis acid–base interfacial free energies, respectively. They can be calculated from Eqn 4.6 and 4.7:[11]

$$\Delta G_{132}^{LW} = 2\left(\sqrt{\gamma_3^{LW}} - \sqrt{\gamma_1^{LW}}\right)\left(\sqrt{\gamma_2^{LW}} - \sqrt{\gamma_3^{LW}}\right) \quad (4.6)$$

$$\Delta G_{132}^{AB} = 2\sqrt{\gamma_3^+}\left(\sqrt{\gamma_1^-} + \sqrt{\gamma_2^-} - \sqrt{\gamma_3^-}\right) + 2\sqrt{\gamma_3^-}\left(\sqrt{\gamma_1^+} + \sqrt{\gamma_2^+} - \sqrt{\gamma_3^+}\right) - 2\sqrt{\gamma_1^+\gamma_2^-} - 2\sqrt{\gamma_1^-\gamma_2^+} \quad (4.7)$$

The membrane zeta potential (ζ_m) was determined by using an electrokinetic analyzer (SurPASS Electrokinetic Analyzer, Anton-Paar GmbH). This analysis can provide a slope of the streaming current versus pressure (dI/dP) from which the membrane zeta potential can be derived. 1 mMol KCl was used as the electrolyte and the zeta potential was measured at pH 7±0.1. Membrane zeta potential was calculated using the Helmholtz-Smoluchowski equation (Eqn. 4.8),

$$\zeta_M = \frac{dI}{dp} \cdot \frac{\mu}{\varepsilon \cdot \varepsilon_0} \cdot \frac{L}{A} \quad (4.8)$$

where ε is the dielectric constant of the solution, ε_0 is the vacuum permittivity, L is the length of the streaming channel and A is the cross-section of the streaming channel. The zeta potential for the unmodified and modified membranes varied slightly (within error of the experiment) and it was found that these changes in the zeta potential produced negligible contributions to the total interfacial force. Therefore the zeta potential was assumed to be constant at -54.5 mV, as measured for the unmodified membrane.

4.3. Materials and methods

4.3.1. Modification of Membrane Surface and Characterization

The surface of a commercial polyethersulphone (PES) membrane (Synder, LX300) is modified by a grafting procedure adapted from a previous publication.[1] The samples of the PES flat sheet membrane are cut into 4x10 cm^2 rectangular sheets and are submerged into solutions of

0.1 mMol of the selected small molecule PFPA, followed by irradiation with a 6W UV lamp (254 nm, 1200 mW/cm^2) for 60 seconds. Then, the samples are immediately rinsed by deionized (DI) water and saved in a DI water bath. Contact angles of the unmodified and modified membranes are measured by a protocol proposed by Jinwen (2014).[12]

As shown in Figure 4.2, three different PFPA compounds are synthesized and coated on the commercial PES membrane. Typically, PFPA target derivatives are synthesized via an activated *N*-hydroxysuccinimide (NHS) intermediate.[35] Although PFPA-NHS is stable enough to enable solid-state surface modifications,[36] several delicate steps with various protecting group manipulations are required to synthesize PFPA-NHS. Furthermore, for its esterification, the synthesis of a PFPA compound via NHS need to utilize *N,N'*-dicyclohexylcarbodiimide, which is a potential irritant hard to remove from the product. In order to develop a more concise and safe fabrication method, we synthesize PFPA-compounds via *para*-azido perfluorophenyl sulfonamides (Compound 3 in Scheme 1). Commercially available pentafluorophenyl sulfonyl chloride (Compound 1) is used as a chemical prototype, which will initiate the synthesis of sulfonamide (Compound 2) by reaction with an amine. The strong electron-withdrawing inductive effect of the sulfonamide enables nucleophilic substitution by an added azide ion to occur in the *para* position to the sulfonamide, forming Compound 3. Compound **3** can be converted to the desired PFPA compounds in a single step such as a given example in the synthesis of Compound **4c**. We expect that the lone pairs of electrons in the sulfonyl group may append the electron-donating functionality to the PFPA modified membrane, improving its electron-donicity (γ^-).

4.3.2. Membrane fouling experiment

The biofouling resistances of the modified and unmodified membranes are tested in a lab-built cross-flow apparatus under a constant flux mode. Each membrane sample cut out by a 19 cm^2 coupon is loaded in the cross-flow cell and compacted with DI water for two hours under 110 kPa pressurized condition. After compaction, the permeate flux is set to 100 LMH (Liter/m^2/h) and transmembrane pressure (TMP) is monitored continuously with pressure transducers in the feed, retentate, and permeate lines. The pressure transducers are connected to an analog-to-digital converter (Data Logger Pro, Vernier Instruments, USA) and pressure readings are transferred to a PC. TMP is calculated by Eqn. 4.9.

$$TMP = \frac{(P_{in} - P_{ret})}{2} - P_{perm} \tag{4.9}$$

where P_{in}, P_{ret}, and P_{perm} are the pressure in the inlet, retentate, and permeate sides, respectively. Unmodified PES, UV-exposed PES, and PFPA modified PES membranes are tested in the same cross-flow apparatus.

Sodium alginate is utilized as a mode biofoulant that can represent a soluble microbial product in MBR. The test membranes are fouled by alginate solution (200 mg sodium alginate/L) for about 90 minutes (300 mL of permeate collected). Then the test membranes are rinsed by DI water for 5 minutes and fouled again at the same condition (2^{nd} fouling stage). Since all of the biofouling tests are performed in an identical and constant flux (100 LMH), increasing rates of TMPs of the test membranes are compared to evaluate their biofouling properties.

In order to evaluate the effects of UV exposure and PFPA-derivatives grafting on rejections of the test membranes, the sodium alginate concentrations in feed solution and

permeate are measured by a total organic carbon (TOC) analyzer with the samples collected during the first fouling stage. The rejection is calculated from Eqn. 4.10:

$$R = \left(1 - \frac{C_p}{C_f}\right) \times 100\% \tag{4.10}$$

where C_f and C_p are the concentrations of total carbon in the feed solution and permeate, respectively.

4.4. Results and Discussion

4.4.1. Effect of acid-base interaction on interfacial force

Figure 4.3a depicted the interfacial forces for several foulants found in MBRs. Sodium alginate (SA) and bovine serum albumin (BSA), which are known to correspondingly represent polysaccharide-based and protein-based soluble microbial products (SMPs) found in MBRs, encounter the lowest repulsive force barriers. These inferior repulsive forces possibly lead alginate and BSA to easily access the surfaces of membranes and foul them quickly. Because small size SMPs with low electron-donicities are also capable to readily deposit on the membrane surface and alter the surface to be more biofouling-friendly to other biofoulants,[13] it is essential to develop a biofouling-resistant membrane that is thermodynamically able to form an elevated free energy barrier against SMPs and prevent them from forming biofouling-friendly frameworks on the membrane surface.

In order to understand the major interfacial interaction that assists the membrane to have a repulsive interaction to biofoulants, the interfacial forces exerted to *E. Coli* and alginate are investigated in terms of their unit interaction components: electrostatic force (F_{EL}), acid-base force (F_{AB}), and Lifshitz-van der Waals force ($F_{LW),}$ as illustrated in Figure 4.3b and 4.3c. For

both of the test biofoulants, the acid-base force dominates the long-distance interaction while Lifshitz-van der Waals force governs the short-distance force. In the case that the acid-base force forms a positive free energy such as *E.coli* - membrane, there is a peak of repulsion between the biofoulant and the membrane, which is caused by competition between the long-distance-governing repulsion (F_{AB}) and the short-distance-governing attraction (F_{LW}). As the biofoulant accesses the membrane surface, the biofoulant experiences an elevated acid-base repulsion. However, the existence of a strong attractive force component (F_{LW}) begins to compromise the interfacial effect of acid-base repulsion when the biofoulant approaches in close proximity to the membrane surface.

The acid-base repulsive force is determined by the acid-base interaction free energy (ΔG_{132}^{AB}), as presented in Eqn. 4.2, and the electron-donicities of biofoulants and membranes critically contribute to ΔG_{132}^{AB} as discussed in Chapter 3. The biofoulants with a low electron-donicity form weak hydration energy barriers and depreciate ΔG_{132}^{AB} , consequently lowering the acid-base repulsion. If the biofoulants possess significantly inferior electron-donicity, they may fail to form a positive ΔG_{132}^{AB} and thus void the repulsive force across all interfacial distances, as shown in alginate-membrane interaction (Figure 4.3c). Absence of a repulsive force component potentially results in rapid adhesion of the biofoulant to the membrane surface and facilitates the biofilm formation, favorably attracting the successive bioadhesion of other biofoulants. However, the deteriorated acid-base free energy due to the inferior electron-donicity of a biofoulant can be revitalized by alternatively enhancing the electron-donicity of membrane. The elevated electron-donicity of the membrane surface is capable to rebuild the hydration energy barrier, augmenting ΔG_{132}^{AB} and thus repulsive feature of F_{AB}.

Figure 4.4 describes how the enhanced electron-donicity of a membrane improves the repulsion against several biofoulants. For polyethylene glycol (PEG), human serum albumin (HSA), and dextran, which have high electron-donicities, a membrane surface with even low level of electron-donicity succeeds to shape a repulsive force against the biofoulants. Because of the low electron-donicity, however, alginate and BSA require much elevated intensity of electron-donicity for the membrane to create repulsion between those biofoulants and the membrane. Several literatures reported that SMPs and the surface of microbial flocs also exhibit downcast electron-donicities comparable to the ones of alginate and BSA.[8,14-17] Thus, this study is motivated to enhance the electron-donicity of a commercial membrane surface (~40 mJ/m^2) in order to successfully form repulsion against the SMPs and microbial flocs, without compromising the membrane permeability and rejection ability.

4.4.2. Surface tension properties of modified membranes

Contact angles and surface tension properties of the test membranes are presented in Table 4.1. Compared to the unmodified PES membrane, UV-exposed and PFPA-modified PES membrane exhibit smaller contact angles with polar liquids (water and ethylene glycol). Because ethylene glycol has high electron-donicity (47.0 mJ/m^2) and low electron-accepticity (1.9 mJ/m^2), the lower contact angle with ethylene glycol may indicate higher electron-accepticity of the membrane. However, as discussed in Chapter 2 and Chapter 3, polymeric membranes tend to be γ^- semi-monopolar, which occurs in the unmodified and modified PES membranes as well. Although the modified PES membranes overall have elevated electron-accepticities, the membranes remain highly γ^- semi-monopolar ($\gamma^+/\gamma^- < \mathbf{0.0012}$) and allow their electron-donicities to critically control their acid-base interactions as well as the interfacial forces.

Decreases in the contact angles of the modified membranes with water apparently indicate the enhanced electron-donicities of the membranes. Especially, zwitterionic PFPA modified membrane demonstrates the lowest contact angle with water, consequently revealing the most enhanced electron-donicity (38.4 mJ/m^2). Due to the greatest electron-donicity, the zwitterionic PFPA modified PES membrane exhibits the highest hydrophilicity (ΔG_{131}) as well. Figure 4.6 depicts the interfacial forces of the test membranes with alginate. The PFPA modified PES membranes succeed to weaken attraction with alginate by intensifying the hydration energy barrier and relieving the negativity of $\Delta \boldsymbol{G}_{\mathbf{132}}^{\boldsymbol{AB}}$.

4.4.3. Biofouling resistances of modified membranes

The experimental results from the short-term biofouling test are plotted in Figure 4.7a. Each membrane is given two distinct fouling stages before and after a 5-minute rinsing process. The unmodified PES membrane demonstrates the greatest fouling rates in both of the first and second stage tests (61.2×10^6 and 80.7×10^6 /m/s, respectively). The modified membranes overall exhibit depressed fouling rates compared to the unmodified membrane and especially zwitterionic PFPA modified membrane shows the lowest fouling rate among the PFPA modified membranes. The zwitterionic PFPA modified membrane demonstrates close-to-zero fouling rates during the initial and second biofouling stages in the short-term test (about 1.5 hours per stage). Although the zwitterionic PFPA modified membrane is inevitably fouled during the longer-term experiment (50 hours) under a continuous filtration mode with no rinsing and relaxation, the zwitterionic PFPA coated membrane significantly suppress the biofouling rate compared to the unmodified membrane as shown in Figure 4.7b. The unmodified PES membrane encounters a severe biofouling as soon as the fouling test begins and the biofouling test should be stopped in

about 7 hours because the TMP reaches the inlet pressure and the pressure in the permeation side becomes less than zero psi, which is under the detection limit of the pressure gauge. In comparison, the zwitterionic PFPA modified membrane maintains the close-to-zero fouling for 16 hours and then begins to be slowly fouled, achieving only 37 kPa of TMP increase during 50 hours.

Overall, the test membranes experience more severe fouling in their second biofouling stages (Table 4.2). Since the rinsing solution does not contain any cleaning chemical, the rinsing solution may not completely remove the alginate particles deposited on the membrane surface and there are presumably residual alginate layers on the membrane surface, which possibly facilitates the adhesion of the alginate in the second biofouling stage. Interestingly, only zwitterionic PFPA modified membrane prevents its second stage biofouling test from causing more acute fouling. This implies that the enhanced electron-donicity may help the zwitterionic PFPA modified membrane to successfully avoid having a strong bioadhesion with alginate and to effectively release the deposited alginates during 5-minute rinse mode. MBRs regularly conduct a rinsing or relaxation mode to unleash the attached biofoulants and the efficient detachment of deposited biofoulants significantly diminishes the irreversible fouling. Therefore, due to the suppressed bioadhesive interaction, a membrane with the enhanced electron-donicity may support MBRs to have better physical cleaning efficacy and thus to experience less irreversible fouling.

Correlation analysis on the biofouling rates with surface tension properties of the test membranes reveals that the biofouling tendency of a membrane is deeply correlated to γ^- and ΔG_{131} (Table 4.2). The hydrophilicity (ΔG_{131}) of membrane represents -0.87 and -0.86 of correlation coefficients with biofouling rates in the initial and second stages, respectively. The

negative sign of the correlation coefficient indicates an inverse relationship between the hydrophilicity and biofouling tendency. In other words, as the membrane surface equips better hydrophilicity, the membrane surface develops higher hydration energy and enhances repulsion between the membrane and biofoulants, which consequently depresses the biofouling rate. The electron-donicity of membrane also exhibits a decent correlation with biofouling rate. The enhanced electron-donicities of PFPA modified membranes apparently correlate with lower biofouling tendencies, disclosing that the intensified γ^- of a membrane may benefit anti-biofouling property.

4.5. Conclusion

The simulation data of interfacial forces revealed that the acid-base interaction significantly contributes to forming repulsion between a biofoulant and a membrane and that the enhanced electron-donicity of membrane can resolve the inferior repulsion with the biofoulant contacting low electron-donor moiety. The simulation result motivated a synthesis of biofouling resistant membrane by grafting PFPA small molecules to intensify the electron-donicity of a commercial PES membrane, aiming to achieve γ^- of 40 mJ/m^2, the threshold quantity to generate repulsion between a membrane and a model biofoulant (alginate). All of PFPA modified PES membranes demonstrated better hydrophilicity and electron-donicity. Among the modified membranes, the zwitterionic PFPA modified membrane exhibited the greatest electron-donicity (38.4 mJ/m^2), which is close to the target value. The hydrophilicity and electron-donicity of a membrane showed meaningful relationships with biofouling resistance of a membrane; greater ΔG_{131} and γ^- apparently correlated to the enhanced anti-biofouling property. Representatively, the zwitterionic PFPA modified membrane demonstrated a remarkably

reinforced biofouling-resistance compared to the unmodified PES membrane both in the short-term and long-term fouling tests.

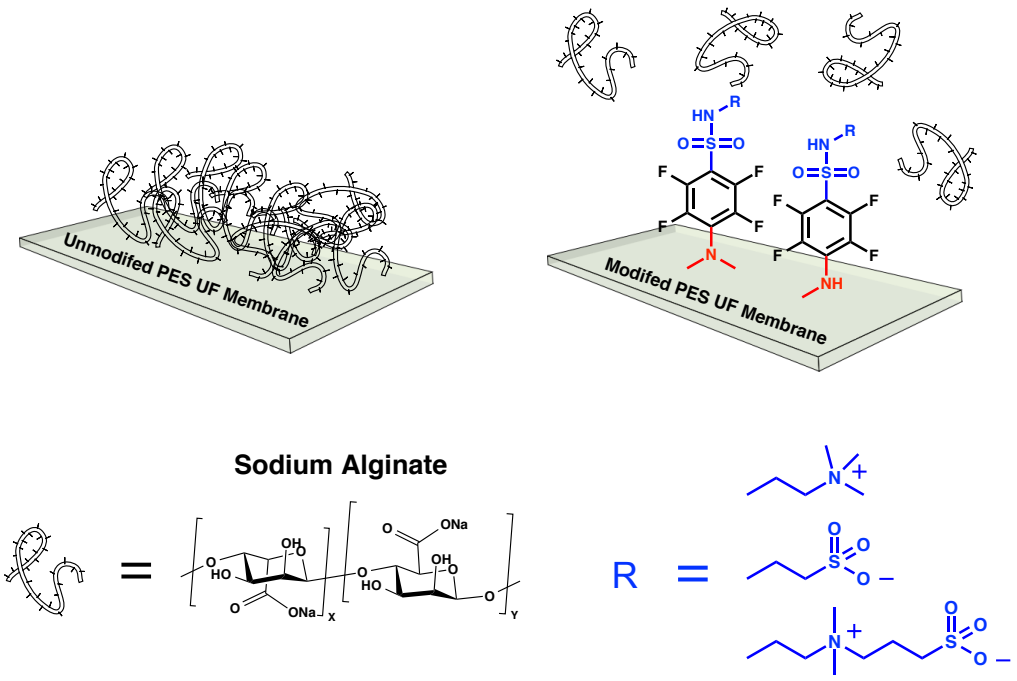

Figure 4.1. Schematic diagram illustrating sodium alginate adhesion to polyethersulfone ultrafiltration membranes unmodified (left) and modified with perfluorophenylazide derivatives (right).

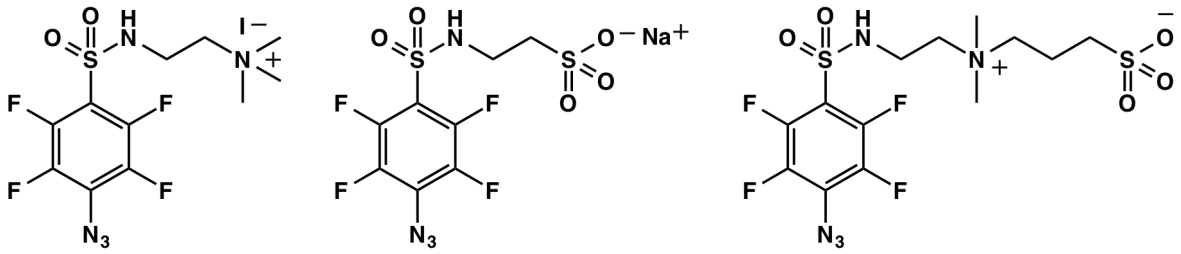

PFPA(+) PFPA(-) PFPA(+-)

Figure 4.2. Target PFPA-derivatives

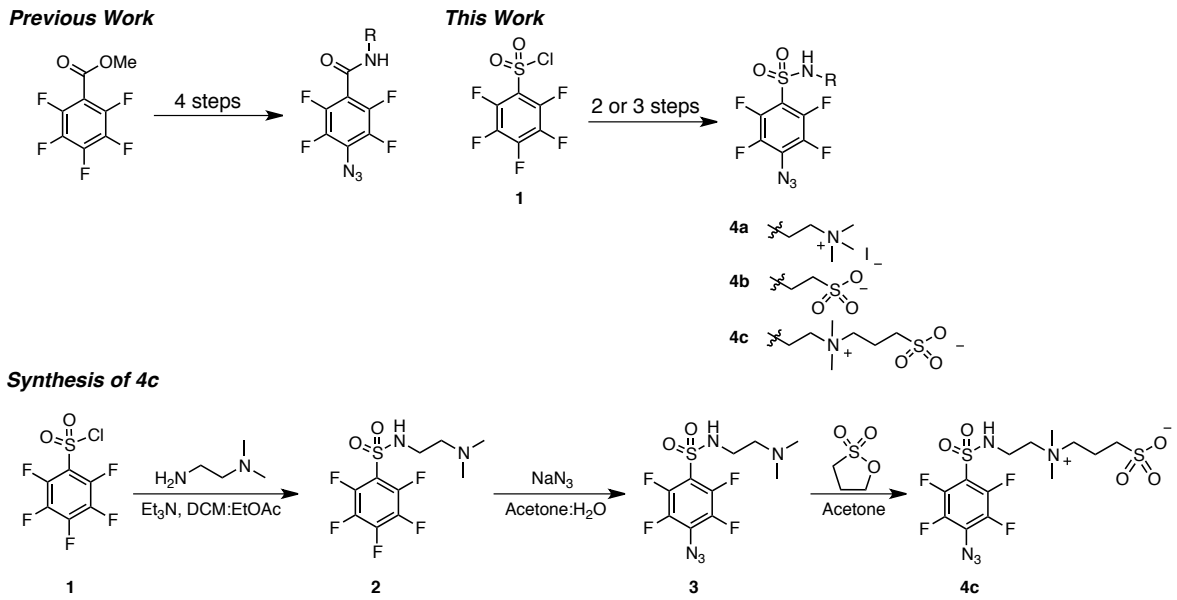

Scheme 1. Synthesis of PFPA small molecules from pentafluorophenyl sulfonyl chloride

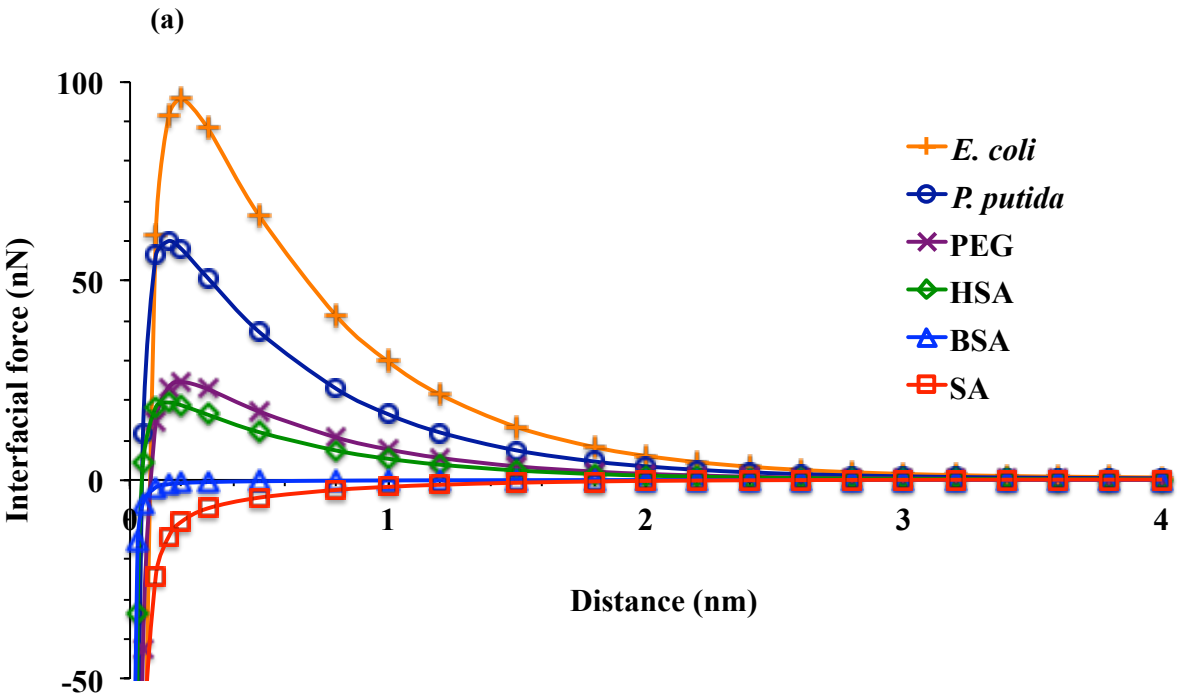

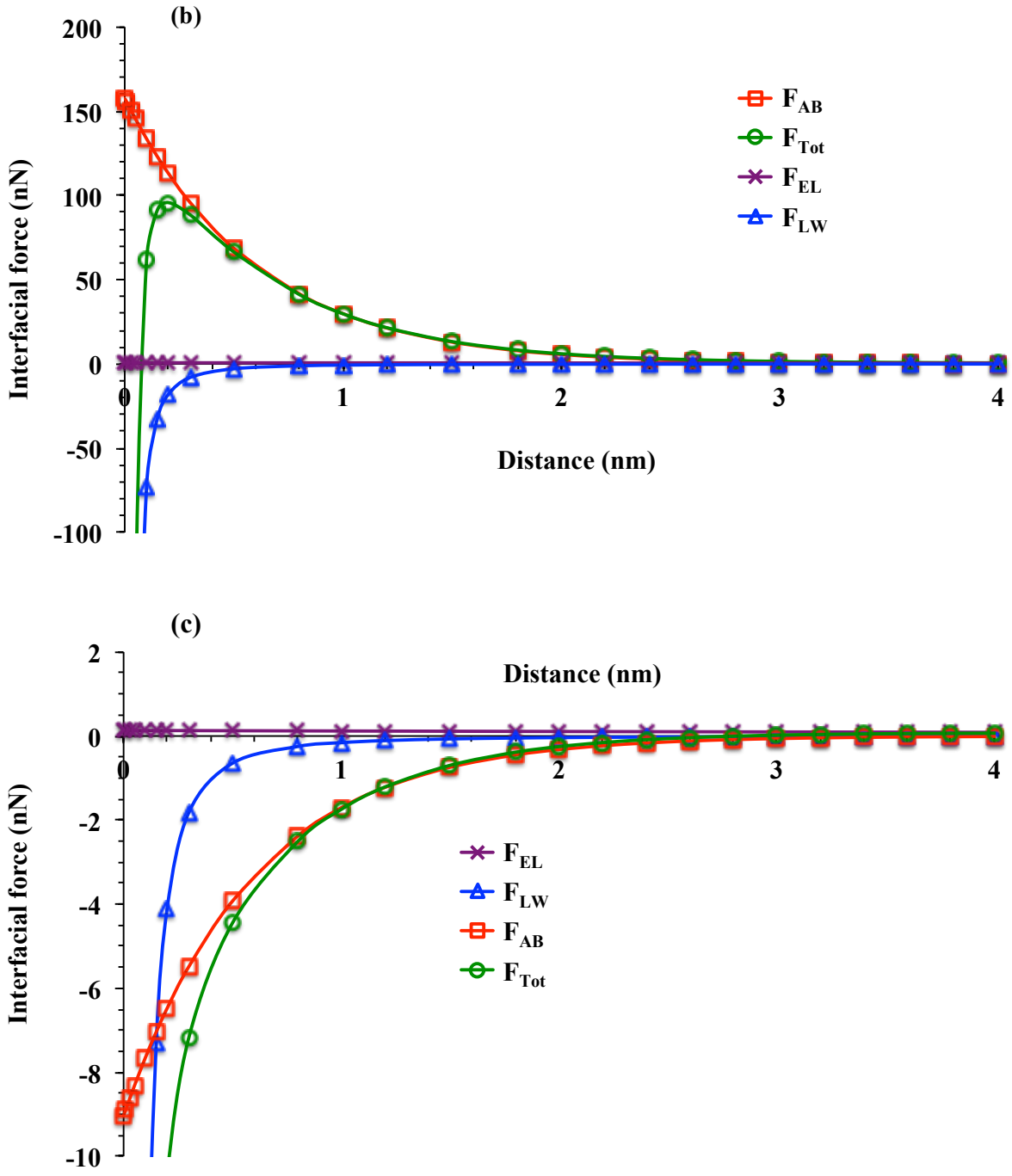

Figure 4.3. a) Interfacial forces between selected foulants in MBRs and PES. *E. coli* = *Escherichia coli*, *P. putida* = *Pseudomonas putida*, PEG = polyethylene glycol, HSA = human serum albumin, BSA = bovine serum albumin, SA = sodium alginate b) The interfacial forces of *E. coli* and PES broken down into its components c) The interfacial forces between sodium alginate and PES broken down into its components. F_{LW} = Lifshitz-van der Waals force, F_{AB} = acid-base force, F_{EL} = electrostatic force, F_{TOT} = total force

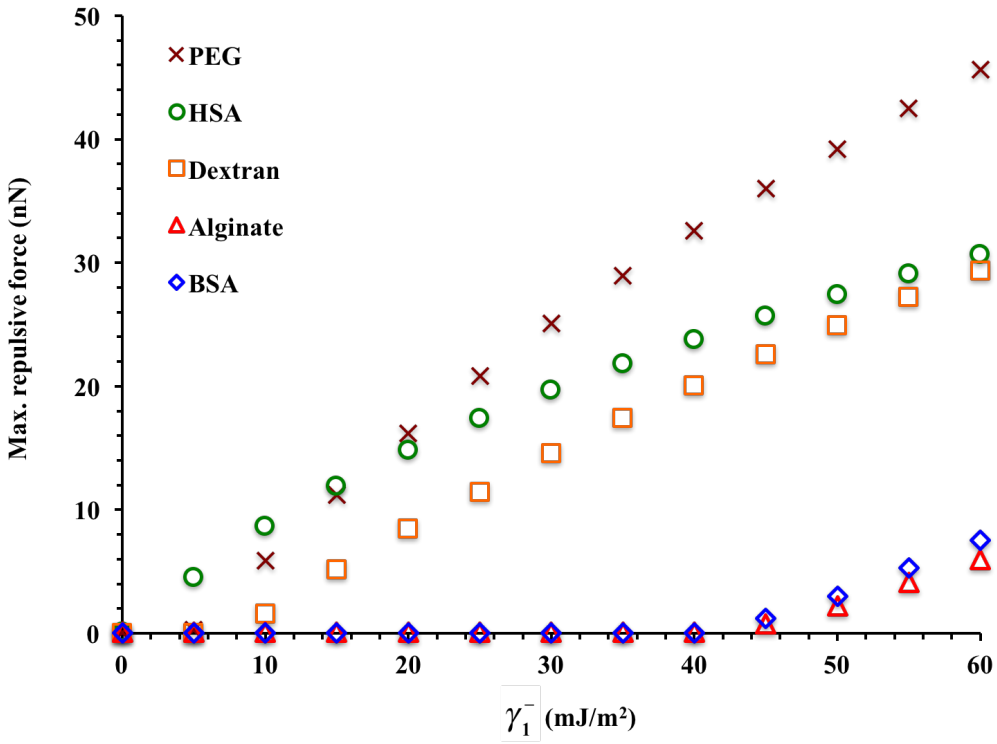

Figure 4.4. The effect of high γ^- on repulsive forces between several foulants and a polyethersulfone membrane. PEG = polyethylene glycol, HSA = human serum albumin, DEX = dextran, BSA = bovine serum albumin

Table 4.4. Surface properties of unmodified and modified PES membranes

Membrane	CA (DI)	CA (EG)	CA (DM)	γ^{LW} (mJ/m^2)	γ^+ (mJ/m^2)	γ^- (mJ/m^2)	ΔG_{131} (mJ/m^2)
PES	49.8	28.9	17.7	48.4	4E-07	29.4	-3.0
PES UV	48.8	29.9	23.3	46.8	1E-03	31.3	1.6
PES PFPA(-)	46.8	25.3	21.6	47.3	1E-02	32.1	2.3
PES PFPA(+)	45.7	23.2	23.7	46.6	4E-02	32.8	3.9
PES PFPA(+-)	40.4	20.1	19.2	48.0	9E-03	38.4	12.5

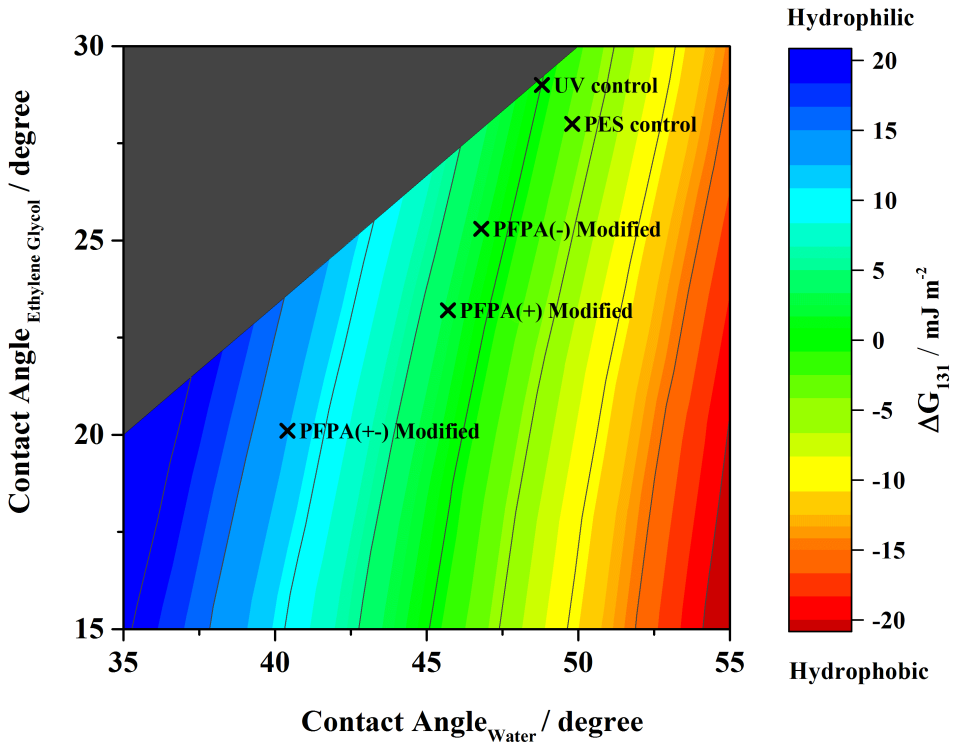

Figure 4.5. Hydrophilicity of unmodified and modified membranes based on the ΔG_{131} surface energy.

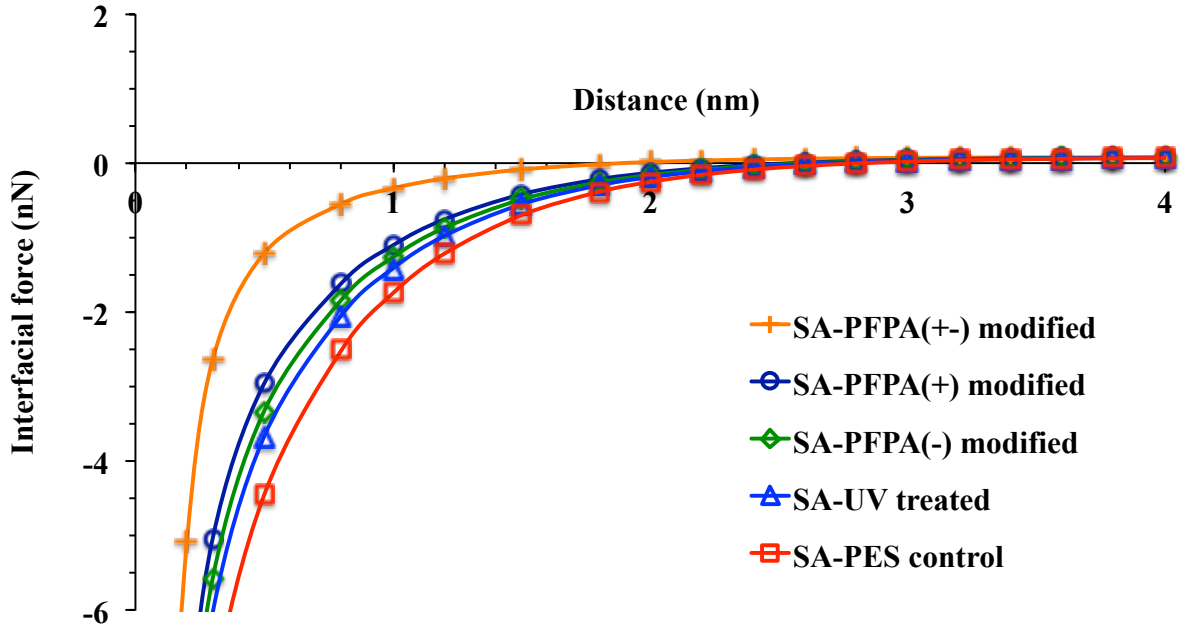

Figure 4.6. Overall interfacial force between sodium alginate and the unmodified and modified membrane surfaces

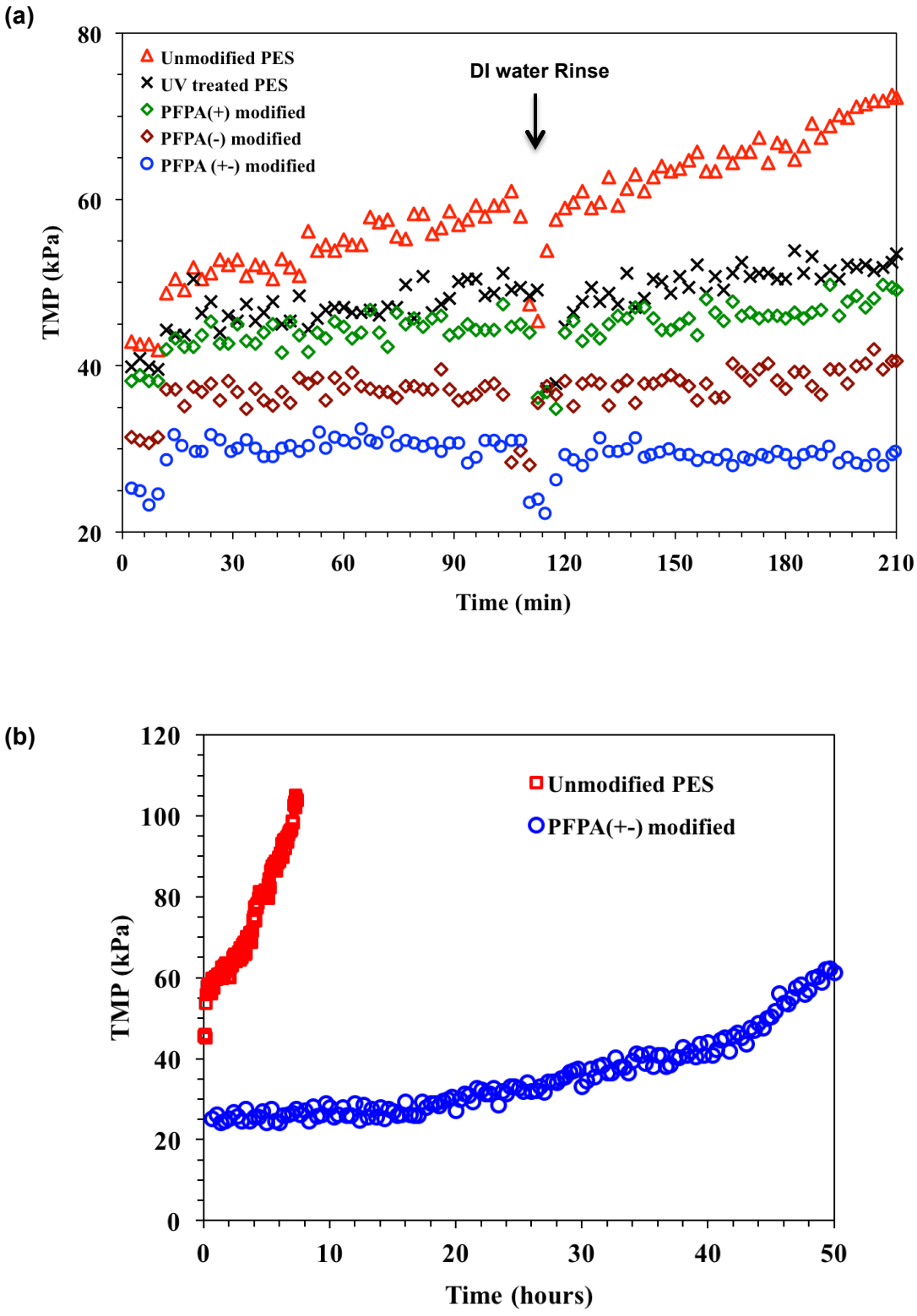

Figure 4.7. Short (a) and long term (b) fouling study of the unmodified and modified membranes

Table 4.5. Performance properties of unmodified and modified membranes

Membrane	1st Stage Fouling Rate (10^6 /m/s)	2nd Stage Fouling Rate (10^6 /m/s)	Pure Water Permeability (LMH/bar)	Rejection of Alginate
Unmodified PES	61.2	80.7	1.07	98.0 %
PES UV Treated	29.9	31.2	1.14	98.8 %
PES-PFPA(+)	13.6	23.3	1.2	98.3 %
PES-PFPA(-)	14.7	18.9	1.6	97.7 %
PES-PFPA(+-)	0	0	1.8	98.7 %
Correlation coefficient				
w/ γ_1^-	(-) 0.83	(-) 0.82	(+) 0.84	
w/ ΔG_{131}	(-) 0.87	(-) 0.86	(+) 0.82	

References

(1) McVerry, B. T.; Wong, M. C. Y.; Marsh, K. L.; Temple, J. A. T.; Marambio-Jones, C.; Hoek, E. M. V.; Kaner, R. B. Scalable Antifouling Reverse Osmosis Membranes Utilizing Perfluorophenyl Azide Photochemistry. *Macromolecular Rapid Communications* **2014**, *35* (17), 1528–1533.

(2) Kim, S.; Marion, M.; Jeong, B.-H.; Hoek, E. M. V. Crossflow membrane filtration of interacting nanoparticle suspensions. *Journal of Membrane Science* **2006**, *284* (1-2), 361–372.

(3) Kang, S. T.; Subramani, A.; Hoek, E. M. V.; Deshusses, M. A.; Matsumoto, M. R. Direct observation of biofouling in cross-flow microfiltration: mechanisms of deposition and release. *Journal of Membrane …* **2004**.

(4) Kim, S.; Marion, M.; Jeong, B.-H.; Hoek, E. M. V. Crossflow membrane filtration of interacting nanoparticle suspensions. *Journal of Membrane Science* **2006**, *284* (1-2), 361–372.

(5) Subramani, A.; Hoek, E. M. V. Direct observation of initial microbial deposition onto reverse osmosis and nanofiltration membranes. *Journal of Membrane Science* **2008**.

(6) Jin, X.; Huang, X.; Hoek, E. M. V. Role of Specific Ion Interactions in Seawater RO Membrane Fouling by Alginic Acid. *Environ. Sci. Technol.* **2009**, *43* (10), 3580–3587.

(7) Cornelissen, E. R.; van den Boomgaard, T.; Strathmann, H. Physicochemical aspects of polymer selection for ultrafiltration and microfiltration membranes. *Colloids and Surfaces A: Physicochemical and Engineering Aspects* **1998**, *138*, 283–289.

(8) Hong, H.; Peng, W.; Zhang, M.; Chen, J.; He, Y.; Wang, F.; Weng, X.; Yu, H.; Lin, H. Thermodynamic analysis of membrane fouling in a submerged membrane bioreactor and its implications. *Bioresource Technology* **2013**, *146* (C), 7–14.

(9) Kim, S.; Hoek, E. M. V. Interactions controlling biopolymer fouling of reverse osmosis membranes. *Desalination* **2007**, *202* (1-3), 333–342.

(10) van Oss, C. J. Development and applications of the interfacial tension between water and organic or biological surfaces. *Colloids and Surfaces B: Biointerfaces* **2007**, *54* (1), 2–9.

(11) van Oss, C. J. Acid—base interfacial interactions in aqueous media. *Colloids and Surfaces A: Physicochemical and Engineering Aspects* **1993**, *78*, 1–49.

(12) Wang, J. *2014_Jinwen_Effects of water chemistry on structure and performance of polyamide composite membranes*; 2014.

(13) Sheng, G.-P.; Yu, H.-Q.; Li, X.-Y. Extracellular polymeric substances (EPS) of microbial aggregates in biological wastewater treatment systems: a review. *Biotechnology Advances* **2010**, *28* (6), 882–894.

(14) Chen, L.; Tian, Y.; Cao, C.-Q.; Zhang, J.; Li, Z.-N. Interaction energy evaluation of soluble microbial products (SMP) on different membrane surfaces: Role of the reconstructed membrane topology. *Water Research* **2012**, *46* (8), 2693–2704.

(15) Li, Z.; Tian, Y.; Ding, Y.; Chen, L.; Wang, H. Fouling potential evaluation of soluble microbial products (SMP) with different membrane surfaces in a hybrid membrane bioreactor using worm reactor for sludge reduction. *Bioresource Technology* **2013**, *140* (C), 111–119.

(16) Lin, H.; Zhang, M.; Wang, F.; Meng, F.; Liao, B.-Q.; Hong, H.; Chen, J.; Gao, W. A critical review of extracellular polymeric substances (EPSs) in membrane bioreactors_

Characteristics, roles in membrane fouling and control strategies. *Journal of Membrane Science* **2014**, *460* (c), 110–125.

(17) Zhang, M.; Liao, B.-Q.; Zhou, X.; He, Y.; Hong, H.; Lin, H.; Chen, J. Effects of hydrophilicity/hydrophobicity of membrane on membrane fouling in a submerged membrane bioreactor. *Bioresource Technology* **2015**, *175* (C), 59–67.

Chapter 5

SUMMARY AND CONCLUSION

In Chapter 1, an overview of biofouling phenomena in MBRs and theoretical backgrounds for the surface tension approach were provided, and the research hypothesis and objectives were outlined.

- According to van Oss approach, in aqueous media, Lewis acid-base interaction occurs between the electron-acceptor in hydrogen atoms of water and lone pairs of atoms of a solid, basically having an analogous concept with hydrogen-bonding.
- Because biofoulants and the membranes are interacting with water and each other and have various extents of the electron-donating and accepting potentials, diverse interfacial interactions occur between biofoulants and membranes in aqueous system.
- Therefore, better thermodynamic understanding on the biofouling phenomena need a perspective that ponders the three different but deeply interconnected interfacial interactions existing in membrane-water, water-biofoulant and biofoulant-membrane.

Chapter 2 investigated the water-membrane interaction in terms of surface tension properties of a membrane and their discrete interactions with water.

- This chapter simulated the available surface tension parameters of polymeric porous membranes using different presumptions on polar properties of water and evaluates the effect of each surface tension parameter of a membrane on water-membrane interactions.
- The simulated libraries of surface tension parameters revealed that polymeric porous membranes highly tend to fall into a category of electron-donor monopolar or semi-monopolar solids.

- The high electron-accepticity of water emphasized the role of γ^- of a membrane in the interfacial interaction between a membrane and water (ΔG_{131}^{tot}) and caused the polar adhesion between electron-donor sites of a membrane and electron-acceptor sites of water to be a major interaction component in ΔG_{131}^{tot} than other components.
- The high Lewis acidity of water highlighted the role of γ^- of a membrane in its wettability as well. A higher electron-donicity of a membrane has little impact on the total surface tension of the membrane surface (γ_1), but successfully favors the electron-acceptor sites of water forming a significantly lower surface tension of the water-membrane interface (γ_{13}) and thus a greater affinity between the membrane and water ($-\Delta G_{13}^{tot}$).

Chapter 3 investigated the effects of water-solids interactions on biofouling phenomena and explored fining key physicochemical properties of a membrane for biofouling resistance.

- The high electron-accepticity of water emphasized the importance of γ^- of a membrane and a biofoulant in their interfacial interaction through water and drove acid-base interaction to be a major interaction component in the interfacial interactions between membranes and a biofoulant (ΔG_{132}).
- The surfaces of various biofoulants were characterized with highly variable electron-donicities and the biofoulant with lower electron donicity can be more vulnerable to biofouling due to the inferior hydration energy formed on the surface of the biofoulant.
- The inferior hydration energy by a low electron-donicity of a biofoulant can be compensated by an enhanced electron-donicity of a membrane; this fact leads to propose a standard of an electron-donicity demand for a membrane to have a positive ΔG_{132} with a given biofoulant.

- Experimental results of a microbial adhesion test and biofouling tests qualitatively correlated well with tendencies of electron-donicities of the test membranes, proving an electron-donicity of a membrane to be a reasonable indicator for the anti-biofouling property of the membrane.

Chapter 4 attempted to impart membranes with hydrophilic and anti-biofouling properties by grafting hydrophilic polymers to the surface.

- Photoactive perfluorophenyl azides (PFPAs) were utilized to generate highly reactive nitrenes (when exposed to UV light) that can covalently bind to the membranes' surfaces. Three different types of small molecule PFPA derivatives were applied and the experimental data directed us to modify the UF membrane surfaces with water-soluble small molecules to maintain the membranes' high permeability.
- The effects of small molecule PFPA derivatives on surface tension characteristics of a polymeric membrane were analyzed by van Oss method. Modeling data indicated that the electron-donicity of membranes plays an essential role in foulant adhesion forces.
- The analyzed physicochemical properties of the modified membranes were compared to the experimental results of a biofouling test with alginate solution. The modified membranes with higher electron-donicity exhibit outstanding foul-resistance against sodium alginate, a model foulant, during operation.